ULTIMATE LOAD ANALYSIS OF FIXED ARCHES

by

Andrew John Mill

B.A.Sc., The University of British Columbia, 1983

A THESIS SUBMITTED IN PARTIAL FULFILLMENT OF

THE REQUIREMENTS FOR THE DEGREE OF

MASTER OF APPLIED SCIENCE

in

THE FACULTY OF GRADUATE STUDIES

Department of Civil Engineering

We accept this thesis as conforming

to the required standard

THE UNIVERSITY OF BRITISH COLUMBIA

October, 1985

In presenting this thesis in partial fulfillment of the requirements for an advanced degree at the University of British Columbia, I agree that the Library shall make it freely available for reference and study. I further agree that permission for extensive copying of this thesis for scholarly purposes may be granted by the Head of my Department or by his or her representatives. It is understood that copying or publication of this thesis for financial gain shall not be allowed without my written permission.

Department of Civil Engineering

The University of British Columbia
1956 Main Mall
Vancouver, Canada
V6T 1Y3

Date October, 1985

ABSTRACT

The advent of Limit States Design has created the necessity for a better understanding of how structures behave when loaded beyond first local yielding and up to collapse. Because the problem of determining the ultimate load capacity of structures is complicated by geometric and material non-linearity, a closed form solution for anything but the simplest of structure is not practical. With this as motivation, the ultimate capacity of fixed arches is examined in this thesis. The results are presented in the form of dimensionless collapse curves. The form of these curves is analogous to column capacity curves in that an ultimate load parameter will be plotted as a function of slenderness.

The ultimate capacity of a structure is often determined by Plastic Collapse analysis or Elastic Buckling. Plastic Collapse is attained when sufficient plastic hinges form in a structure to create a mechanism. This analysis has been proven valid for moment resisting frames subjected to large amounts of bending and whose second order effects are minimal. Elastic buckling is defined when a second order structure stiffness matrix becomes singular or negative definite. Pure elastic buckling correctly predicts the ultimate load if all components of the structure remain elastic. This may occur in slender structures loaded to produce large axial forces and small amounts of bending. Because arches are subject to a considerable amount of both axial and bending, it is clear that a reasonable ultimate load analysis must include both plastic hinge formation and second order effects in order to evaluate all ranges of arch slenderness.

A computer program available at the University of British Columbia accomplishes the task of combining second order analysis with plastic hinge formation. This ultimate load anaysis program, called "ULA", is interactive, allowing the user to monitor the behaviour of the structure as the load level is increased to ultimate. A second order analysis is continually performed on the structure. Whenever the load level is sufficient to cause the formation of a plastic hinge, the stiffness matrix and load vector are altered to reflect this hinge formation, and a new structure is created. Instability occurs when a sufficient loss of stiffness brought on by the formation of hinges causes the determinant of the stiffness matrix to become zero or negative.

Two different load cases were considered in this work. These are a point load and a uniformly distributed load. Both load cases included a dead load distributed over the entire span of the arch. The load, either point load or uniform load, at which collapse occurs is a function of several independent parameters. It is convenient to use the Buckingham π Theorem to reduce the number of parameters which govern the behaviour of the system. For both load cases, it was necessary to numerically vary the location or pattern of the loading to produce a minimum dimensionless load. Because of the multitude of parameters governing arch action it was not possible to describe all arches. Instead, the dimensionless behaviour of a standard arch was examined and the sensitivity of this standard to various parameter variations was given.

Being three times redundant, a fixed arch plastic collapse mechanism requires four hinges. This indeed was the case at low L/r. However, at intermediate and high values of slenderness, the loss of stiffness due to

the formation of fewer hinges than required for a plastic mehanism was sufficient to cause instability. As well, it was determined that pure elastic buckling rarely, if ever, governs the design of fixed arches.

Finally, the collapse curves were applied to three existing arch bridges; one aluminum arch, one concrete arch, and one steel arch. The ultimate capacity tended to be between three and five times the service level live loads.

TABLE OF CONTENTS

TABLE OF CONTENTS (Continued)

TABLE OF CONTENTS (Continued)

LIST OF TABLES

LIST OF FIGURES

LIST OF FIGURES (Continued)

LIST OF SYMBOLS

A	Cross sectional area
a_i	Intercept of facet i of a yield surface with the p axis
b_i	Intercept of facet i of a yield surface with the m axis
c	Distance from the centroid of a symmetrical cross-section to the outer fibre
E	Young's Modulus
e	Eccentricity of applied load
f	Rise of an arch
F_i	Load cases
$F_D, F_O, F_P, \bar{F}$	Load Vectors
h_i	Height to location i on an arch
I	Moment of inertia of a cross-section
K	Stiffness matrix
k	Effective length factor
L	Span of an arch
M	Bending moment
M_p	Plastic moment
M_y	Yield moment
m	$\lvert M \rvert M_p$
P	Point load
P_i	Point load of which event i occurs
P_p	Axial force required to cause full cross sections yielding with no moment present
p	P/P_p
r	Radius of gyration of a cross section

LIST OF SYMBOLS (Continued)

S	Elastic section modulus
V_L, V_R	Vertical reactions
w	Uniformly distributed load (U.D.L.)
w_d	Uniformly distributed dead load
w_i	Unbalanced U.D.L. at which event i occurs
w_u	Ultimate U.D.L.
x	Parameter indicating loading pattern
y	The distance from the center of gravity of a symmetrical cross section to the centre of gravity of either the upper or lower half
Z	Plastic section modulus
α	Dead load ratio
α_i	Load factors applied to load cases F_i
λ	Load level
ϕ	Curvature
ϕ_i	$m/b_i + p/\alpha_i$
σ_y	Yield stress

ACKNOWLEDGEMENT

The author wishes to thank Dr. Roy F. Hooley for his invaluable inspiration and assistance towards the completion of this work.

This research might never have been started without the generous financial support of the Natural Sciences and Engineering Research Council. Their efforts in aiding Canadian research is acknowledged.

Finally the author would like to extend his thanks to the UBC Computing Center for their provision of such excellent services.

CHAPTER 1

INTRODUCTION

1.1 Basic Design Philosophies

The basic philosophy of structural design has seen many changes. Allowable stress design has been very common and is still used today in many applications. In allowable stress design, dead and live loads are applied to a structure such that nowhere in the structure does any stress exceed allowable. The allowable stress is normally the yield stress divided by some factor of safety, i.e.;

$$\text{STRESSES DUE TO D.L. + L.L.} < \sigma_y/N \qquad (1.1)$$

where D.L. = dead load,

L.L. = live load,

σ_y = yield stress,

N = factor of safety.

Eq. (1.1) implies that both the dead load and live load are subject to the same factor of safety.

Statistical studies of loads and materials have been used to develop a contemporary design philosophy. The object of this new design method, called Limit States Design, is to ensure that the probability of reaching a given limit state, such as collapse or unserviceability is below an acceptable value. To accomplish this, the dead and live loads must each have their own factors of safety, N_1 and N_2 simply because the dead load is better defined than the live load. The basic Limit State Design philosophy can now be summarized as follows:

$$N_1 \text{ D.L.} + N_2 \text{ L.L.} \leq \phi R \qquad (1.2)$$

where N_1 D.L. + N_2 L.L. = Effect of applied loads

R = the resistance of a member, connection or structure, and

ϕ = the capacity reduction factor accounting for material variation.

A slight change in nomenclature accompanies the new design method such that N_1 and N_2 are now referred to as load factors.

1.2 Reserve Capacity

It is common today to use elastic analysis to find the response of the structure to the factored loads. If R is taken as first yield, there exists additional capacity beyond that load level. This will be referred to as reserve capacity.

Unless a structure is exceedingly slender and fails due to elastic buckling prior to reaching first yield, the reserve capacity is at least the increase in load required to form the first plastic hinge, and at most, the increase in load required to obtain a plastic collapse mechanism. A determinate structure fails after the formation of one plastic hinge, therefore a more redundant structure would generally possess a higher reserve capacity.

1.3 Application to Arches

With the preceeding discussion of Limit States Design and reserve capacity as motivation, this thesis will examine the ultimate load, or collapse limit state of fixed arched ribs. This will ultimately lead to

a better understanding of the reserve capacity of fixed arches as well as the factors on which it depends.

The key to the success of this work is a reliable analysis technique which must include all prevalent types of behaviour. Conventionally, plastic analysis is used in determining collapse loads for moment resisting frames and continuous beams. Elastic buckling is used in the evaluation of the ultimate capacity of slender columns. Considering that an arch is basically a compression member subject to bending by unsymmetrical live loads, the ultimate strength may be governed by plastic collapse, elastic buckling, or by some intermediate form of instability with less plastic hinges than required for a collapse mechanism. The reserve capacity of an arch is therefore governed by non-linear behaviour. This non-linearity arises from plastic hinging and P-Δ second order effects. A computer analysis combining both these factors is outlined in Section 1.2.

In an age of increasing accessibility to computer hardware and software, a difficult question faces the researcher. Is it a researcher's responsibility to present his results in the form of design or analytical equations based on curve fitting or similar conventional techniques? Or, is it the researcher's responsibility to present the result of hours of computer analysis so as to inform and enlighten the reader and to give the reader conceptual ideas and guidelines, assuming that the reader has the computer facilities to duplicate some part of the researcher's work and to use the results for his or her own particular and specialized purpose? The latter approach has been chosen here.

1.4 Computer Program Theory and Underlying Assumptions

The computer program used in this work is "ULA" (Ultimate Load Analysis)[1]. It is a plane frame stiffness program which combines second order analysis with plastic hinge formation. ULA is an interactive program which allows the user to monitor the structure and to place plastic hinges when necessary as the load is increased to ultimate.

One of the requirements of limit states design is that the structure not fail when subjected to each of a number of load vector F_0 where

$$\begin{aligned} F_0 &= \alpha_1 F_1 + \alpha_2 F_2 + \alpha_3 F_3 + \ldots . \\ &= F_D + \bar{F} \end{aligned} \tag{1.3}$$

F_0 is then a linear combination of load cases F_i augmented by the appropriate load factor α_i. In analyzing for ultimate load, the response of the structure at any load level λ to the force vector F must be determined where

$$F = F_D + \lambda \bar{F} \tag{1.4}$$

The original load vector F_0 is the sum of vectors F_D and $\bar{F}$. In performing the analysis to determine ultimate load, only $\bar{F}$ is augmented by load vector λ. This makes it possible to maintain a constant dead load factor, for example, and increase only the live load until collapse.

1.4.1 Elasto-Plastic Analysis

There are two basic methods of elasto-plastic analysis. The first is an energy method whereby the external energy created by the loading is equated to the internal energy for different mechanisms and mechanism

combinations. The second method is by load increments whereby the structure is analyzed as linear elastic until a member moment reaches the plastic moment M_p at which point it remains at M_p with free relative rotation of adjacent members. The load level is then increased and the structure is analyzed linearly until another hinge is to form. This continues until a collapse mechanism is obtained. The second method is preferred because it lends itself to computer simulation and it makes the inclusion of second order effects practical.

Fig. 1 shows a typical hinge formation sequence with increasing λ for a single bay frame. It is important to note that each of the structures No. 0 through 4 are different and each is valid only for a specific range of λ. Each structure has a different stiffness matrix K and each will be analyzed under the loads shown.

To actually place a hinge in the structure at the appropriate load level, an additional slave joint is created at the hinge location which has the same translation as the master joint, but different rotation. The load vector F is then augmented by $\pm M_p$ between each master and slave pair, so the new load vector is now $F = F_D + \lambda\bar{F} + F_p$, where F_p contains only $\pm M_p$. This hinge placement is depicted in Fig. 2. Full details are given in reference 1.

The linear elasto-plastic response of the single bay frame of Fig. 1 forms the polygonal shape in Fig. 3 indicating the loss of stiffness in the structure as each hinge forms. In the method described above for hinge placement, a hinge can be placed at any load level. Because each of the structures of Fig. 1 is unique, the response at load level λ_B, for example, can be obtained by a first order analysis of structure #2 from zero load level to λ_B along a secant OB, and not along the facets of the polygon.

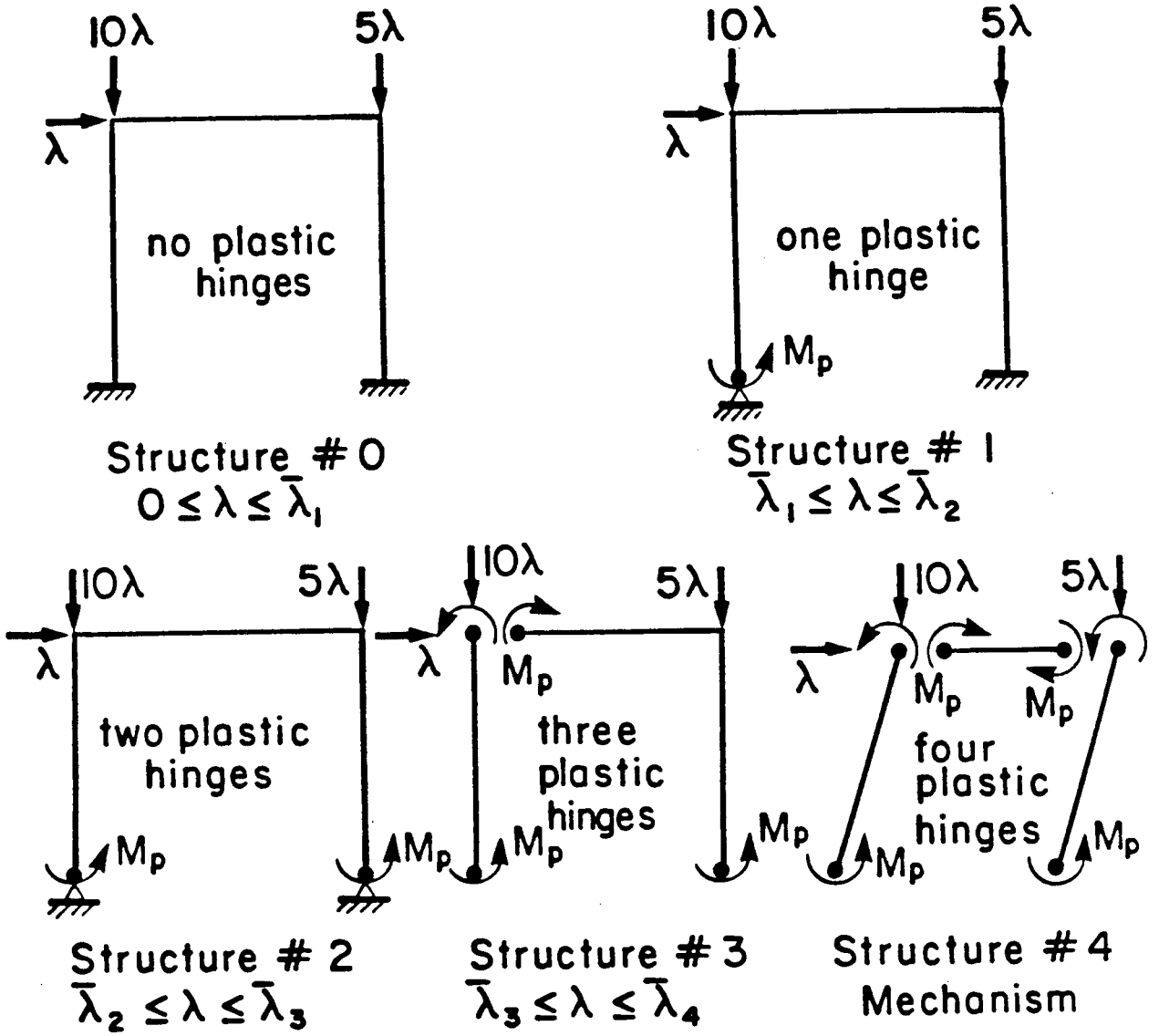

Fig. 1. Elasto-Plastic Hinge Formation.

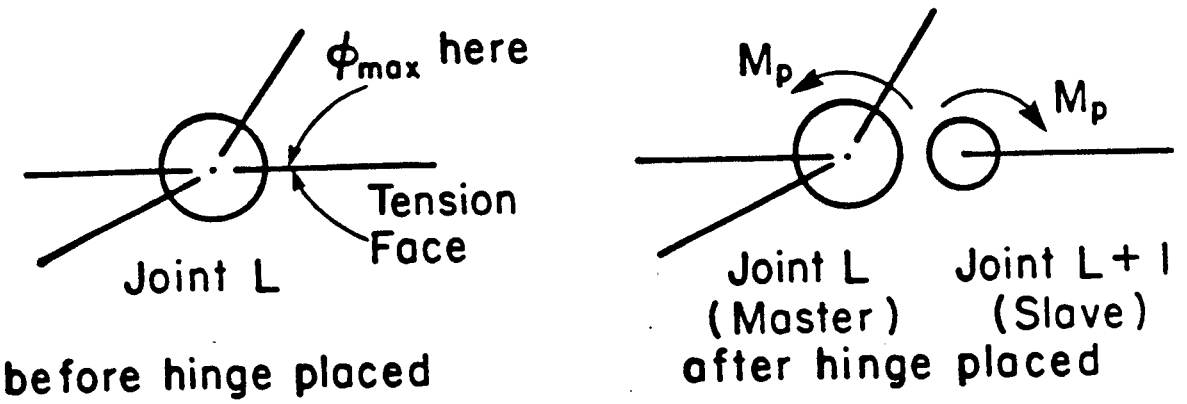

Fig. 2. Hinge Placement.

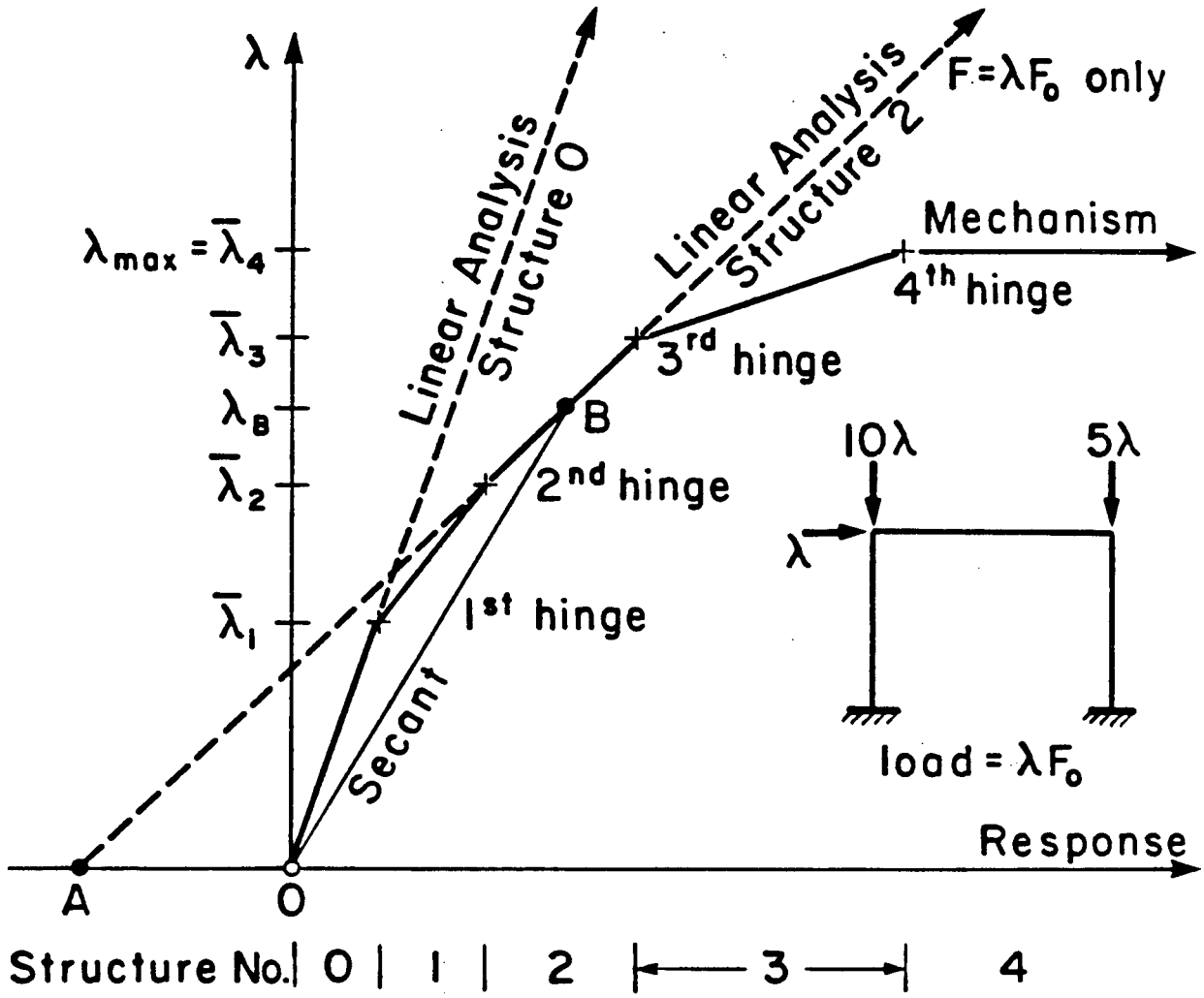

Fig. 3. First Order Elasto-Plastic Response.

1.4.2 Second Order Analysis

Second order analysis requires the structure to be elastic and to be in equilibrium in the deformed shape. The latter is achieved by using stability functions in the member matrix. Details of these stability functions will not be discussed here as they are standard and presented by many other authors including Gere and Weaver[2]. The stability functions depend on the axial forces, and the axial forces depend on the

deflected shape. It is therefore necessary to iterate towards a solution several times at each load level. This is nicely handled by the interactive format of the program because the analyst can view the determinant of the structure stiffness matrix and use that as a criteria for convergence.

Normally, only a small number of cycles, perhaps two, is required for convergence as the axial force changes only slightly with the inclusion of the second order effects. Of course a few more cycles are required when more hinges are placed due to the increased flexibility and load level.

The two previously mentioned ultimate load theories, plastic collapse and elastic instability, would each give a collapse load. However, unless a particular structure is either especially stubby to collapse plastically, or slender to buckle elastically, then the actual ultimate load behaviour is somewhere between these two extremes, and the value of the ultimate load is lower than that obtained by plastic or second order analysis. It is apparent that in order to establish the maximum load capacity, and hence an idea of the probability of reaching the ultimate limit state, a combination of the two theories is needed for many practical structures.

1.4.3 Second Order Elasto-Plastic Analysis

An incremental approach is a common method for combining second order and elasto-plastic analysis. The incremental forces and deflections due to a small increment, $d\lambda$, in load level, λ_1 are obtained using a tangent stiffness matrix. At each load level, the ratio of moment to plastic moment, M/M_p, is checked to determine the necessity of placing a

plastic hinge. The total response is then the sum of all the incremental responses. However, errors arise because the tangent stiffness matrix is approximate, hinges may not be placed at $M/M_p = 1$, and round off occurs due to a multitude of steps. These cumulative errors can be minimized by using a small $d\lambda$. This, however, becomes more expensive and does not assure convergence. This incremental approach is not adopted for this work. A simpler ultimate load analysis system is used which should require less computing time and certainly avoids any cumulative errors.

The system adopted is a simple combination of second order analysis, and hinge placement. A second order elasto-plastic response curve shown in Fig. 4 is similar to the first order elasto-plastic response curve shown in Fig. 3; the difference being the presence of arc segments

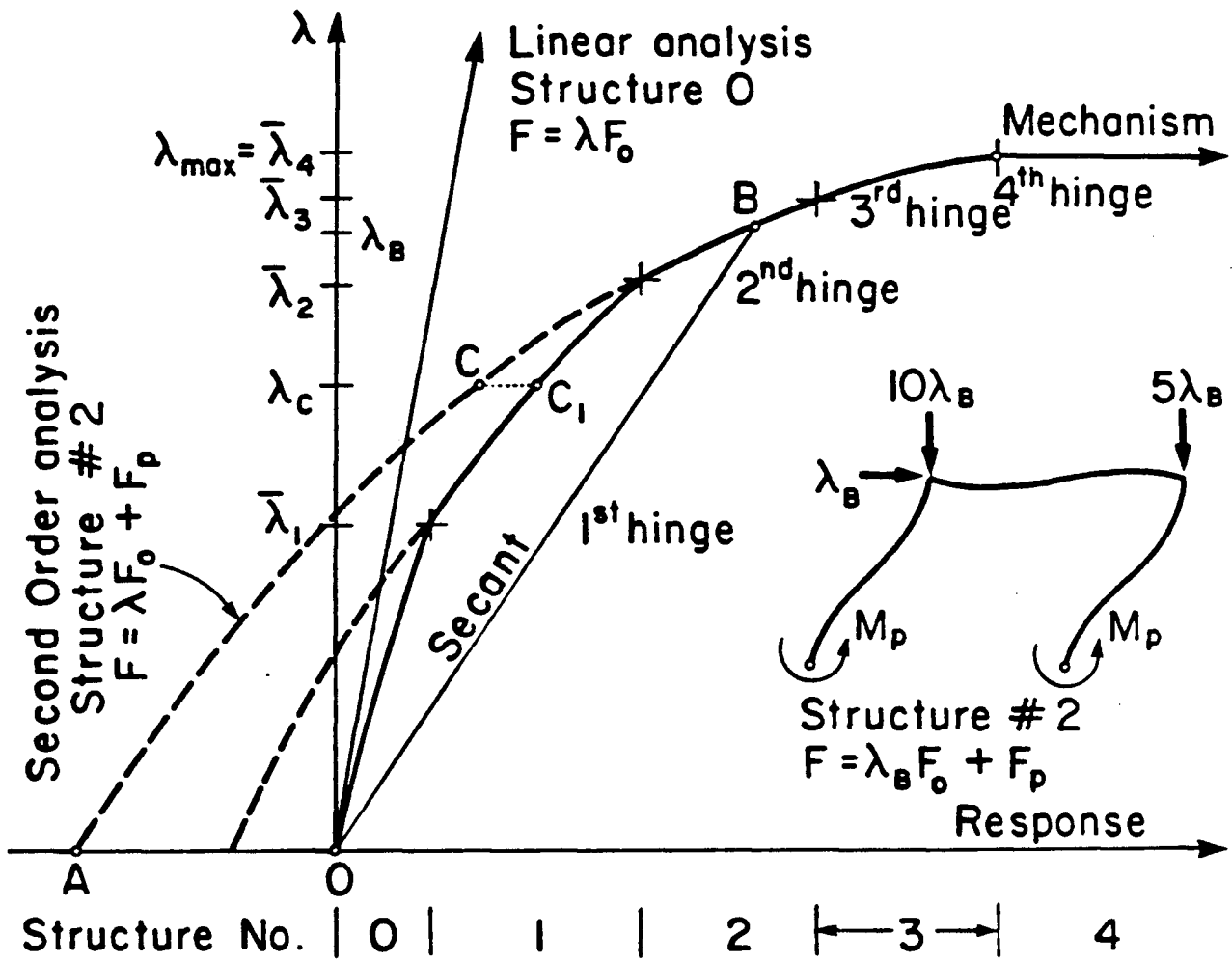

Fig. 4. Second Order Elasto-Plastic Response.

between hinge formations instead of linear facets. To determine the response at a certain load level, first order (linear) analysis is simply replaced by second order analysis, for each of the four structures.

To determine the response of the structure at load level λ_B, for example, it is not necesasry to methodically increment the load level and follow the arced segments from 0 to B. As long as the location of the hinge is known, in this case at the base of the frame, then all that is required is a second order analysis with the structure #2 loaded with $\lambda_B F_0$ and the plastic moments shown. The total response from zero load level to λ_B is along secant OB. Unlike the incremental approach, any errors due to placing a hinge when $M/M_p \neq 1$ is a local error and not cumulative, so that the response at higher load levels will not be affected.

1.4.4 Moment Axial Interaction

Consideration must now be given to the reduction of the plastic moment due to the presence of an axial load P in the member. To do this, the analyst must first decide on an appropriate yield surface for the cross-section being analyzed. The yield surface can be defined by a series of straight lines, and is described to the program by the intersections of the facets. By including only symmetrical sections, and hence the absolute value of the bending moment, only the top half of a yield surface need be considered.

The yield surface used throughout this work is shown in Fig. 5. It is a slight variation on CAN3-S16.1-M84. A plastic hinge forms when moments and axials becomes large enough to reach the yield surface. A parameter ϕ_i is defined for each facet i such that when the maximum $\phi_i = 1$, the yield surface has been reached and a hinge should be placed. The quantity ϕ_i is defined as follows:

$$\phi_i = m/b_i + p/a_i$$

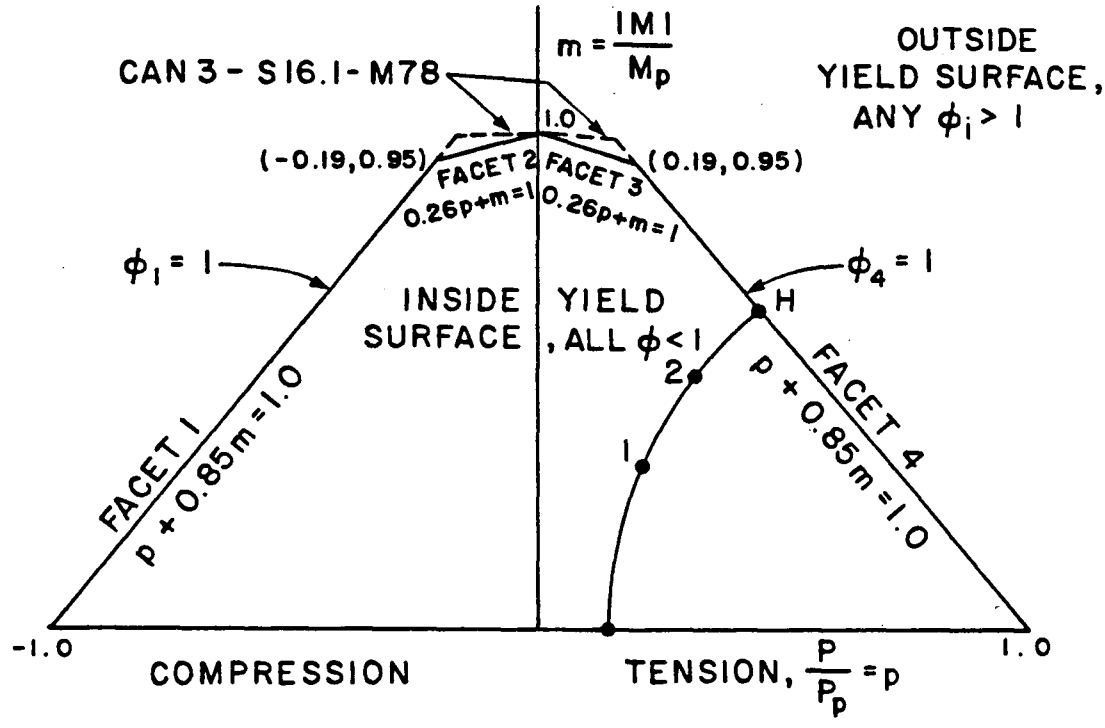

Fig. 5. Yield Surface

where $m = |M|/M_p$, $p = P/P_p = P/A\sigma_y$, and a_i and b_i are the intercepts of each facet with the p and m axis respectively.

Now the convenience of an interactive format becomes apparent. At each load level, once the second order convergence is obtained, a plot of the structure appears on the screen with a list of the five maximum ϕ_j values, where ϕ_j is the maximum of all ϕ_i for member end j. At a glance, the analyst can tell how close the structure is to forming a plastic hinge, and where this hinge will form. To facilitate the analyst's choice of load level, the program estimates the load level at which the next hinge should form. This is accomplished by extrapolating linearly from two known points inside the yield surface to the yield surface itself. The basic assumptions here are that line 1-2-H in Fig. 5 is straight and that p is linear with λ.

1.4.5 Moment Curvature

A perfect elasto-plastic behaviour is assumed for the analysis of fixed arches. Fig. 6 shows an idealized moment curvature relationship. A loss of bending stiffness in any section occurs from the first yield moment, M_y, to the plastic moment, M_p, as the cross-section becomes fully plastic. This, as well as the effect of residual stresses are neglected in this work. Chapter 2 will examine the consequences of these assumptions.

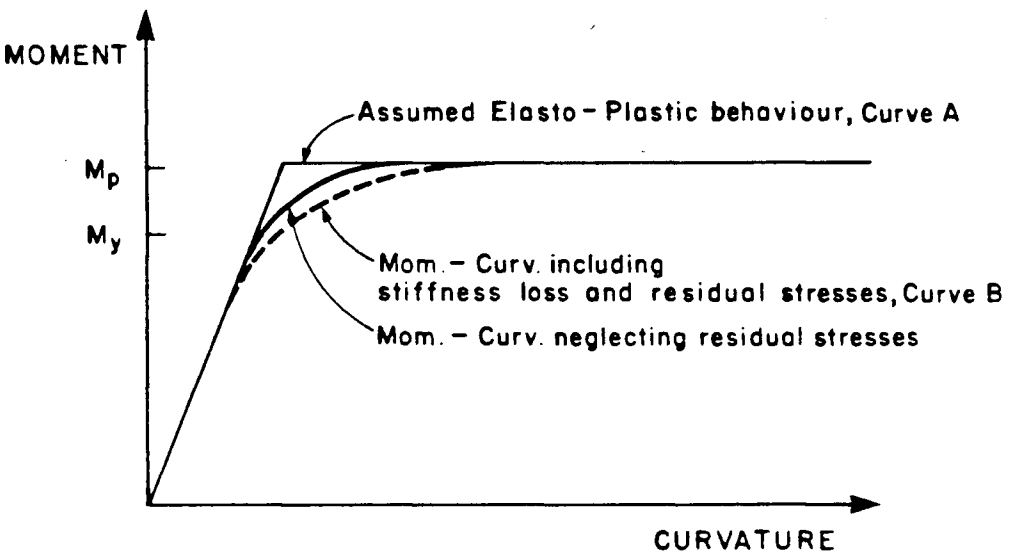

Fig. 6. Idealized Elasto-Plastic Behaviour.

The effect of neglecting stiffness loss and residual stresses is examined in Chapter 2.

1.4.6 Criteria for Reaching Ultimate Load

Ultimate load is defined here as the load level at which the second order elasto-plastic stiffness matrix K assembled in the ULA program becomes singular. This is accomplished by monitoring the determinant of K. A zero determinate implies a singular and unsolvable matrix. A negative definite stiffness matrix occurs when the determinant is negative,

and although an equilibrium solution is then possible, it corresponds to unstable equilibrium and will not be permitted.

Fig. 7 shows a beam-column bent in double curvature due to equal and opposite end eccentricities. The load-deflection curve shows diagrammatically the collapse criteria discussed above. The Choleski method used for the solution of the stiffness equations is only coded for real numbers. Because of this, the routine stops when $|K| = 0$ and signals an unstable structure.

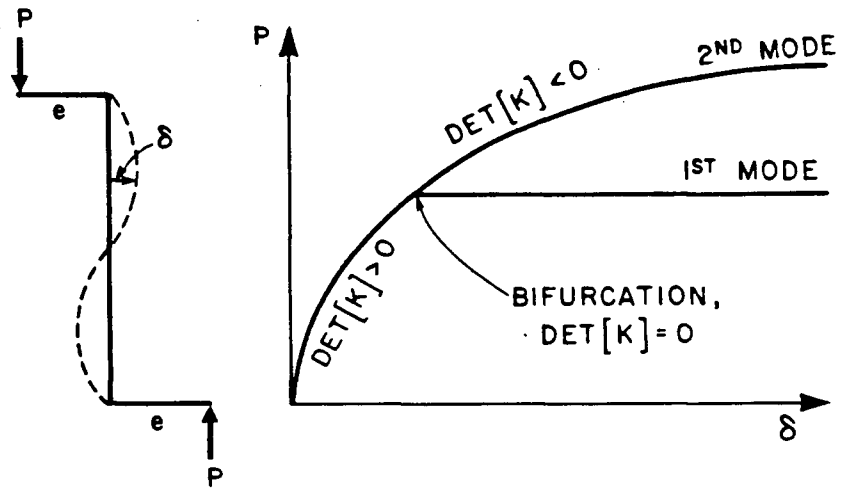

Fig. 7. Failure Criteria Applied to a Beam-Column in Double Curvature.

1.4.7 Interactive Graphic Display

Interactive graphic display helps the user in making necessary decisions such as the number of P-delta convergence cycles, hinge placement, and selection of the next load level. Of course, the standard displays such as member bending moments, axials, shears, and deflected shape, are available on command at any given load level. Other displays are available which give the analyst enlightened appreciation of how the structure is behaving. The first of these is a display of the yield

surface, as shown in Fig. 5. Superimposed on the yield surface is a trace of the m and p coordinates for each member end from load level to load level. This gives the analyst a quick and easy way of determining whether groups of members are behaving as bending members, compression or tension members, or some combination. The final feature is a display of the reserve capacity of each member. A self-explanatory example of this display is shown in Fig. 8.

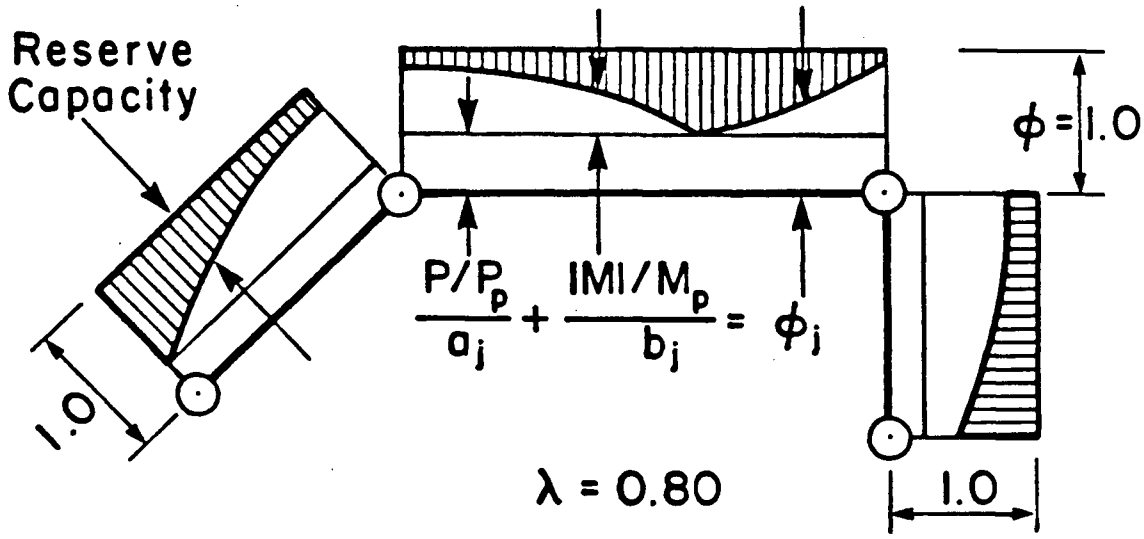

Fig. 8. Member Reserve Capacity.

The analyst can now determine at a glance how much of each cross-section is being used up by axial forces, or bending moments. It is also apparent where the next hinges should form, as the reserve capacities of the locations are approaching zero. Other features such as strain hardening and hinge closure are also available. The program ULA, with its interactive graphic format, gives the analyst a complete and quickly understood appreciation of how a particular structure is behaving with

increasing load level, and where it may need redesign or where material is not being used efficiently. It is this program that will be used to investigate the non-linear and ultimate behaviour of fixed arches.

CHAPTER 2

AN ECCENTRICALLY LOADED COLUMN

2.1 Governing Parameters

An arch and a column posess many similarities. They are both compression members subject to bending. A column bends when loaded eccentrically, and an arch bends when loaded unsymmetrically. Rather than start with the discussion of arches, the similar, more familiar, and simpler problem of eccentrically loaded columns will be considered. It is the intention of this chapter to develop an analytical solution for an eccentrically loaded column based on the same assumptions to be used for the ultimate load of arches as outlined in Section 1.4. This analytical solution will then be compared to an existing more exact solution and experimental results. An indication of error due to the original assumptions will be shown. Fig. 9 shows the eccentrically loaded column chosen for comparison.

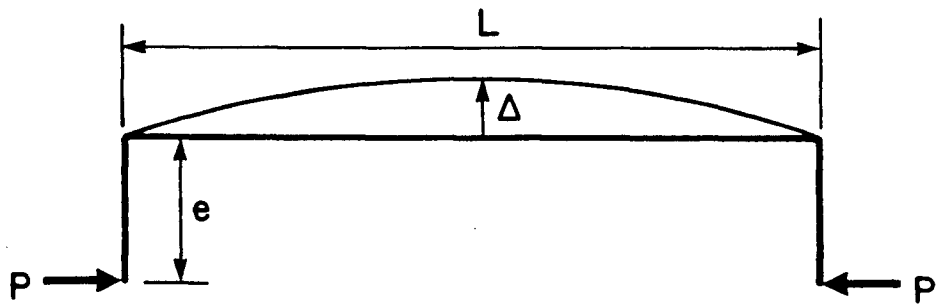

Fig. 9. An Eccentrically Loaded Column.

As outlined in Chapter 1, elasto-plastic material behaviour will be assumed neglecting strain hardening and residual stresses. The elasto-plastic assumption essentially means that moment curvature remain linear up to M_p. Neglecting the loss of stiffness between M_y and M_p produces a stiffer structure and a non-conservative result.

The ultimate column capacity P_u is a function of the following six parameters;

$$P_u = f\{e, L, EI, AE, P_p, M_p\} \tag{2.1}$$

where EI = linear elastic bending stiffness

AE = linear elastic axial stiffness

$P_p = A\sigma_y$

= maximum possible axial load with no moment present

and

$M_p = Z\sigma_y$

= maximum possible bending moment with no axial present.

With several independent parameters, it is convenient to use the Buckingham Π Theorem to reduce the number of parameters which govern the behaviour of the system. With seven parameters in Eq. (2.1) dependent on the two dimensions of force and length, only five dimensionless ratios are needed to describe the system as follows:

$$P_u/P_p = f\left\{\frac{e}{M_p/P_p}, \frac{L}{\sqrt{EI/AE}}, \frac{AE}{P_p}, \frac{M_p}{P_p\sqrt{EI/AE}}\right\} \tag{2.2}$$

The awkward parameters of Eq. (2.2) are chosen because they simplify into the more familiar ratios shown below;

$$P_u/P_p = f\{e/y,\ L/r,\ E/\sigma_y,\ y/r\} \tag{2.3}$$

where E = Young's modulus,

A = cross-section (area)

I = moment of inertia

$r = \sqrt{I/A} = \sqrt{EI/AE}$ = radius of gyration,

y = the distance from the centre of gravity of the symmetrical section to the centre of gravity of either the upper or lower half,

and σ_y = yield stress,

so that

$$AE/P_p = AE/A\sigma_y = E/\sigma_y,$$

$$\frac{L}{\sqrt{EI/AE}} = \frac{L}{r},$$

$$\frac{e}{M_p/P_p} = e/y$$

and

$$\frac{M_p}{P_p\sqrt{EI/AE}} = y/r$$

The maximum moment of the eccentrically loaded column of Fig. 9 occurs at the midspan. According to Timoshenko[3],

$$M_{max} = P(e + \Delta) = Pe \sec(kL/2) \qquad (2.4)$$

where

$$k^2 = P/EI$$

The column is determinate and will therefore fail once the hinge forms at the midspan. The plastic moment must be reduced in the presence of an axial load according to the yield surface of Fig. 5. To develop an analytical solution for the column capacity, we need an interaction equation. Facet 1 of Fig. 5 will be used as it is valid for $|M/M_p| <$ 0.95. Eq. (2.5) describes this interaction;

$$0.85\ M/M_p + P/P_p = 1 \qquad (2.5)$$

where $M_p = \sigma_y Ay = P_p y$

and $P_p = \sigma_y A$

Therefore:

$$M_{max} = Pe \sec \frac{kl}{2} = 1.18\ M_p\ (1 - P/P_p)$$

or

$$(1 - P/P_p) = 0.85\ (P/P_p)\ (e/y) \sec \frac{k\ell}{2} \qquad (2.6)$$

where $$\frac{k\ell}{2} = \sqrt{\frac{P}{EI}\frac{\ell}{2}} = \sqrt{\frac{P}{AE}\frac{\ell}{2r}} = \sqrt{\frac{P}{P_p}\frac{\sigma_y}{E}}\ \frac{\ell}{2r}$$

Eq. (2.6) becomes

$$P_u/P_p = \frac{1}{1 + 0.85\ e/y\ \sec\left(\sqrt{\frac{P}{P_p}\frac{\sigma_y}{E}}\ \frac{\ell}{2r}\right.} \qquad (2.7)$$

Eq. (2.7) is an analytical expression for column capacity under eccentric loading based on the same assumptions that will be used to analyse the ultimate capacity of arches.

2.2 Comparison of Analytical Equation with Correct Analysis and Experimental Results for a Particular Cross-Section

Galambos and Ketter[4] present dimensionless curves for the ultimate strength of a typical I-beam under axial load with equal end eccentricities causing bending in the strong direction. The fundamental difference between the derivation of Eq. 2.7 and the Galambos and Ketter approach is the assumed moment versus curvature relation. Galambos and Ketter use a correct relation like curve B of Fig. 6. In this thesis, the moment curvature relation is simplified by idealizing elasto-plastic behaviour, similar to curve A of Fig. 6.

The method used by Galambos and Keffer is based on numerically integrating values on a specific M-ϕ curve and iterating towards a correct deflected shape. Instability arises when the iterations do not converge. Because this method relies on a known moment-axial-curvature relation, which is unique for every different cross-section, a closed form solution is not available.

It is now possible to compare the results of Eq. 2.7 with Galambos and Ketter for a specific I-beam, namely a 3I5.7. The required moment-axial-curvature relation for this beam is shown in Fig. 10, based on an assumed residual stress pattern shown in Fig. 11. Of course, the

reduction of M_p due to the presence of axial in the derivation of Eq. 2.7 is handled by incorporating the yield surface of Fig. 5.

Fig. 12 is a dimensionless plot of an ultimate load parameter P_o/P_y versus slenderness L/r against an eccentricity parameter ec/r^2. The quantity c is measured from the centroid of the symmetric cross section to the outer fibre. The results according to the assumptions of this thesis, labelled "ULA" are clearly non-conservative compared to the more analytically correct results of Galambos and Ketter. The discrepancy is indicated by a shaded region and is as much as ten percent. Experimental results have also been included in the plot of Fig. 12 and appear to be bounded by the two analytical solutions.

It was necessary to make a slight modification to Eq. 2.7 in order to plot the ULA curve. The dimensionless parameter chosen by Galambos and Ketter to reflect eccentricity was ec/r^2. This differs from the ratio e/y used in Eq. 2.7 and it is a simple matter of arithmetic to transform from one to the other once the cross-section properties are known. In this case, $ec/r^2 = cy/r^2\ (e/y) = 0.85\ e/y$. Also, $E/\sigma y = 30{,}000/33 = 909$. Therefore, Eq. 2.7 becomes:

$$\frac{P_u}{P_p} = \frac{P_o}{P_y} + \frac{1}{1 + 0.73\ ec/r^2\ \sec\left(\sqrt{P/P_p}\ L/60.3\right)} \qquad (2.8)$$

It is Eq. 2.8 that is actually plotted on Fig. 12 and labelled "ULA".

An eccentrically loaded column is a determinate structure which fails after the formation of one plastic hinge. The purpose of the comparison presented in Fig. 12 was to extrapolate the results and make some judgement on the effect of idealizing behaviour as elasto-plastic on

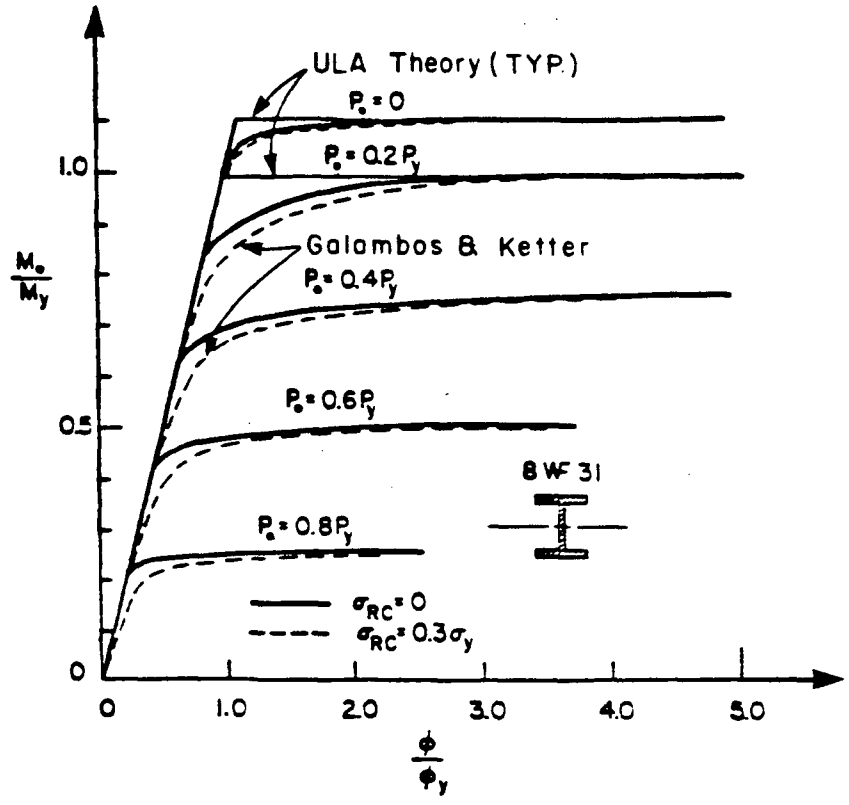

Fig. 10. Moment-Axial-Curvature Relation.

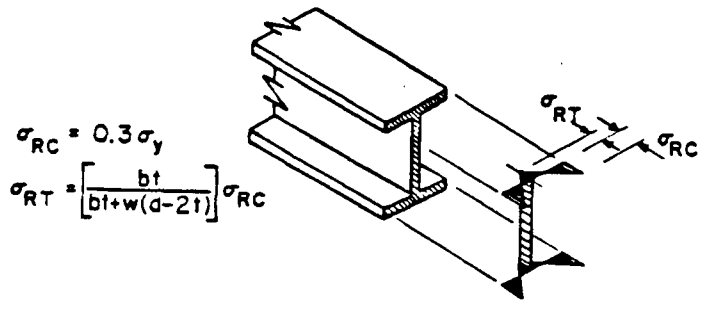

Fig. 11. Cooling Residual Stress Pattern Assumed by Galambos & Ketter.

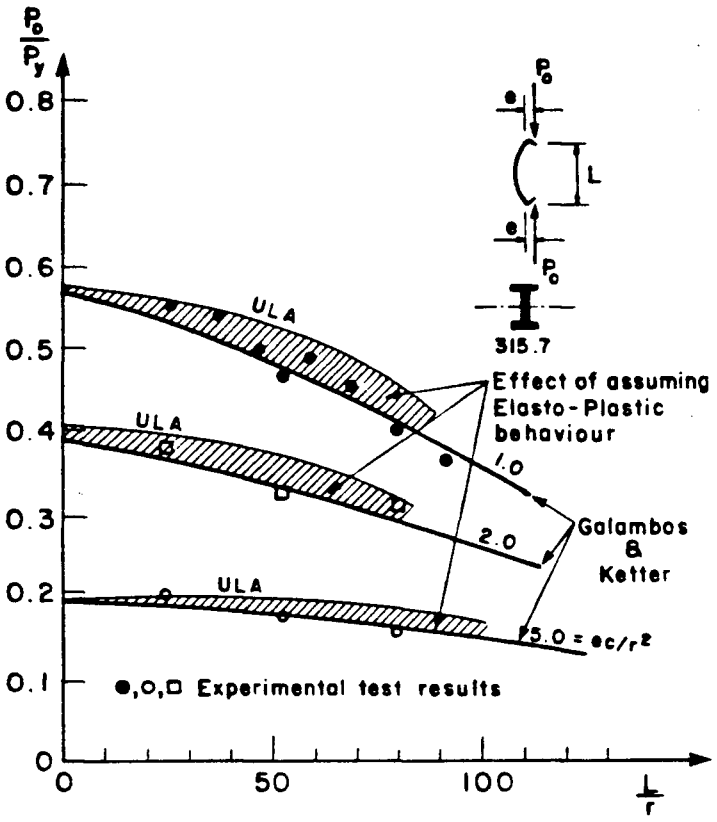

Fig. 12. Effect of Elasto-Plastic Assumption on Column Capacity.

the ultimate strength of fixed arches. A fixed arch is three times redundant. Most plastic hinges formed prior to collapse would already be in the plastic region where the moment-curvature behaviour (Fig. 10) levels out to constant M_p reduced only by the presence of axial forces. Any errors during the formation of plastic hinges prior to the last hinge are local errors, not cumulative, and do not effect the final result. Any non-conservatism should only occur in the last hinge formed. This is demonstrated qualitatively in Fig. 14. It is therefore proposed that the

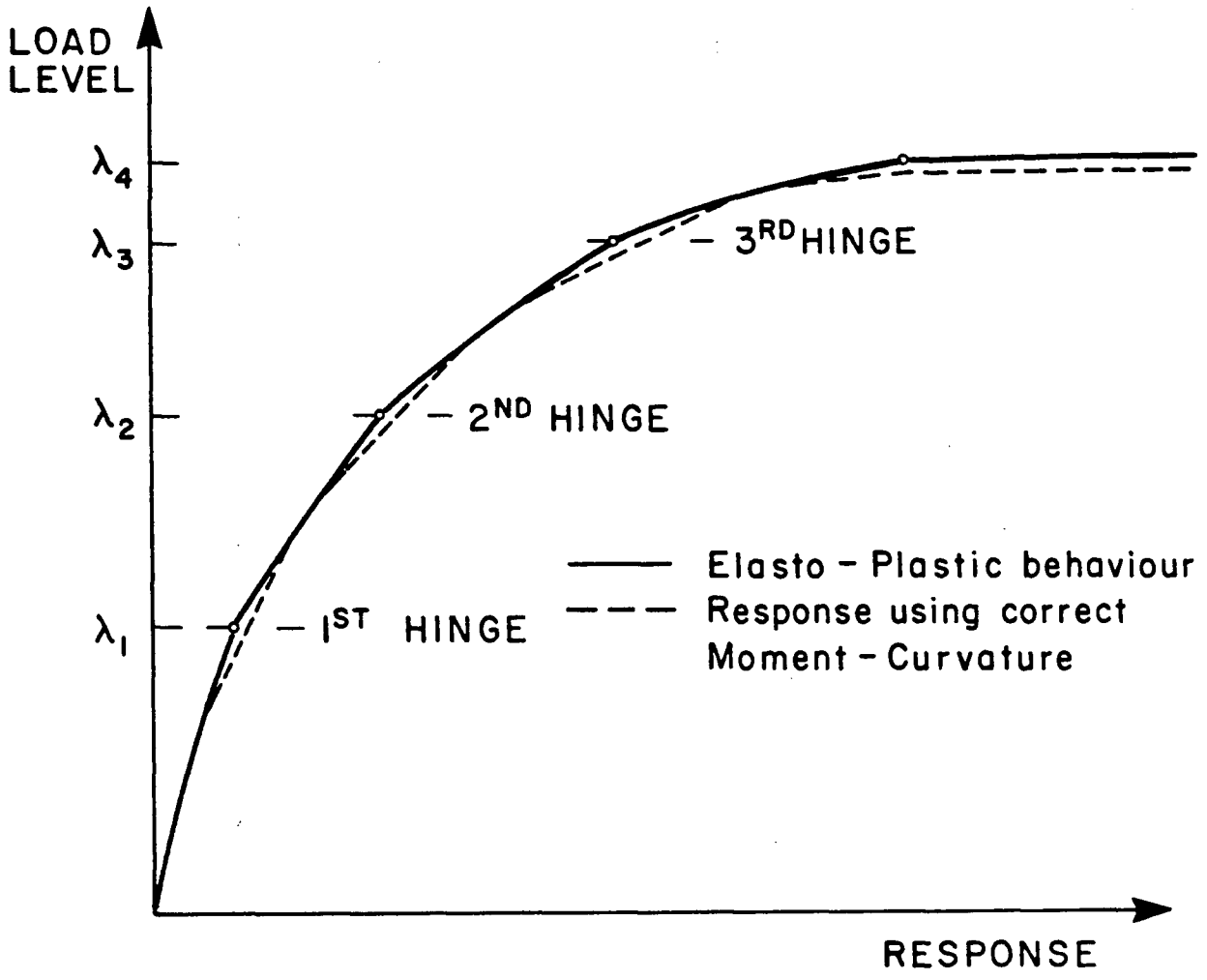

Fig. 14. Effect of Elasto-Plastic Assumption on a Typical Load-Response Curve.

effect of idealizing behaviour as elastic-plastic is not as significant in the case of fixed arched ribs as it is in the case of a beam-column and would therefore be appreciably less than ten percent. It is worth pointing out at this time that the beneficial effect of strain hardening is not considered here, and might serve to further eliminate any small non-conservatism.

The basic case of an eccentrically loaded column will now be expanded to the study of the ultimate strength of fixed arches.

CHAPTER 3

PRESENTATION AND DISCUSSION OF STANDARD ARCH BEHAVIOUR CURVES

3.1 Nonlinear Arch Behaviour

It is the object of this chapter to present the nonlinear behaviour of fixed arches. Because of the multitude of parameters governing arch action it will not be possible to describe all arches. Instead, the dimensionless behaviour of a standard arch will be given. In Chapter 5 the sensitivity of this standard to various parameter variations will be investigated.

3.1.1 Computer Model

Since ULA considers only straight members between nodes, the rib will be a polygon. This polygon was chosen to be twenty segments connecting twenty-one nodes because experience has shown that the difference between this and a continuous curve would be less than 1%. If the real arch really has twenty straight segments then of course the error in this model is zero. If, on the other hand, the real arch has say, four segments, then the error may be too large for practical applications.

Most arches are designed so that the dead load produces no moment except, perhaps, from rib shortening. The shape is then the moment diagram for dead load; a shape somewhere between a parabola and a catinary. The 21 nodes were placed on a parabola for this study together with 19 equal point loads so as to produce no moment under dead load except for rib shortening. Rib shortening is automatically included in a stiffness analysis and no attempt was made to factor it out. Arches

constructed so that dead load moment due to rib shortening is minimized will then have smaller moments than calculated with this model. In summary then, the model consisted of a twenty sided polygon with the nodes lying on a parabola.

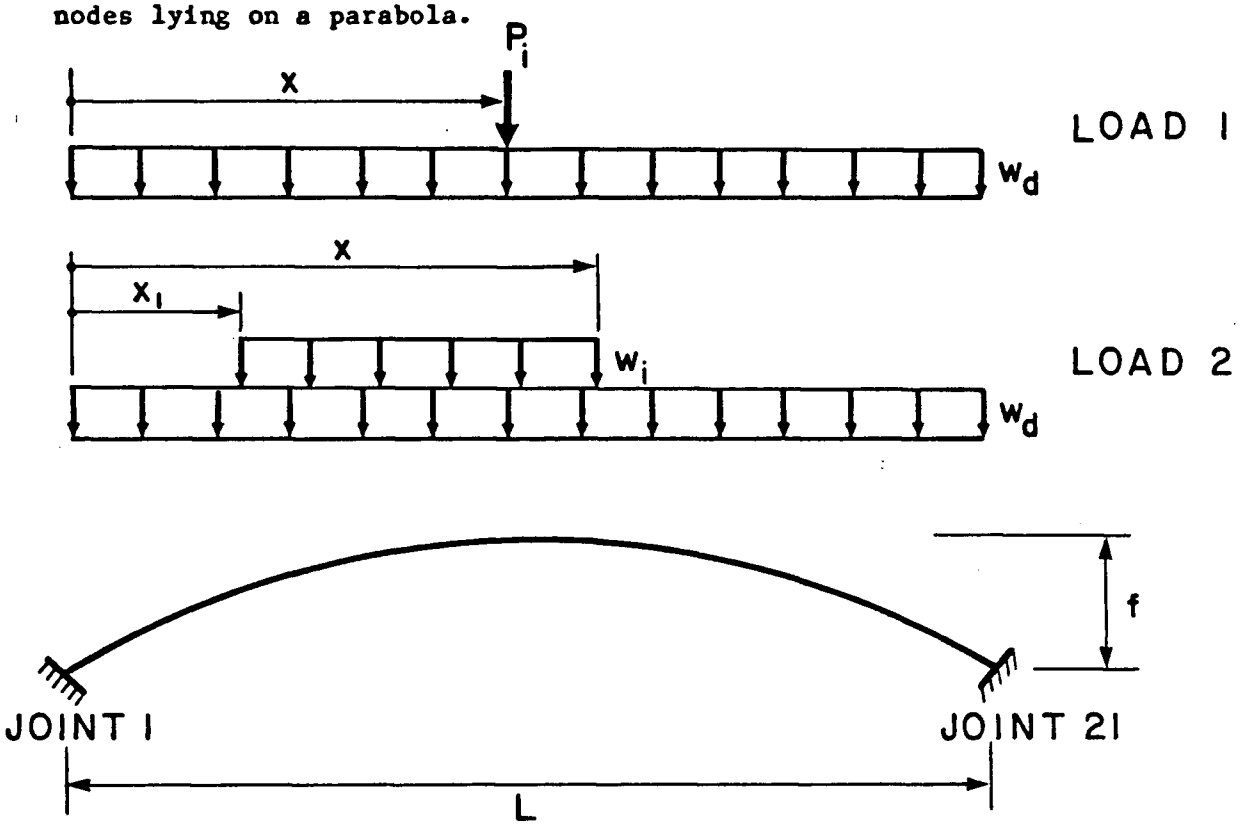

Fig. 16. Arch Loading.

Two load cases were considered to act on the model as shown in Fig. 16. Load one consists of the dead load plus w_d a point load P_i located x from the left end. Load two consists of a dead load w_d plus a live w_i on a loaded length of $x-x_1$. The distributed loads w_i and w_d were modelled as point loads at the polygon nodes in order to eliminate local bending on the straight segments.

The live load w_i or P_i was gradually increased in ULA with w_d held constant. The subscript i is used to denote the load at which specific events occured as follows:

w_e or P_e Load at which yield stress first occurred at some point on the rib

w_1 or P_1 Load at which first hinge formed

w_2 or P_2 Load at which second hinge formed

w_3 or P_3 Load at which third hinge formed

w_4 or P_4 Load at which fourth hinge formed

w_u or P_u is the ultimate load which may be any of the above loads as will be explained later.

Since the arch is three times redundant, up to four hinge will form before failure occurs. For very slender arches, the system may buckle as soon as the first hinge forms so that w_1 or P_1 is the ultimate load. For stocky arches, all four hinges will form before failure occurs as a mechanism so that w_4 and P_4 is the ultimate.

Each of w_i and P_i was minimized by varying x (and x_i). In general it was found that x_1 was zero and x for minimum load varied with i.

3.1.2 Governing Parameters

The load w_i or P_i is a function of nine parameters as follows:

$$w_i \text{ (or } P_i) = f[L, f, x, w_d, EI, AE, P_p, M_p, M_y]$$

where L = span

f = rise

w_d = dead load

EI = bending stiffness

AE = axial stiffness

$P_p = A\sigma_y$ = plastic axial load with no moment action

$M_p = A_y\sigma_y = z\sigma_y$ = plastic moment with no axial load action

$M_y = S\sigma_y$ = moment at which yield occurs with no axial

Since these ten parameters link only the two dimensions of force and length, the Buckingham Π theorem shows that only eight dimensionless parameters govern the system. The following eight are chosen for convenience:

$$\frac{w_i L^2}{M_p} \left(\text{or } \frac{P_i L}{M_p}\right) = f\left[\frac{f}{L}, \frac{x}{L}, \frac{L}{r}, \frac{y}{r}, \frac{z}{s}, \frac{E}{\sigma_y}, \frac{w_d L^2}{8fP_p}\right] \qquad (3.1)$$

The parameter Z/S will only effect the first yield condition and not hinge formation. The parameter $w_d L^2/8fP_p$ is chosen to represent, approximately, the fraction of axial capacity P_p used up by dead load thrust.

3.1.3 The Standard Arch

It is clearly impractical to evaluate numerically the dimensionless load of Eq. (3.1) as a function of seven independent parameters. It is practical though to define a standard, or average, or practical arch by assigning specific values to these seven parameters and then to run a sensitivity analysis to show their relative importance. Such a system will give the specific behaviour in a practical region and an indication of what might happen some distance from that region. In general though it will be necessary to run a full analysis for cases remote from this standard arch.

With the above in mind, four parameters were given specific values to define the standard arch as follows:

E/σ_y = 30,000 ksi / 40 ksi ≅ 210,000 MPa / 280 MPa = 750

f/L = 0.15

y/r = 0.95

Z/S = 1.15

An E/σ_y of 750 is definitely applicable to steel and close to concrete. Behaviour of other materials will come from the sensitivity analysis. An f/L of 0.15 has been used for many bridges but higher structures will be covered in the sensitivity analysis. A solid rectangular section has y/r = 0.866 while two flanges with no web has y/r = 1.00. The chosen y/r = 0.95 is then a reasonable value. The shape factor Z/S varies from 1.5 for a solid rectangle to 1.00 for two flanges with no web. The chosen value of 1.15 is then closer to a steel box or wide flange.

With x/L chosen so as to minimize the dimensionless load this leaves

$$\frac{w_i L^2}{M_p} \left(\text{or } \frac{P_i L}{M_p}\right) = f\left[\frac{L}{r}, \frac{w_d L^2}{8 f P_p}\right]$$

for the standard arch. A study of existing arches shows that

$$\alpha = w_d L^2 / 8 f P_p$$

ranges from near zero to approximately 0.2. It was decided to produce curves of

$$\frac{w_i L^2}{M_p} \left(\text{or } \frac{P_i L}{M_p}\right) = f\left(\frac{L}{r}\right) \quad \text{for } \alpha = 0,\ 0.1,\ 0.2$$

to give the behaviour of the standard arch.

Numerous runs on the Amdahl V8 of the UBC computing centre then defined the functions of Eq. (3.1) which are shown plotted in Figs. 17 through 24.

It should be noted that the parameter L/r involves the span length and not the classic "effective" length kL. For a fixed arch, the effective slenderness is given by $kL/r \cong 0.37\ L/r$.

3.1.4 Loading for Minimum Strength

Influence lines have been invaluable in the linear analysis of arches to determine the loading for maximum moment, thrust, stress, etc. They are of little use though with nonlinear behaviour because superposition is not applicable. For the case at hand it is necessary to numerically vary x_1/L and x/L to produce a minimum dimensionless load. This method was necessary for all w_i and P_i since x/L and x_1/L depend upon i.

3.1.5 Point Loading for Minimum Strength

To minimize P_iL/M_p it is only necessary to vary the one parameter x/L. Fig. 25 shows a typical variation of P_iL/M_p as a function of x/L for the standard arch with a given value of L/r. It is apparent from this behaviour that a single minimum exists for the ultimate load and all hinges formed after the first hinge. However, two local minima exist for the first yield and first hinge curves. These two minima arise because the first hinge may form at two different locations on the arch, each location corresponding to a different value of x/L. However, once the

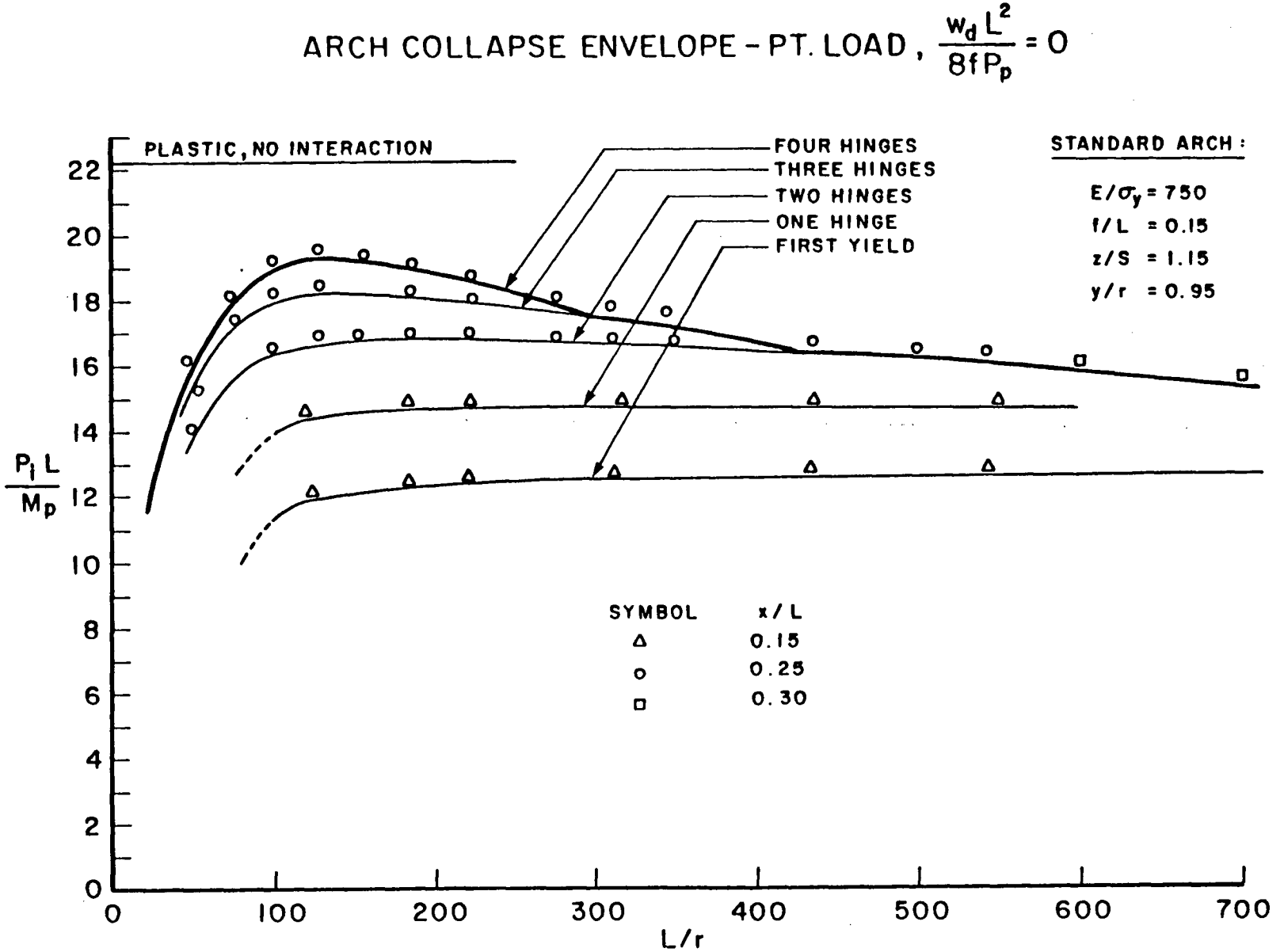

Fig. 17. Hinge Formation Curves and Collapse Envelope, Point Loading $\alpha = 0.0$.

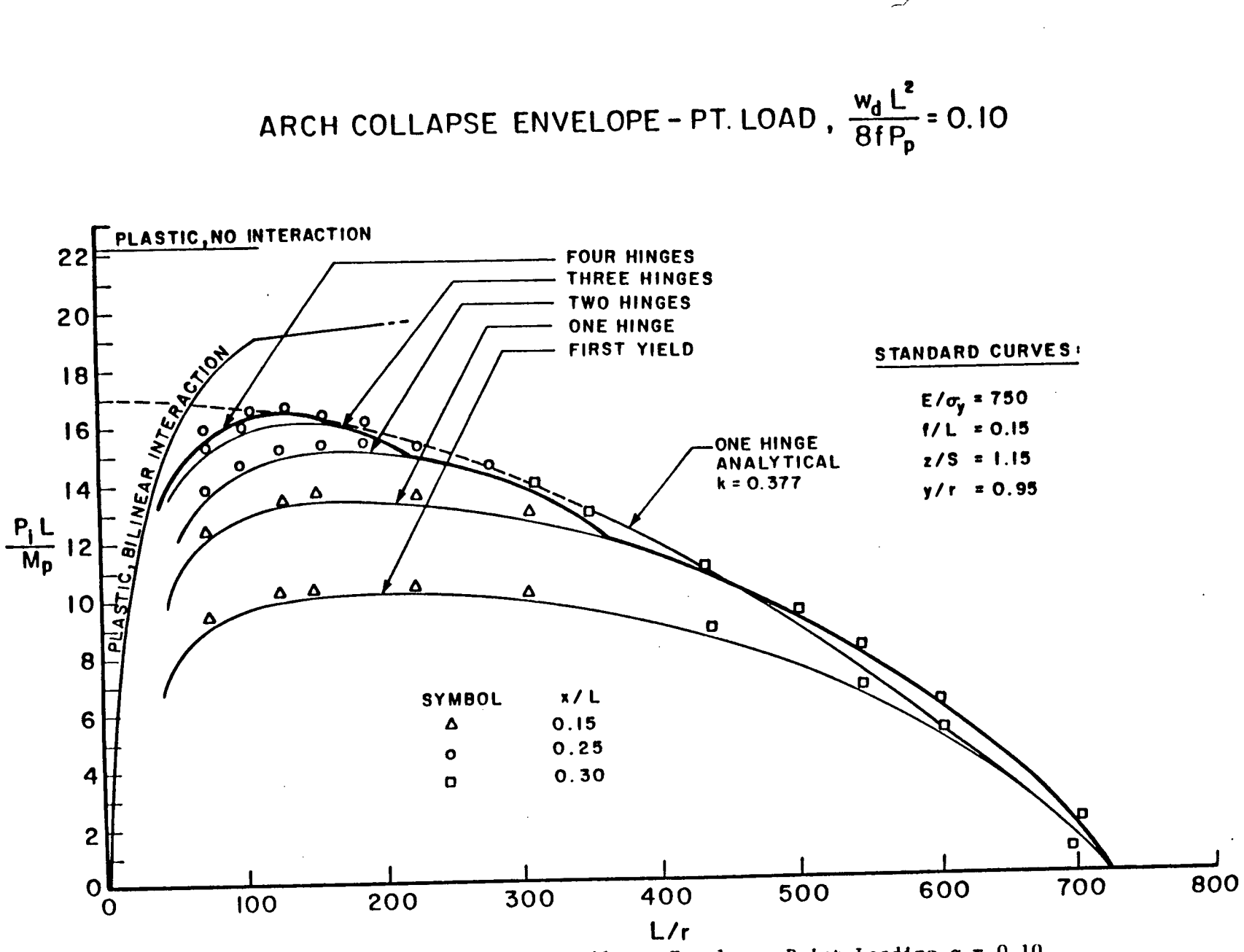

Fig. 18. Hinge Formation Curves and Collapse Envelope, Point Loading α = 0.10.

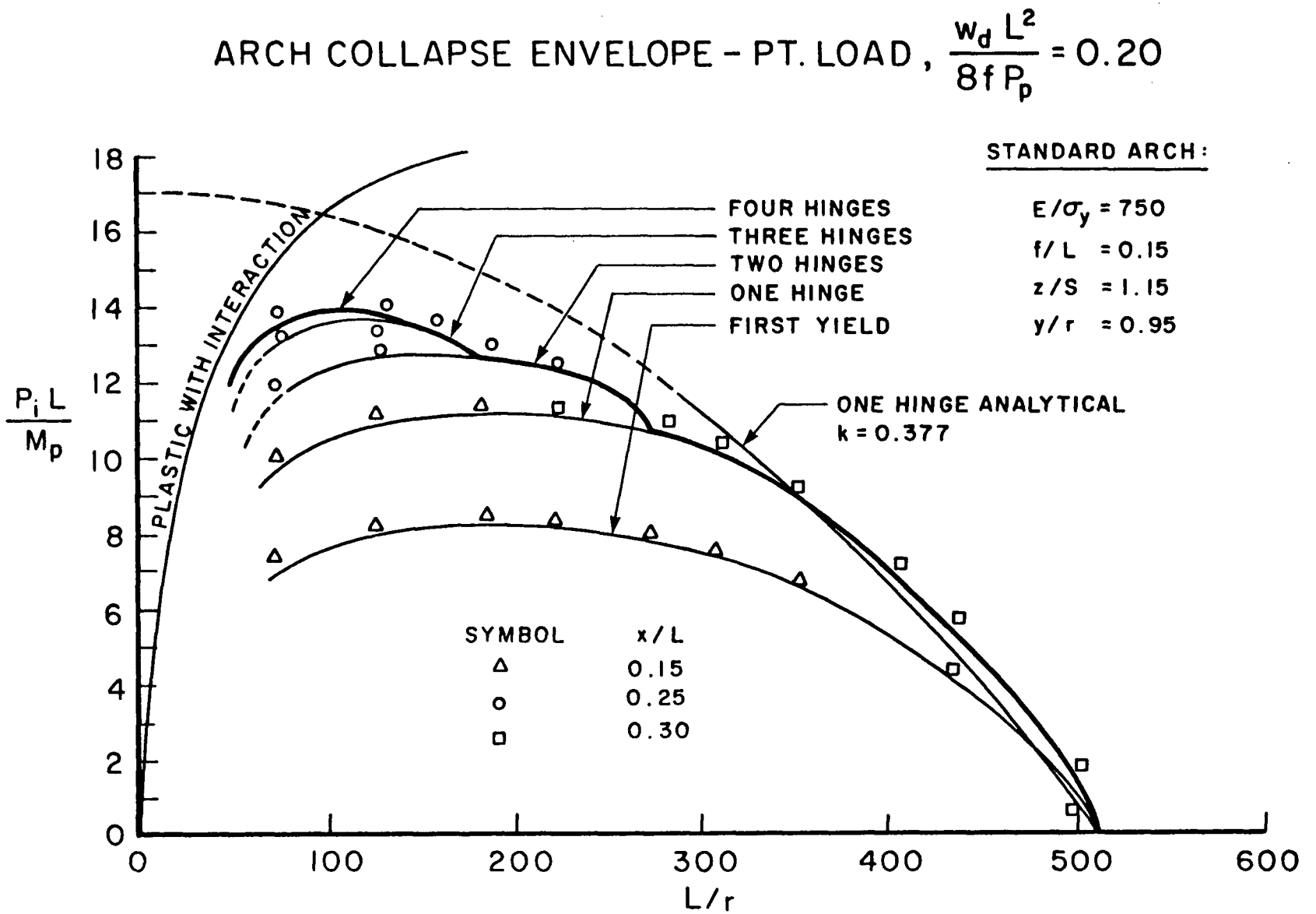

Fig. 19. Hinge Formation Curves and Collapse Envelope, Point Loading α = 0.20.

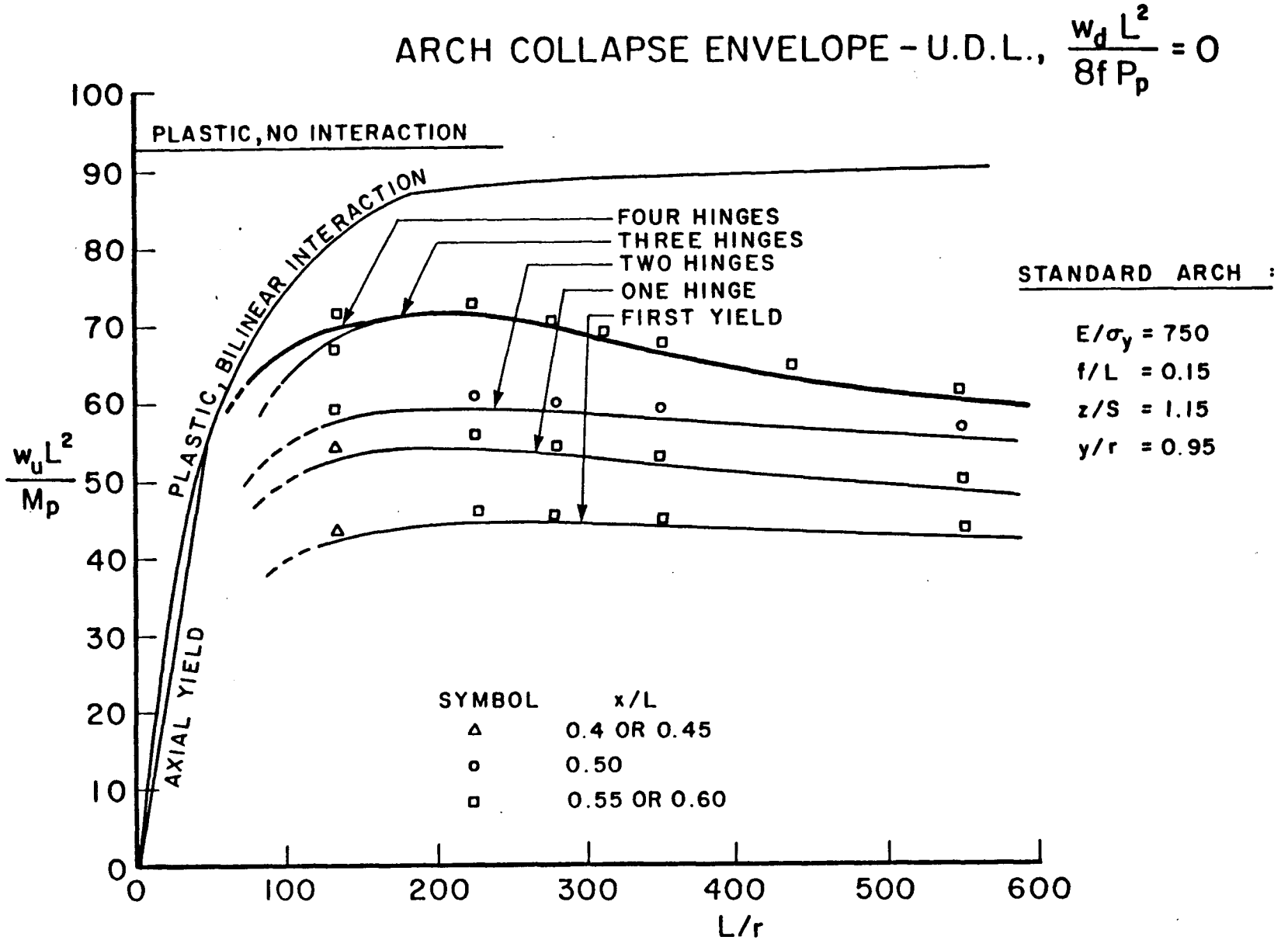

Fig. 20. Hinge Formation Curves and Collapse Envelope, Uniform Loading $\alpha = 0.0$.

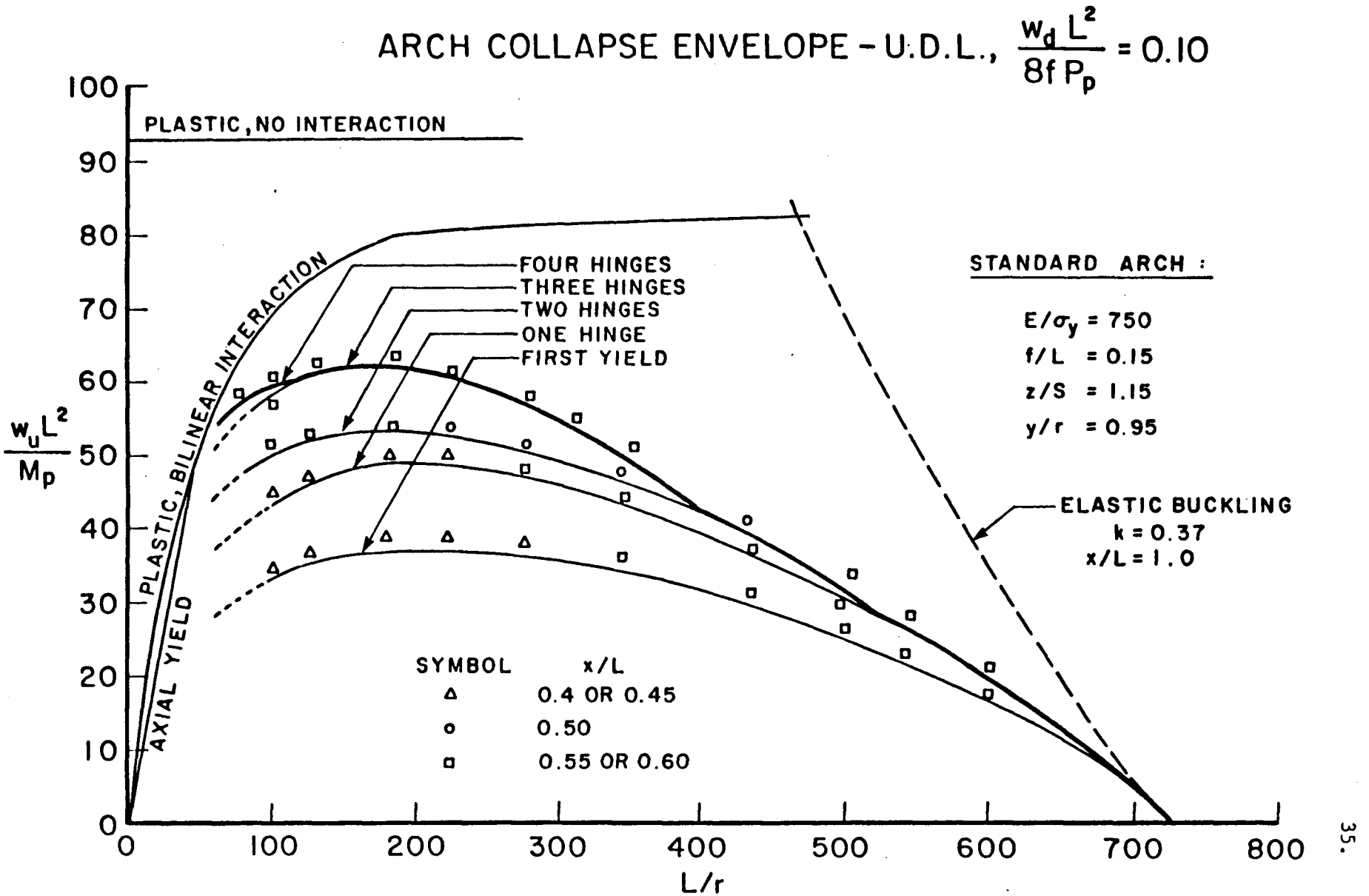

Fig. 21. Hinge Formation Curves and Collapse Envelope, Uniform Loading $\alpha = 0.10$.

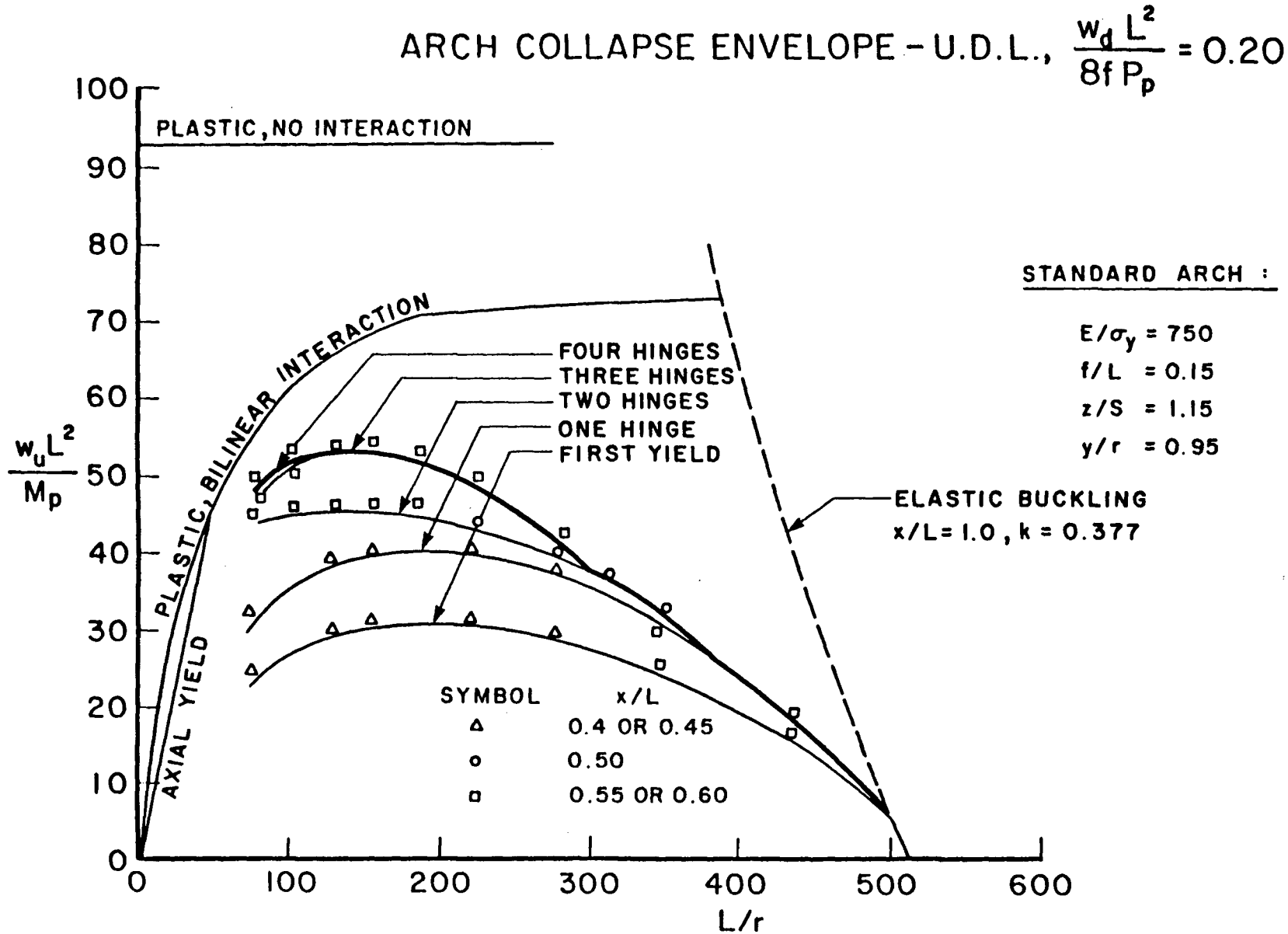

Fig. 22. Hinge Formation Curves and Collapse Envelope, Uniform Loading $\alpha = 0.20$.

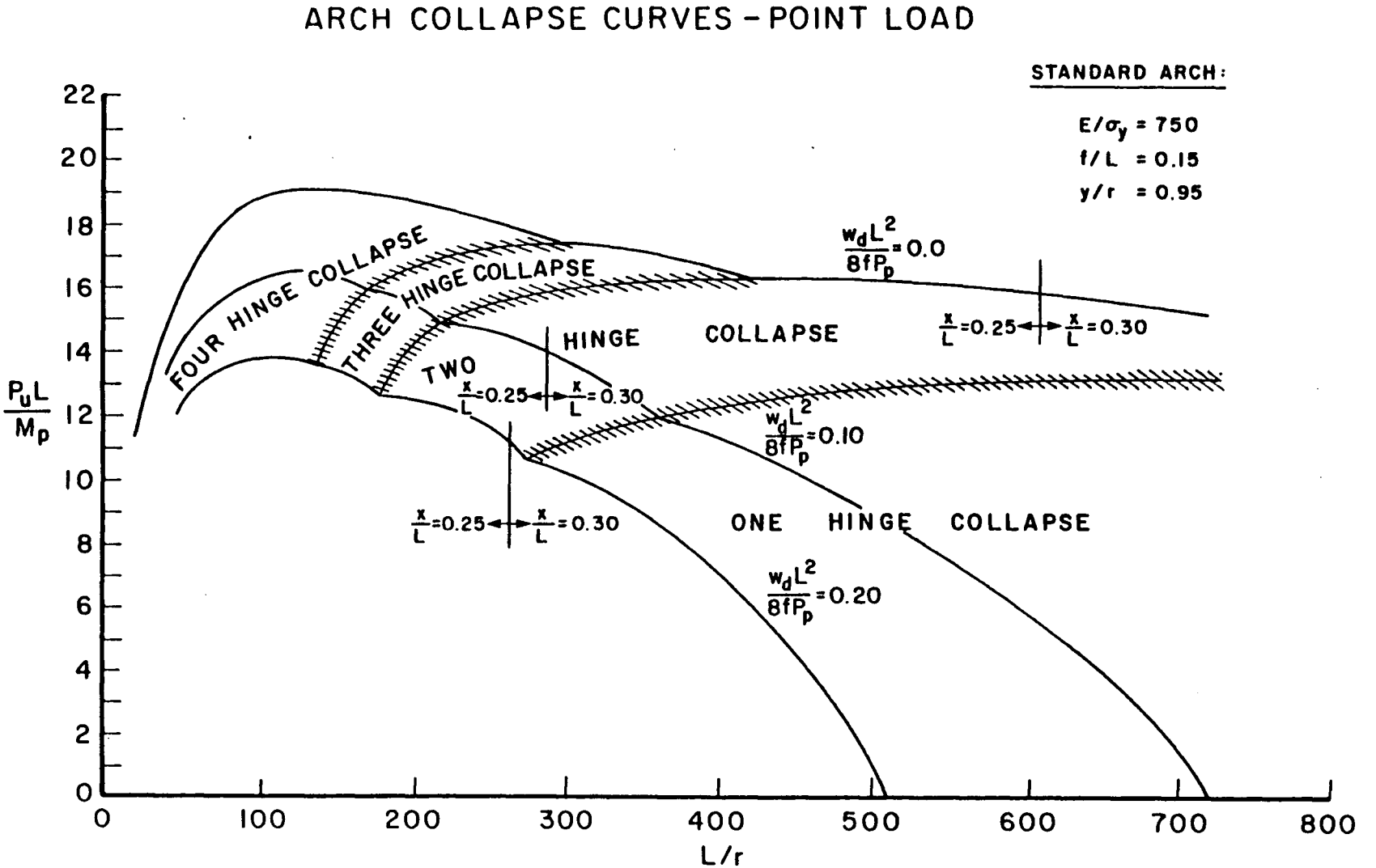

Fig. 23. Fixed Arch Collapse Envelopes, Point Loading.

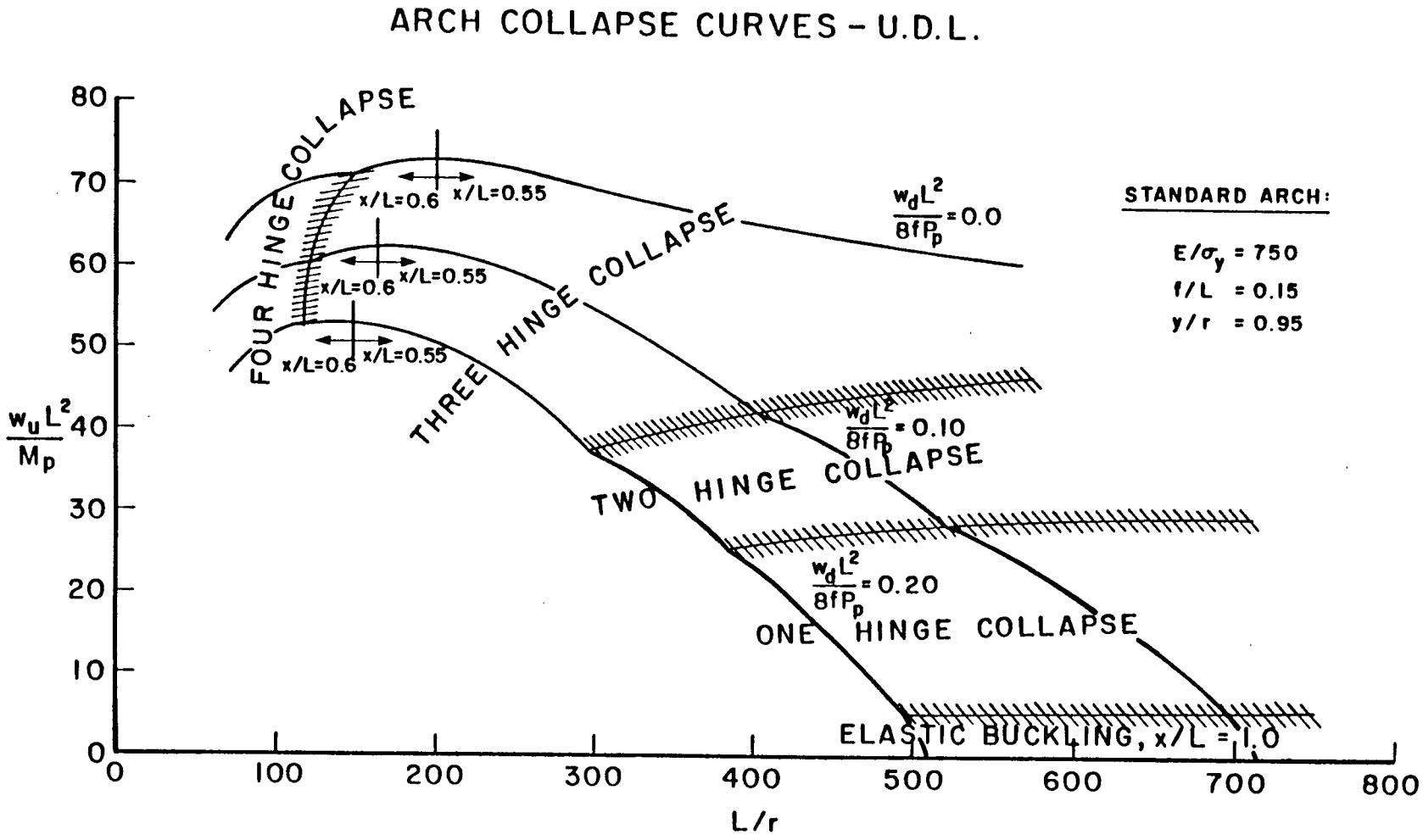

Fig. 24. Fixed Arch Collapse Envelopes, Uniform Loading.

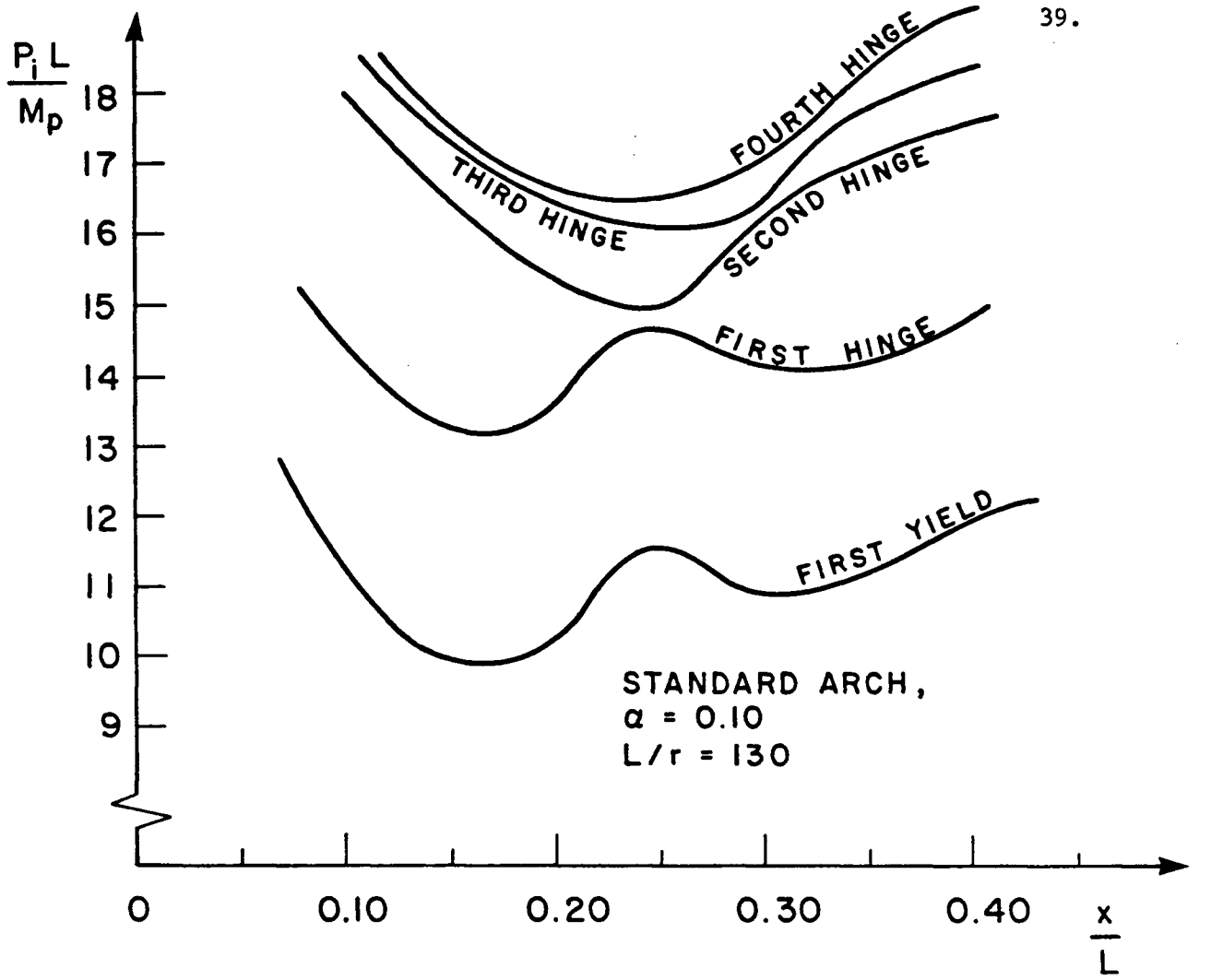

Fig. 25. Variation of Dimensionless Load Parameter with Load Location.

first hinge forms, there exists only one possible remaining location for each of the subsequent hinges, therefore, their behaviour yields a single minimum.

The first hinge forms either at the left haunch or at the location of the point load. If the first hinge forms at the left haunch, then the second hinge will always form at the location of the point load. If the first hinge forms at the location of the point load, then the second hinge will form at the left haunch. The third hinge forms at the right haunch and the fourth hinge forms at, or near the right quarter point.

This assumes of course that stability permits the formation of all the hinges. It was necessary to examine both local minima on the first yield and first hinge curves because either one may govern depending on the slenderness.

3.1.6 Unbalanced Uniform Loading for Minimum Strength

Two dimensionless parameters, x_1/L and x/L, are required to describe the location of the unbalanced uniform load. During preliminary analysis, it quickly became evident that the value of x_1/L required to load for minimum strength was zero. This means that a uniformly distributed load starting at the left haunch and extending part way along the span will minimize $w_i L^2/M_p$. This loading was used for all w_i so that only x/L needed variation to produce a minimum.

The behaviour of the load parameter $w_i L^2/M_p$ as a function of x/L is similar to that of the point load of Fig. 25. Two local minima exist for the first yield and first hinge conditions, and one unique minimum exists for each of the subsequent hinges. As before, once the first hinge forms, the location of each of the subsequent hinges is uniquely defined.

The first hinge forms at one of the haunches, depending on L/r. The second hinge will then always form at the opposite haunch. The third hinge forms near the right quarter point, and the fourth hinge forms near the left quarter point, assuming instability has not already occurred prior to the formation of any of these hinges.

As previously mentioned, the arch was discretized into twenty members. This means that the values of x/L for minimum strength for either the point loaded arch, or the uniformly loaded arch, could be

incorrect by as much as ±2 1/2%. This would result in only negligible errors in the minimum load parameters.

3.2 Discussion of Hinge Formation Curves and Collapse Envelopes

The standard arch behaviour curves of Figs. 17 to 24 are the fundamental results of this thesis. The curves are bounded by analytical solutions which will be derived in Chapter 4. It is the purpose of this segment of the work to discuss the collapse envelopes and the hinge formation curves themselves. The discussion will include a summary of arch behaviour by regions on the plots.

3.2.1 Collapse Envelopes

The curve which defines the ultimate load as a function of L/r is actually an envelope of the hinge formation curves, Figs. 17 to 23.

Once the hinge formation curves are plotted, and the collapse envelope generated, the results can be summarized on a separate graph showing the collapse envelopes only. Two such plots are required; one for the point loaded arch, Fig. 23, and one for the uniformly loaded arch, Fig. 24. These graphs of $P_u L/M_p$ or $w_u L^2/M_p$ versus L/r each show three collapse envelopes corresponding to α = 0.0, 0.10, and 0.20.

As expected, there are five different types of collapse; elastic buckling, and one, two, three, or four hinge collapse. The governing collapse mechanism for the standard arches examined is dependent on the slenderness L/r, and the dead load ratio α. This gives rise to regions on the arch collapse curves of Figs. 23 and 24 corresponding to the different mechanisms of collapse.

3.2.2 Effect of L/r on Type of Collapse

It is of no surprise by now that less hinges are required for collapse with increasing slenderness. On any given collapse envelope, the value of L/r which marks the transition from one type of failure to another is clearly visible by a cusp in the curve. The cusp is actually the end of a hinge formation curve. For example, the transition between three hinge failure and two hinge failure is the end of the third hinge formation curve. For any value of slenderness beyond this point, the formation of a third hinge is not possible because loss of stiffness causes instability to occur before the third hinge has a chance to form.

The effect of L/r can be summarized by contrasting the failure modes at low L/r and high L/r. A four hinge plastic collapse mechanism as dictated by classical plastic theory occurs only at low L/r where second order effects are minimial. The opposite occurs at high L/r where second order effects are prevalent and failure is instigated by the loss of stiffness due to the formation of the first hinge or complete elastic buckling.

3.2.3 Effect of Dead Load on Type of Collapse

Having discussed the effect of slenderness on the type of collapse, it remains to discuss how and why the dead load ratio α influences the mode of collapse. The values of slenderness marking the transition between two different collapse mechanisms will be termed $(L/r)_{trans}$.

The ratio α is the only parameter which contains the dead load w_d. Any increase in dead load would increase the dead load thrust and hence increase any second order effects. It is therefore correct to conclude that the collapse curves corresponding to higher values of α are

influenced more by second order effect. Therefore, it is not surprising that P_i and w_i decrease with increasing α.

The dead load also effects the value of $(L/r)_{trans}$ marking the location of a cusp. There must exist some values of L/r for which a lower value of α would permit an additional hinge to form due to a lessening of the second order effect. A typical segment of two superimposed collapse envelopes is shown in Fig. 29 to show qualitatively the range of L/r for which two different types of collapse are prevalent. Because the range of L/r described by Fig. 29 must exist, $(L/r)_{trans}$ must be lower for higher values of α.

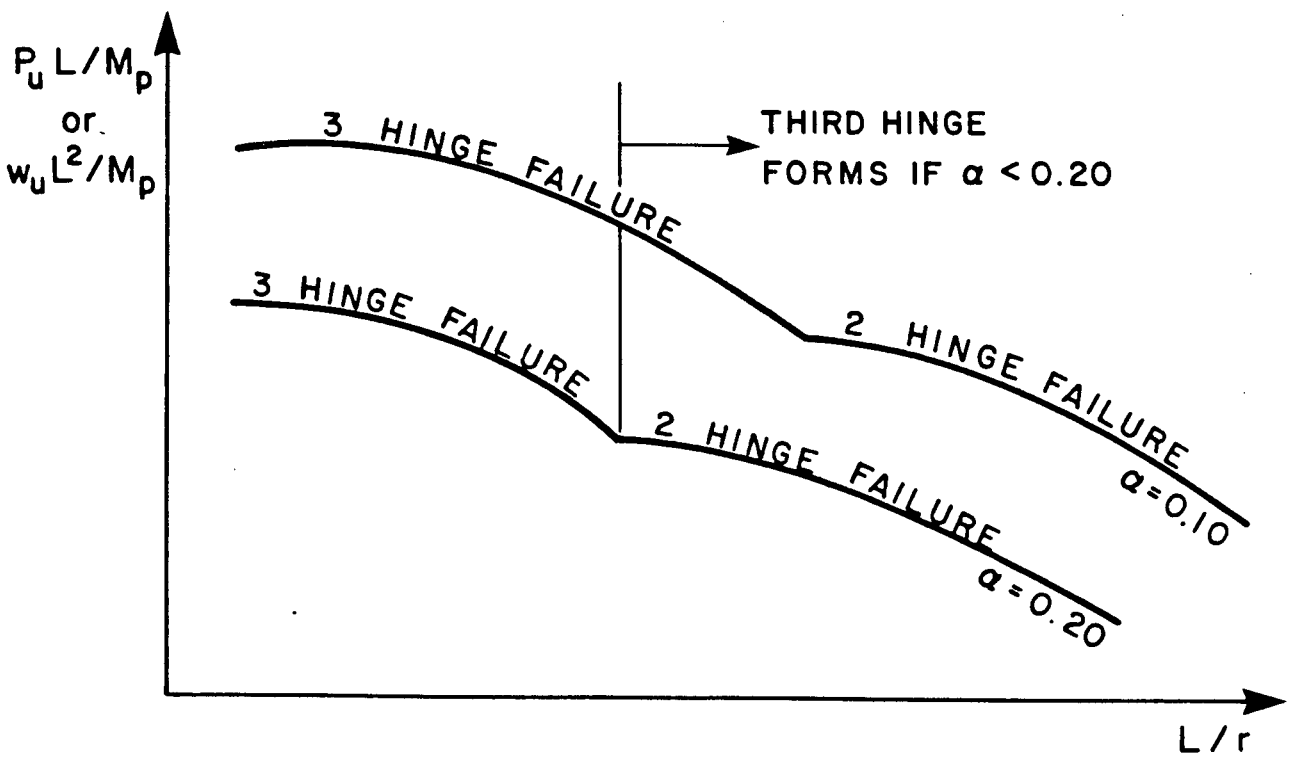

Fig. 29. Variation of $(L/r)_{trans}$.

3.2.4 Elastic Buckling and the Limiting Slenderness Ratio

Examining Figs. 23 and 24, it is apparent that the collapse envelopes cross the horizontal axis where the live load is zero. At this point, the dead load alone is sufficient to cause elastic buckling. Theoretically, this is the maximum possible slenderness for a given dead load ratio α, and is referred to as the slenderness limit. Figs. 23 and 24 also show that the behaviour of arches just prior to reaching this slenderness limit is different for the point loaded arch than for the uniformly loaded arch and so each will be discussed separately.

Nowhere on the point load collapse curve, Fig. 23, does elastic buckling govern the ultimate load except in the limit as P approaches zero where the dead load alone causes elastic buckling. Under uniform loading, the region of elastic buckling is very small. In this region $x/L = 1.0$, which means the live load was applied over the entire span of the standard arch. The uniform load w required to cause elastic buckling was smaller than the half span load required to form the first hinge. This elastic buckling region is so close to the theoretical slenderness limit, where the live load to dead load ratio becomes zero that it is impractical and likely impossible to attain.

In summary, in-plane elastic buckling of a fixed arch will rarely, if ever, govern design.

3.2.5 Critical Loading Pattern, x/L Results

Indicated on all the hinge formation curves is the value of x/L which minimized the dimensionless load. These are shown by the use of symbols plotted slightly above the actual data points for clarity. The results for the ultimate load for each loading condition are reasonably

consistent. In general, the non-linear behaviour dictates that loading 55 to 60 percent of the span governs for the ultimate capacity of a uniformly loaded arch, and placing the point load at x/L = 0.25 or 0.30 governs for a point loaded arch.

There are two distinct values of x/L governing first yield and the formation of the first hinge. This was expected because, as previously explained, when either load parameter is plotted as a function of x/L only, two local minima arise, each corresponding to different first hinge locations. However, it remains to explain why one local minima governs for low L/r, and the other for higher L/r.

Under uniform loading, the first hinge (and first yield) curves show a definite transition from x/L = 0.4, corresponding to a hinge forming at the left haunch, to x/L = 0.6, corresponding to a hinge forming at the right haunch. To explain this phenomena, it is necessary to define a moment due to rib shortening, M_{rs}, and a second order amplification factor ϕ. Two separate cases will be examined, a stubby arch with L/r approaching zero and a very slender arch with high L/r. Fig. 27 shows the approximate haunch moments in a stubby arch loaded with 40% and then 60% of full live load. The maximum haunch moment caused by the unbalanced uniform live load w alone is given the symbol M_w. The opposite haunch moment is less than M_w and is arbitrarily taken as 0.75 M_w to emphasize the difference. Simple superposition says that the left haunch moment with x/L = 0.4 and the right haunch moment with x/L = 0.6 are equal, however this excludes the effect of rib shortening. It is important to note that M_{rs} acts to increase the left haunch moment, but decrease the right haunch moment. This explains why the total moment at joint 1 with x/L = 0.4 is the largest, thus allowing the first hinge to

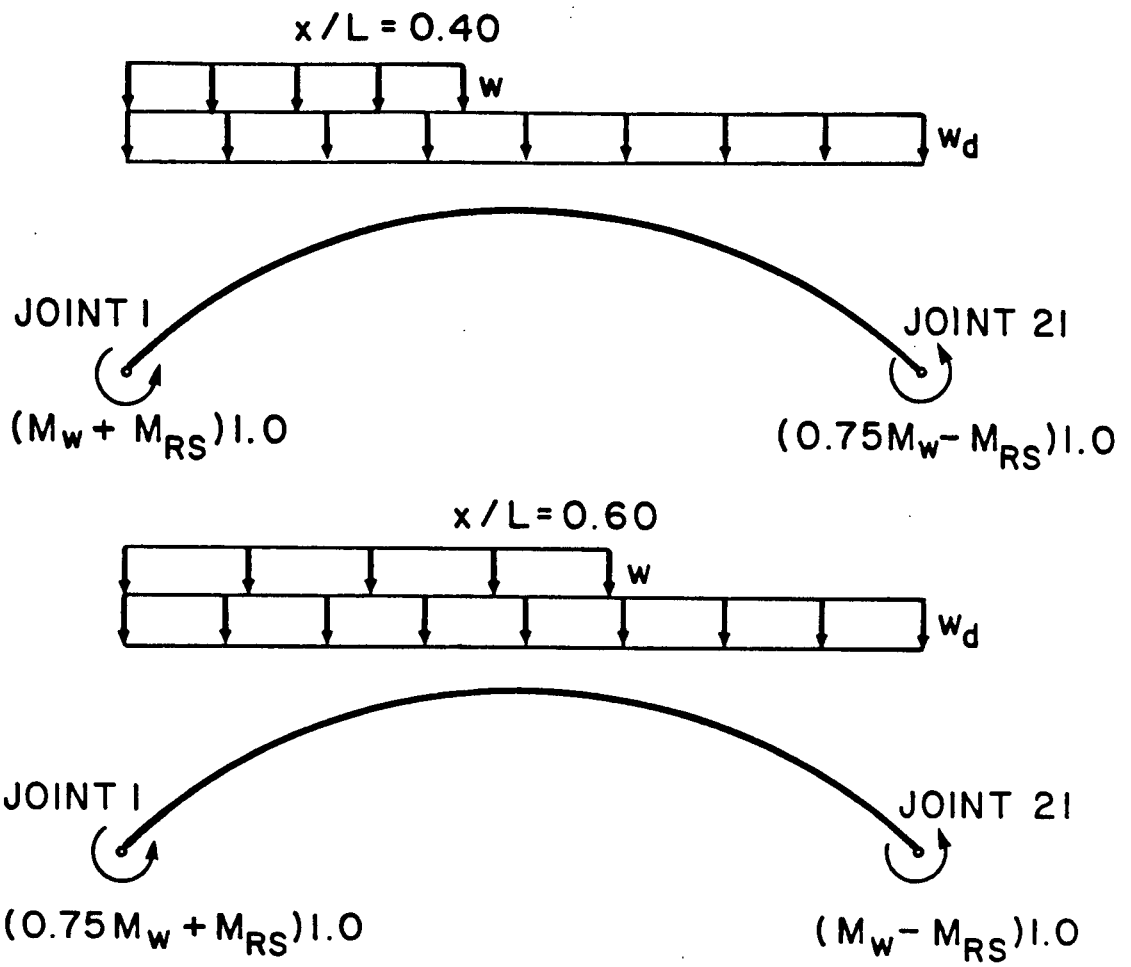

Fig. 27. Stubby Arches, No Second Order Amplification, ϕ = 1.0.

form there at low L/r.

Fig. 28 shows the haunch moments of two slender arches loaded by 40% and 60% of full live load respectively. The moment due to rib shortening becomes insignificant at large L/r because the ratio M_{rs}/M_w varies inversely with L/r. For large L/r, the second order effect now overshadows any effect of rib shortening. The maximum joint 1 moment is $\phi_1 M_w$. The maximum joint 21 moment is $\phi_2 M_w$. The second order magnification

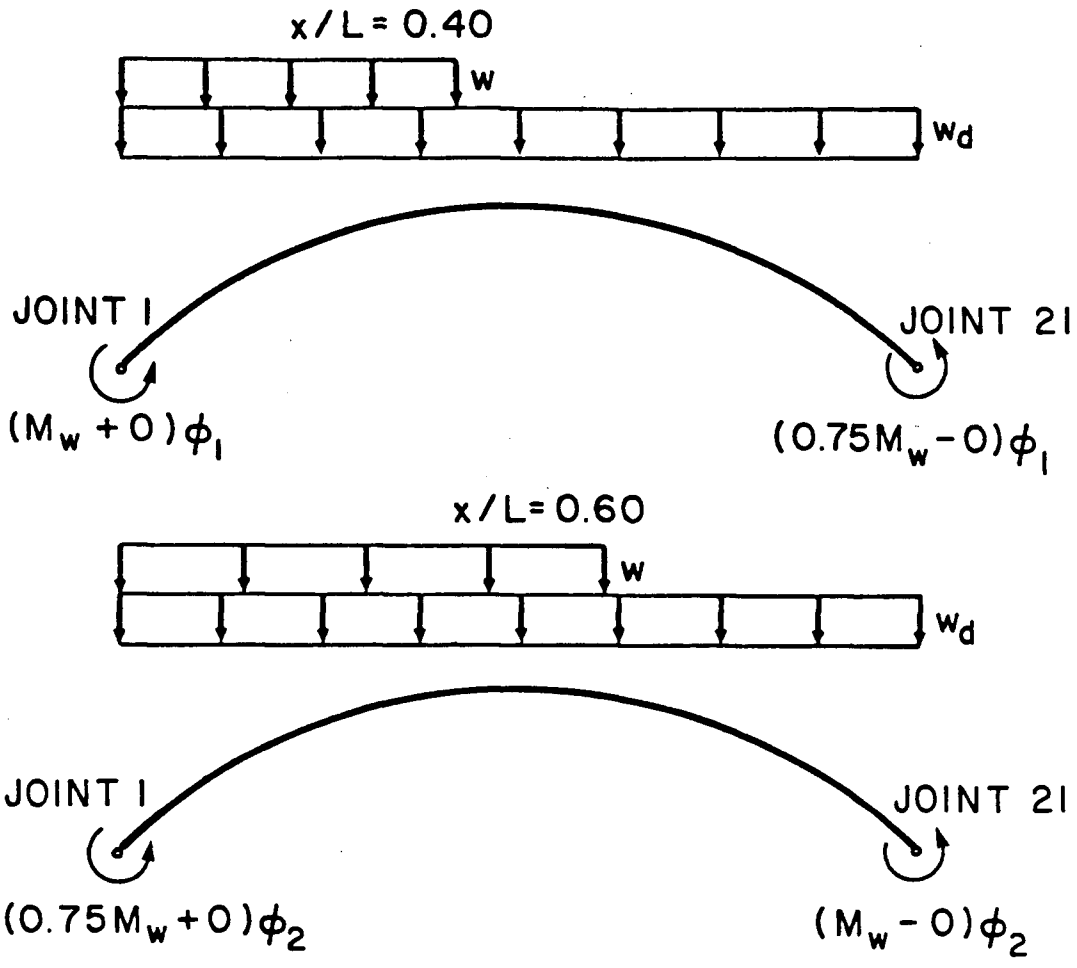

Fig. 28. Haunch Moments in Slender Arches.

60% loaded than for a load over only 40% of the span. Therefore, ϕ_2 is greater than ϕ_1 and the moment at joint 21 with x/L = 0.6 is the largest. For slender arches, the first hinge will form at the right haunch, joint 21, with the span 60% loaded.

A similar phenomenon arises when an arch is loaded by a point load. Lower L/r implies that x/L = 0.15 and the first hinge forms at the left haunch. At higher L/r, the first hinge forms with x/L = 0.30 at the location of the point load. Thus, the reason for this is similar to the explanation given for a uniform loading and will not be repeated.

In this chapter, the main results of this thesis were presented in the form of hinge formation curves and collapse envelopes, Figs. 17 through 22. Conventional analytical solutions for ultimate load are plotted on these figures as analytical bounds to the results generated. It remains to derive these bounds and to discuss any discrepancies between the collapse curves and the analytical solutions. The following chapter will accomplish this.

CHAPTER 4

ANALYTICAL BOUNDS

The fixed arch collapse curves were presented and discussed in Chapter 3. Analytical bounds were also plotted to served as reference. It is the aim of this chapter to derive these analytical solutions based on traditional analysis and to compare these to the collapse envelopes.

The analytical solutions serve as bounds at low L/r and high L/r. At low L/r, the ultimate load approaches that for a four hinge plastic collapse mechanism. The analytical solution is therefore based on conventional plastic analysis with no second order effects. At high L/r, the point loaded arch is bounded by one hinge collapse, and the uniformly loaded arch by elastic buckling.

4.1 Analytical Bounds for Low L/r

Two solutions will be derived for each of the two loading cases. The first solution will neglect the effect of any reduction of M_p due to the presence of axial force, and the second solution will include this axial reduction of M_p. In both cases, no second order magnification is considered.

4.1.1 Low L/r; Neglecting Axial Reduction of M_p

The point loaded arch will be examined first. The point load is placed at the left quarter point. This is a reasonable assumption and is confirmed by the results of Chapter 3 which indicated that x/L = 0.25 at low L/r. Fig. 30 shows three free body diagrams. One diagram of a parabolic arch under dead load and a point live load, the second of the left

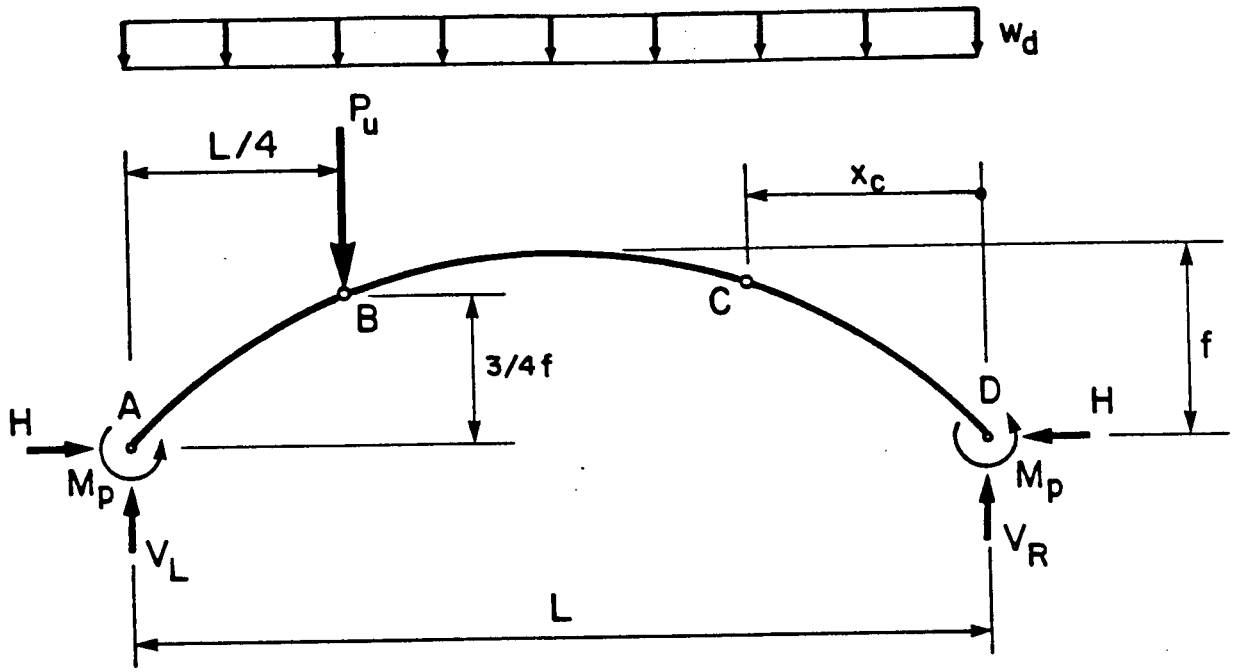

F.B.D. #1 - Full Arch

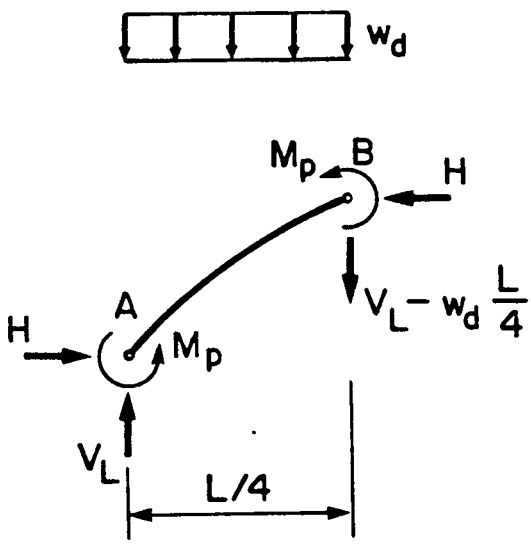

F.B.D. #2 - Left Quarter

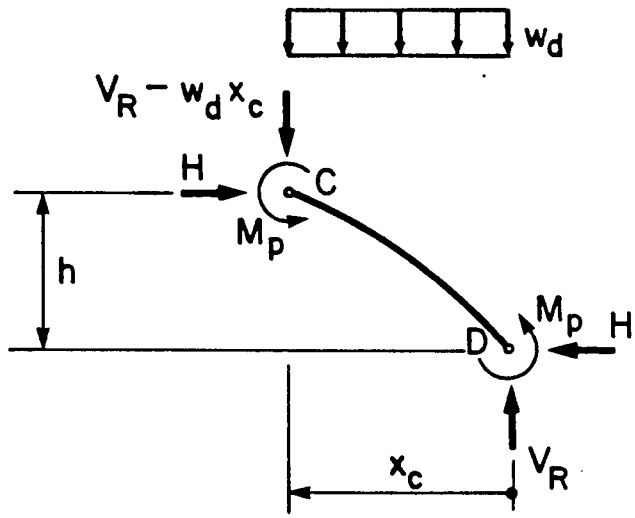

F.B.D. #3 - Right Side

Fig. 30. Free Body Diagrams of Point Loaded Arch.

quarter of the arch, and the third of the right. The locations A, B and D of three of the four hinges are known to be at the haunches and at the point load. However, the location C of the fourth hinge must be established and is represented by the unknown variable x_c.

The following equilibrium equations apply to the three free body diagrams of Fig. 30:

F.B.D. #1, $\Sigma V = 0$ gives

$$V_L + V_R = P_u + w_d L, \tag{4.1}$$

F.B.D. #1, $\Sigma M_A = 0$ gives

$$2M_p + V_R L - P_u L/4 - (w_d L)(L/2) = 0, \tag{4.2}$$

F.B.D. #2, $\Sigma M_B = 0$ gives

$$H(\tfrac{3}{4}f) + 2M_p + w_d(L/4)(L/8) = V_L(L/4) \tag{4.3}$$

and F.B.D. #3, $\Sigma M_c = 0$ gives

$$2M_p + V_R x_c = Hh + w_d \frac{w_c^2}{2} \tag{4.4}$$

A fifth equation can be obtained from the geometry of the parabolic arch

$$\frac{h}{f} = -4(\frac{x_c}{L})^2 + 4(\frac{x_c}{L}) \tag{4.5}$$

The solution to this problem involves the six unknowns, H, V_L, V_R, x_c, P_u and h and only five equations. The five equations 4.1 to 4.5 relate the six unknowns. Elimination of H, V_L, V_R and h gives

$$\frac{P_u L}{M_p} = 8\left(1 + \frac{1}{3(x_c/L) + 4(x_c/L)^2}\right) \tag{4.6}$$

It is important to note that the dead load has no effect on the result for four hinge plastic collapse if axial reduction of M_p and second order effects of neglected. This arises because in the analytical solution the dead load only causes axial forces and no bending, and axial forces contribute only to second order effects and reduction of M_p.

It remains to determine the location of the fourth hinge by minimizing $P_u L/M_p$ in Eq. (4.6) with respect to x_c/L. This can be accomplished by maximizing D where $D = 3(x_c/L) - 4(x_c/L)^2$. Differentiating and setting dD/dx equal to zero gives $x_c/L = .318$ for minimum collapse load. This minimum collapse load is then

$$\frac{P_u L}{M_p} = 22\,\frac{2}{9} = 22.22 \tag{4.7}$$

This means that the ultimate point load parameter is constant if axial reduction of M_p and second order effects are neglected. Eq. (4.7) is plotted on Figs. 17, 18 and 19 as a straight line labelled, "Plastic, No Interaction". This result is grossly non-conservative because axial interaction to reduce M_p is prevalent at low L/r, and second order effects are not negligible, especially at intermediate and high L/r.

A similar analytical solution for low L/r and neglecting reduced plastic moment must now be derived for the uniformly loaded arch. This

loading case is slightly more complicated because only two of the four hinge locations are known. Fig. 33 is a free body diagram of a parabolic arch loaded by an unbalanced uniform load. For the purposes of this analysis, the dead load is not considered because, as we have just seen, it is of no consequence if axial interaction and second order effects are neglected.

The method of solution is exactly analogous to the point load case. Moment and force equilibrium arch yields expressions for V_R and V_L. As well, moment equilibrium of a free body diagram from A to B will result in an expression for horizontal thrust H, just as for the point load case. These three reactions are as follows:

$$V_R = \frac{wx^2/2}{L} - 2\frac{M_p}{L}$$

$$V_L = wx(1 - \frac{x}{2L}) + \frac{2M_p}{L}$$

and

$$H = \frac{1}{h_b}\{wxb(1 - \frac{x}{2L}) + 2M_p\frac{b}{L} - 2M_p - \frac{wb^2}{2}\} \qquad (4.8)$$

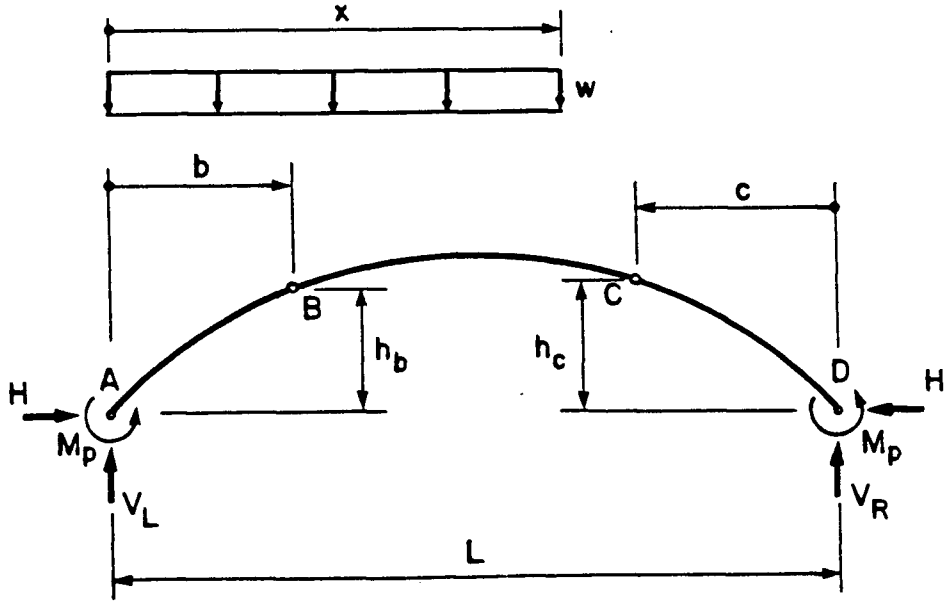

Fig. 33. Four Hinge Plastic Collapse Under Unbalanced U.D.L. Loading.

Now, moment equilbrium about C of the free body from C to D in Fig. 34 will yield the final equation as $2M_p + V_R c = H(h_c)$. Substituting for the known reactions H and V_R gives the following:

$$2M_p + \left(\frac{wx^2}{2L} - \frac{2M_p}{L}\right)c = \frac{h_c}{h_b}\left\{wxb\left(1 - \frac{x}{2L}\right) - \frac{wb^2}{2} + 2M_p\frac{b}{L} - 2M_p\right\} \qquad (4.9)$$

in order to simplify, let

$$\gamma = \frac{h_c}{h_b} = \frac{-4\frac{f}{L^2}c^2 + 4\frac{f}{L}c}{-4\frac{f}{L^2}b^2 + 4\frac{f}{L}b} = \frac{\frac{c}{L} - \left(\frac{c}{L}\right)^2}{\left(\frac{b}{L}\right) - \left(\frac{b}{L}\right)^2}$$

Eq. 4.9 now is a function of the hinge locations b/L and c/L as shown below.

$$\frac{w_u L^2}{M_p} = \frac{2(c/L + \gamma\, b/L - \gamma - 1)}{\frac{a^2 c}{2L^3} - \gamma\frac{ab}{L^2}\left(1 - \frac{a}{2L}\right) + \frac{\gamma b^2}{2L^2}} \qquad (4.10)$$

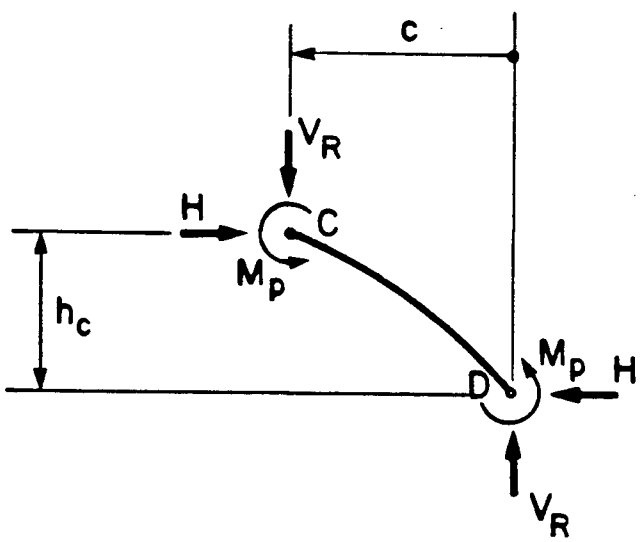

Fig. 34. F.B.D. of Right Side.

It now remains to minimize the ultimate load parameter with respect to hinge locations and loaded length. To accomplish this, a simple computer program was written which evaluted $w_u L^2/M_p$ for various combinations of b/L, c/L and x/L, to determine the minimum. The results were as follows;

$$b/L = 0.30,\ c/L = 0.30,\ x/L = 0.50$$

and

$$\frac{w_u L^2}{M_p} = 93.33 \qquad (4.11)$$

Eq. 4.9 is the result of a four hinge plastic collapse analysis neglecting axial interaction and second order effects. It is plotted as a horizontal line in Figs. 20, 21 and 22 and is evidently grossly non-conservative.

It is worth noting that for both loading cases, the ultimate load ratios are independent of f/L, E/σ_y and y/r and α.

4.1.2 Low L/r, Including Axial Interaction

Neglecting axial reduction of M_p at low L/r is a serious omission. This will now be included in the analytical solution to obtain a more reasonable bound at low L/r.

To make the arch behaviour amendable to a closed form solution, two assumptions are now made. First, the distribution of axial force over the entire span of the arch is assumed constant and equal to the thrust H. This is a fair assumption for arches whose rise to span ratio, f/L, is not abnormally high. Second, the interaction between axial and bending is assumed bilinear as shown by the yield surface of Fig. 5.

This is the same yield surface used for the non-linear analysis in ULA so the comparisons should be valid.

4.1.2.1 Plastic Collapse, Low L/r, Including Axial Interaction, in Point Load Case

Now, for the point load case, Eq. (4.7) must be rewritten as

$$P_u L/\bar{M} = 22.22 \tag{4.12}$$

where $\bar{M}$ is the reduced plastic moment due to axial $\bar{P}$. For the same reason, Eq. 4.3 is simplified and rewritten as

$$\bar{P} \cong H = \frac{P_u L}{4f} + \frac{w_d L^2}{8f} - \frac{2\bar{M}}{f}$$

$$= \frac{P_u L}{4f} + \alpha P_p - \frac{2\bar{M}}{f} \tag{4.13}$$

The yield surface is represented by the following two equations:

$$\bar{P}/P_p + 0.85\ \bar{M}/M_p = 1.0 \qquad \text{for} \quad \bar{M}/M_p \leq 0.95 \tag{4.14}$$

and

$$0.26\ \bar{P}/P_p + \bar{M}/M_p = 1.0 \qquad \text{for} \quad \bar{M}/M_p > 0.95 \tag{4.15}$$

Combining Eqs. 4.12 and 4.13 with 4.14 and then 4.15 gives

$$\frac{P_u L}{M_p} = \frac{(L/r)(1.0-\alpha)}{0.16\ \frac{(y/r)}{(f/L)} + .0385\ L/r} \qquad \text{for} \quad \bar{M}/M_p \geq 0.95 \tag{4.16}$$

and

$$\frac{P_u L}{M_p} = \frac{(L/r)(1.0-\alpha)}{0.0416\,\frac{(y/r)}{(f/L)} + .045(L/r)} \quad \text{for} \quad \bar{M}/M_p < 0.95 \qquad (4.17)$$

Substituting the standard arch values of $y/r = 0.95$ and $f/L = 0.15$ into the above equations gives:

$$\frac{P_u L}{M_p} = \frac{(L/r)(1.0-\alpha)}{1.013 + .0383\,(L/r)} \quad \text{for} \quad \bar{M}/M_p \leq 0.95 \qquad (4.18)$$

and

$$\frac{P_u L}{M_p} = \frac{(L/r)(1.0-\alpha)}{0.263 + 0.045\,(L/r)} \quad \text{for} \quad \bar{M}/M_p > 0.95 \qquad (4.19)$$

By equating Eqs. 4.18 and 4.19 it is easily shown that Eq. 4.18 governs for $L/r \leq 111$ and Eq. 4.19 governs for $L/r > 111$. These two equations are plotted on Figs. 17, 18 and 19 and labelled as "Plastic, Bilinear Interaction". As expected this curve is vastly different from the "Plastic, No Interaction" curve for low L/r. This is because the hinges do not form at a moment M_p, they form at $\bar{M}$, and $\bar{M} \ll M_p$ as L/r approaches zero. The limit of $P_u L/M_p$ as L/r approaches zero is zero, however the limit of $P_u L/\bar{M}$ as L/r approaches zero is 22.22.

4.1.2.2 Plastic Collapse, Low L/r, Including Axial Interaction, U.D.L. Case

Having derived expressions for four hinge plastic collapse including axial interaction for a point loaded arch, it remains to repeat this derivation for an arch loaded by unbalanced U.D.L.

Eq. 4.11 must be rewritten as follows:

$$\omega_u L^2/\bar{M} = 93.33 \qquad (4.20)$$

Substituting x/L = 0.5, b/L = 0.3, c/L = 0.3 into Eq. (4.8) and adding the dead load thrust, the expression for axial force in the arch becomes:

$$\bar{P} \cong H = \frac{8.036\times10^{-2}\, w_u L}{f/L} - \frac{5}{3}\frac{M_p}{L(f/L)} + \alpha P_p \qquad (4.21)$$

Combining Eqs. (4.20) and (4.21) with each of the interaction Eqs. (4.14) and (4.15) gives

$$\frac{w_u L^2}{M_p} = \frac{(L/r)(1.0-\alpha)}{0.0625\,\frac{(y/r)}{(f/L)} + 9.1071\times10^{-3}(L/r)} \quad \text{for } \bar{M}/M_p \leq 0.95 \qquad (4.22)$$

and

$$\frac{w_u L^2}{M_p} = \frac{(L/r)(1.0-\alpha)}{0.01625\,\frac{(y/r)}{(f/L)} + 1.0714\times10^{-2}(L/r)} \quad \text{for } \bar{M}/M_p > 0.95 \qquad (4.23)$$

Substituting the standard values of f/L = 0.15 and y/r = 0.15 results in the following two equations:

$$\frac{w_u L^2}{M_p} = \frac{(L/r)(1.0-\alpha)}{0.396 + 9.11\times10^{-3}(L/r)} \quad \text{for } \bar{M}/M_p \leq 0.95 \qquad (4.24)$$

and

$$\frac{w_u L^2}{M_p} = \frac{(L/r)(1.0-\alpha)}{0.103 + 1.071\times10^{-2}(L/r)} \quad \text{for } \bar{M}/M_p > 0.95 \qquad (4.25)$$

Equating (4.24) and (4.25) indicates that for L/r ≤ 182 Eq. (4.24) will govern, and for L/r > 182 Eq. (4.25) will govern. This result is plotted

on Figs. 20, 21 and 22 and labelled, "Plastic, Bilinear Interaction".

Unlike the point load case, the arch behaviour at low L/r under U.D.L. is not entirely governed by four hinge collapse. At very low L/r, the governing failure mechanism could be full cross-section axial yielding under full span live load (x/L = 1.0). An analytical solution for this behaviour is obtained simply by equating the thrust caused by full dead and live laod to full axial yield $P_p = A\sigma_y$ as follows:

$$P \cong H = \frac{w_u L^2}{8f} + \frac{w_d L^2}{8f}$$

$$= \frac{w_u L^2}{8f} + \alpha P_p = P_p$$

Substituting $M_p/P_p r = 0.95$ yields:

$$\frac{w_u L^2}{8fM_p}(.95r) = 1.0 - \alpha$$

Simplifying and substituting f/L = 0.15 results in the following:

$$\frac{w_u L^2}{M_p} = 1.263(1.0-\alpha)(L/r) \qquad (4.26)$$

Eq. (4.26) describes the ultimate full span uniform live load required to cause axial yielding of a standard arch. Equating Eq. (4.26) with four hinge plastic collapse Eq. (4.24) shows that full live load axial yielding only governs for L/r < 43. Eq. (4.26) is plotted on Figs. 20, 21 and 22 and labelled "Axial Yield".

4.2 Analytical Bounds for High L/r

As the slenderness, L/r, approaches the theoretical slenderness limit, the arch under unbalanced U.D.L. collapses by elastic buckling, whereas the point loaded arch buckles after the formation of the first hinge. Analytical solutions wil now be derived for each of the slender collapses mentioned. Axial reduction of M_p is not significant at high L/r and is therefore not included in this analytical derivation.

4.2.1 High L/r, Full Uniform Live Load Elastic Buckling

An expression for the elastic buckling load parameter as a function of L/r can be derived by equating full live load and dead load thrust to the Euler buckling load. Again, it is assumed that the axial force in the arch is constant and equal to the horizontal thrust so that

$$\frac{w_d L^2}{8f} + \frac{w_u L^2}{8f} = \frac{\pi^2 EI}{(kL)^2}$$

or

$$\alpha P_p + \frac{w_u L^2}{8f} = \frac{\pi^2 EAr^2}{(kL)^2}$$

where kL is the effective length of a fixed arch. Including the identity $y/r = M_p/P_p r$ and simplifying gives

$$\frac{w_u L^2}{M_p} = \frac{8f/L}{y/r}\left(\frac{\pi^2}{K^2}\frac{E}{\sigma y}\frac{1}{L/r} - \alpha\, L/r\right) \qquad (4.27)$$

The analytical solution requires a value of the effective length factor k. This was obtained by examining the result of a standard arch ULA analysis at L/r = 700 for α = 0.10 where the governing ultimate load behaviour was elastic buckling under full live load. A value of k = 0.377 was chosen such that Eq. 4.27 would agree with the ULA result. Substituting standard arch values of f/L = 0.15, E/σy = 750 and y/r =

0.95 as well as k = 0.377 gives a final result:

$$\frac{w_u L^2}{M_p} = \frac{65,800}{(L/r)} - 1.26\ \alpha\ (L/r) \qquad (4.28)$$

Eq. (4.28) describes the uniform ultimate load parameter for elastic buckling as a function of the dead load ratio α and slenderness L/r. This is plotted on Figs. 20, 21 and 22 under the label "Elastic Buckling, k = 0.377".

4.2.2 High L/r, Point Load, One Hinge Buckling

An expression for one hinge instability is derived by equating the plastic moment M_p to the approximate linear first order moment PL/17 with second order magnification.

$$\frac{PL}{17}\left(\frac{1}{1 - H/H_{cr}}\right) = M_p \qquad (4.29)$$

PL/17 was determined by evaluating the maximum moment from linear first order stiffness analysis.

For large L/r, virtually all the thrust comes from the dead load. Therefore, it is assumed that $H = \frac{w_d L^2}{8f} = \alpha P_p$. Now, Eq. (4.29) becomes:

$$M_p = \frac{PL}{17}\left(\frac{1}{1 - \frac{\alpha P}{\pi^2 EI}(kL)^2}\right)$$

Setting $P = P_u$ and rearranging:

$$\frac{P_u L}{M_p} = 17\left(1 - \frac{\alpha}{\pi^2}\frac{\sigma_y}{E}\left(\frac{kL}{r}\right)^2\right)$$

Substituting k = 0.37 and $E/\sigma y = 750$ yields the final result:

$$\frac{P_u L}{M_p} = 17\left(1 - 1.920\times10^{-5}\ \alpha(L/r)^2\right) \qquad (4.30)$$

Eq. (4.30) is an analytical solution for the point load ratio required for one hinge instability as a function of the dead load ratio α and the slenderness L/r. It is plotted as "One Hinge Analytical, k = 0.377" on Figs. 17, 18 and 19.

4.2.3 Analytical Solution for the Theoretical Slenderness Limit

An expression for the theoretical slenderness limit can be obtained by solving either Eq. (4.27) or Eq. (4.29) for L/r when $w_u L^2/M_p$ or $P_u L/M_p$ are zero. If $P_u L/M_p = 17\left(1 - \frac{\alpha}{\pi^2}\frac{\sigma_y}{E}\left(\frac{kL}{r}\right)^2\right) = 0$

then
$$(L/r)_0 = \frac{1}{K}\sqrt{\frac{\pi^2}{\alpha}\frac{E}{\sigma_y}} \qquad (4.31)$$

where $(L/r)_0$ is the slenderness limit. Substituting K = 0.377, E/σ_y = 750 and α = 0.1 then 0.2 indicates that

$$(L/r)_0 = 720 \qquad \text{for} \qquad \alpha = 0.1$$

and

$$(L/r)_0 = 510 \qquad \text{for} \qquad \alpha = 0.2$$

4.3 Comparison of Analytical Bounds With Collapse Envelopes

There exists a discrepancy between the analytical bounds derived in this chapter and the collapse curves generated by non-linear ultimate load analysis. These arise due to the inadequacies of the conventional analytical solutions. The graphical explanations for the discrepancies

are presented by slenderness regions in Figs. 35 and 36. The plots of $\alpha = 0.1$ were arbitrarily chosen here, however the explanation holds for all three dead load ratios examined.

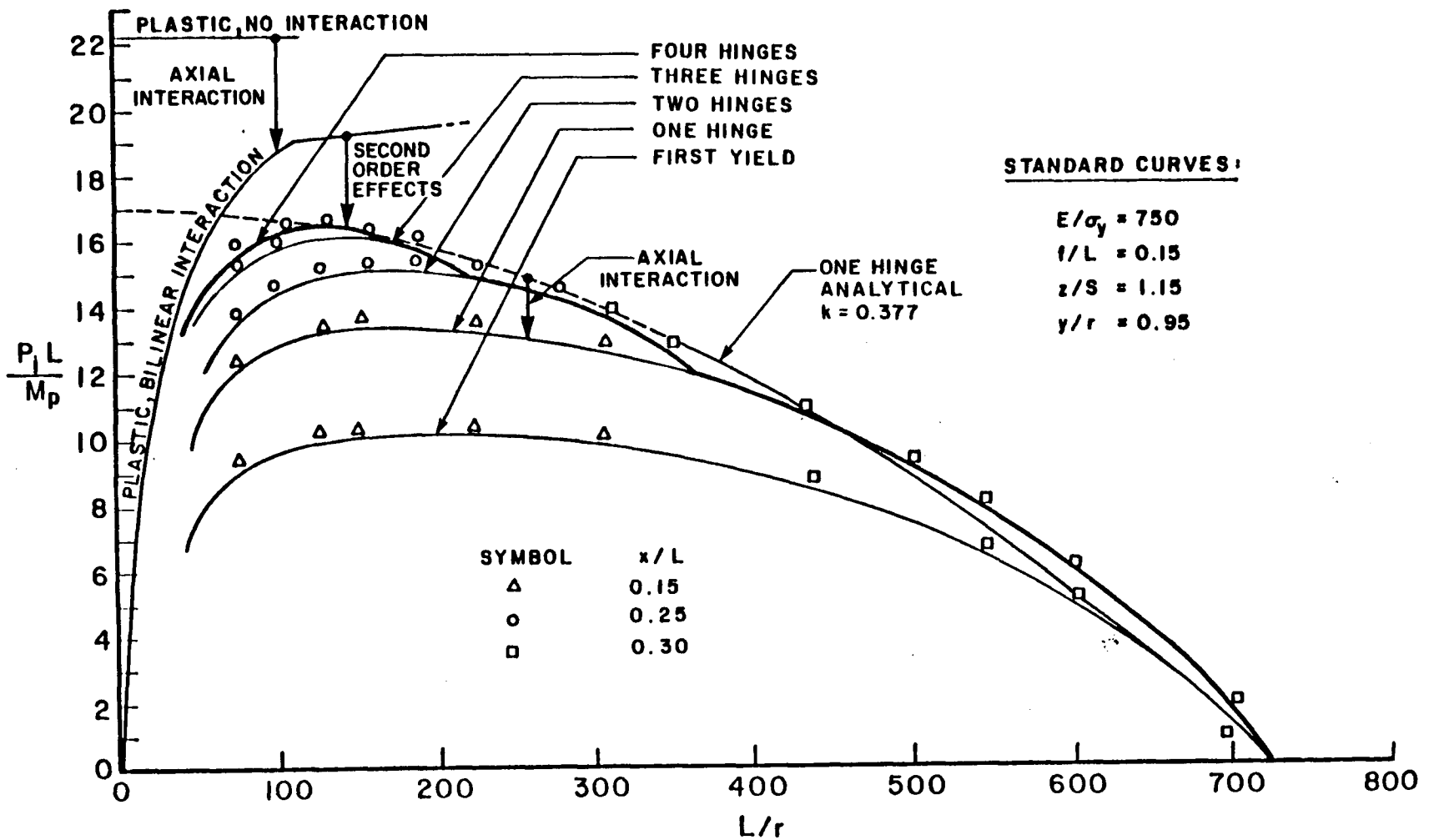

Fig. 35. Discrepancies Between Analytical Solutions and Collapse Curves, Point Loading.

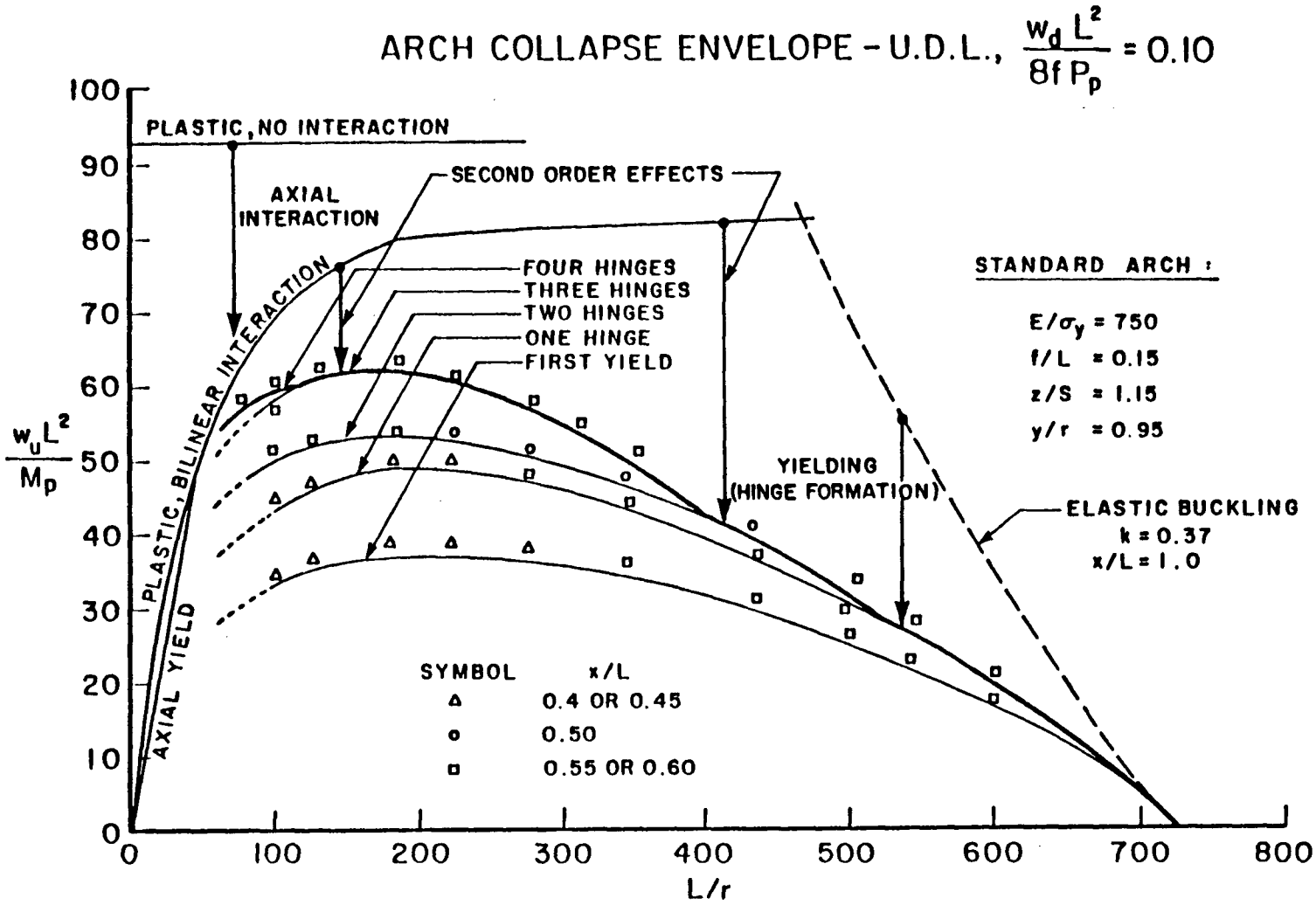

Fig. 36. Discrepancies Between Analytical Solutions and Collapse Curves, U.D.L. Loading.

CHAPTER 5

VARIATION OF STANDARD PARAMETERS

The non-linear behaviour of standard fixed arches are summarized by hinge formation curves and collapse envelopes in Chapter 3. To make this examination of arch behaviour possible it was necessary to define a standard arch by assuming that $E/\sigma_y = 750$, $f/L = 0.15$, $Z/s = 1.15$ and $y/r = 0.95$. These standard values are indicative of a typical steel box girder or wide flange arch. It is the purpose of this chapter to vary these four standard parameters and examine the effect on the non-linear performance of fixed arches. This should facilitate the extrapolation of the results of this thesis to include actual arches whose parameters will certainly deviate from the standard values. In the following sections only one parameter at a time is altered; all others are kept at the standard value.

5.1 Variation of E/σ_y

The dimensionless parameter E/σ_y is a material property and not a function of arch geometry or cross-section. It ranges typically from approximately 375 or 400 for aluminum to about 900 for reinforced concrete.

Eqs. 4.26 and 4.29 serve as analytical bounds for behaviour at long L/r for uniform loading and point loading respectively. The second order reduction terms are $[1 - (\alpha/\pi^2)(\sigma_y/E(kL/r)]$ for point loading and $[\frac{\pi^2}{K^2}\frac{E}{\sigma_y}\frac{1}{L/r} - \alpha L/r]$ for uniform loading. It is apparent from these terms that second order effects are proportional to E/σ_y. Thus, a reduction of

E/σ_y from the standard value of 750 will increase any second order effects and therefore decrease the capacity of the arch. This has been confirmed by computer analysis and is presented in Fig. 37 through 40 for $E/\sigma_y = 375$.

Upon examination of these variation of parameter curves for E/σ_y, it is obvious that the effect of reducing E/σ_y becomes less pronounced with decreasing L/r. This is because any second order effects are proportional to $(L/r)^2$ and therefore die out at low L/r. Extending this argument to the limiting case as L/r approaches zero, it is evident that E/σ_y has no effect on the ultimate load parameter. This limiting case is governed by a four hinge plastic collapse mechanism according to Eqs. 4.16 and 4.17 which do not contain the parameter E/σ_y.

The limiting slenderness limit defined by Eq. 4.37 is proportional to the square root of E/σ_y. This supports the reduction of the slenderness limit due to the halving of E/σ_y indicated by Figs. 37 through 40.

5.2 Variation of f/L

The rise to span ratio, f/L, is commonly in the range of 0.10 to 0.30 for bridge arch ribs in steel, concrete or aluminum. The standard arch has an assumed value of 0.15.

At low L/r, four hinge plastic collapse is described by Eqs. 4.16 and 4.17 for point loading and Eqs. 4.22 and 4.23 for unbalanced uniform loading. The quantity f/L appears in both these analytical solutions. It is evident from these equations that increasing only f/L results in an increase in the ultimate load ratios $P_u L/M_p$ or $w_u L^2/M_p$. Also, the effect of varying f/L diminishes with increasing L/r and is almost non-existant in the intermediate range of L/r. For example, at a relatively low value

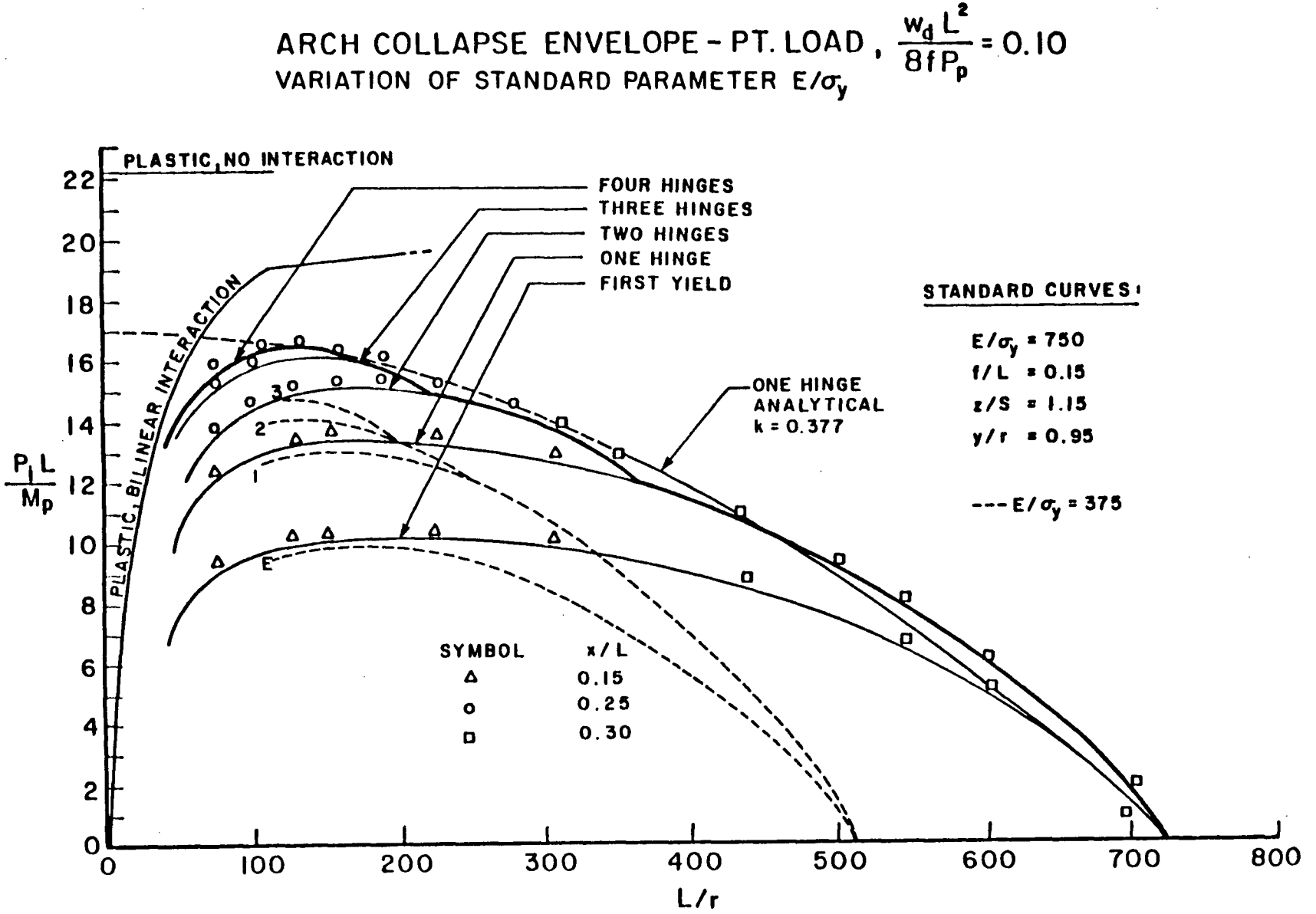

Fig. 37. Sensitivity Analysis of E/σ_y, Point Loading, $\alpha = 0.10$

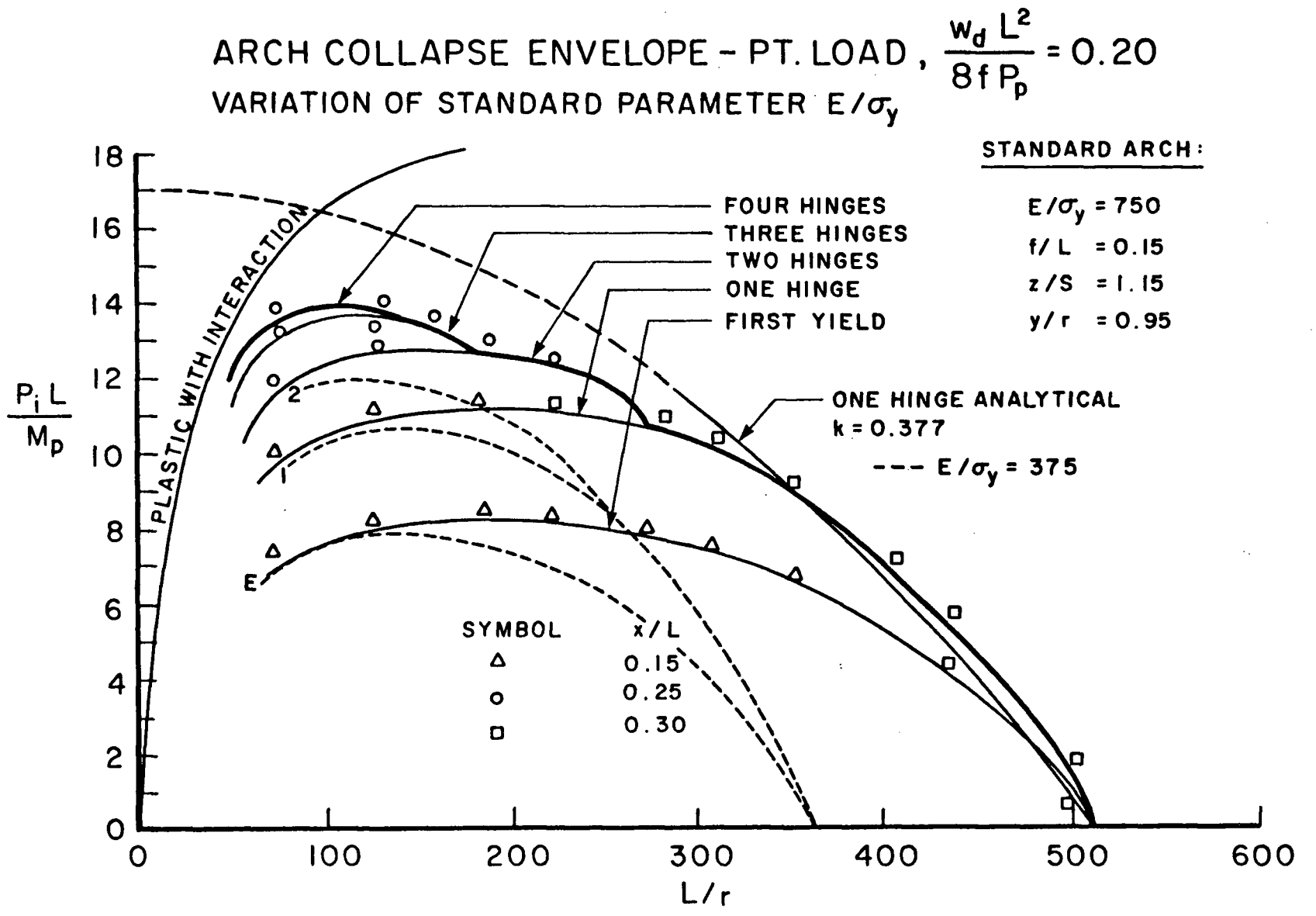

Fig. 38. Sensitivity Analysis of E/σ_y, Point Loading, $\alpha = 0.20$

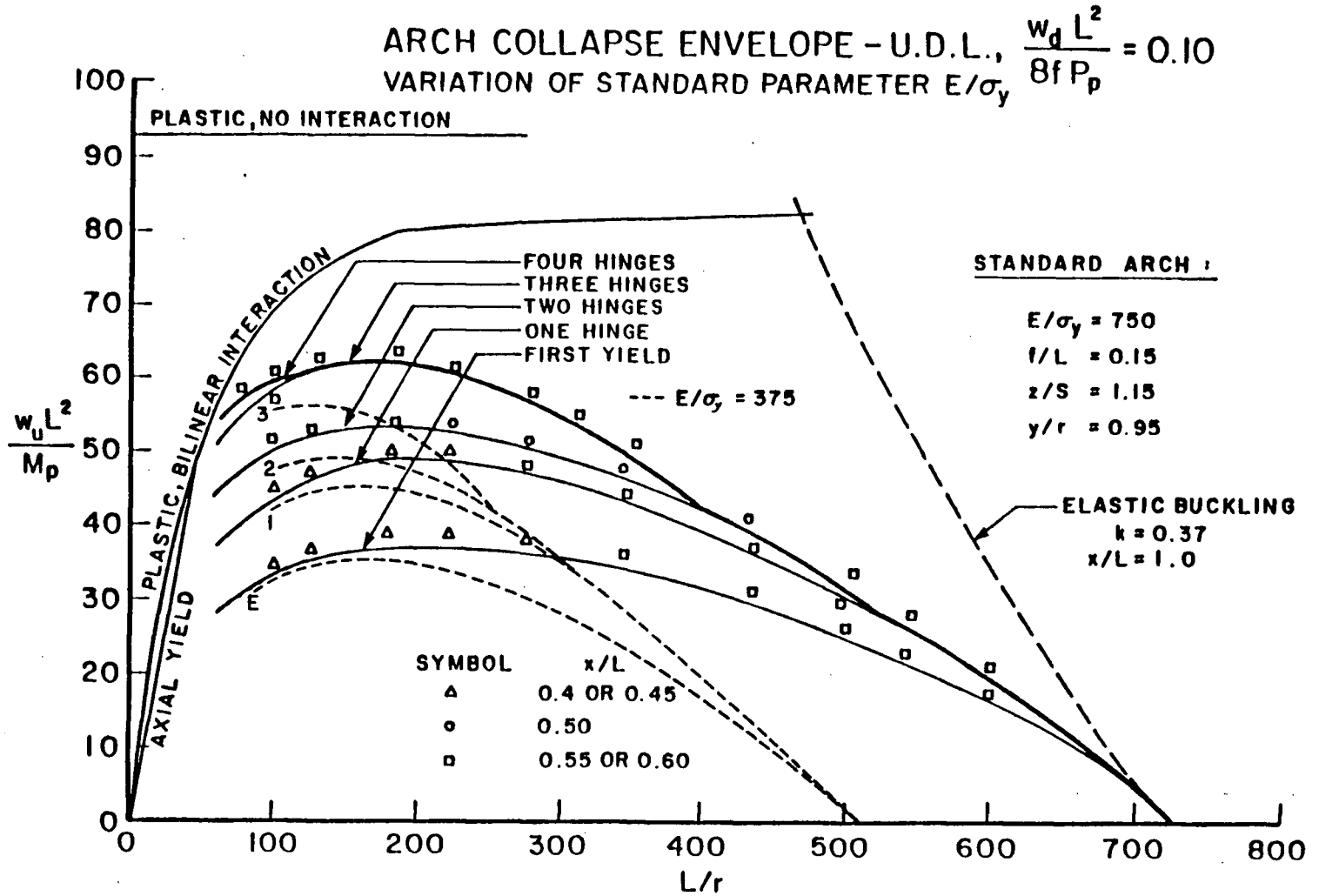

Fig. 39. Sensitivity Analysis of E/σ_y, Uniform Loading, $\alpha = 0.10$

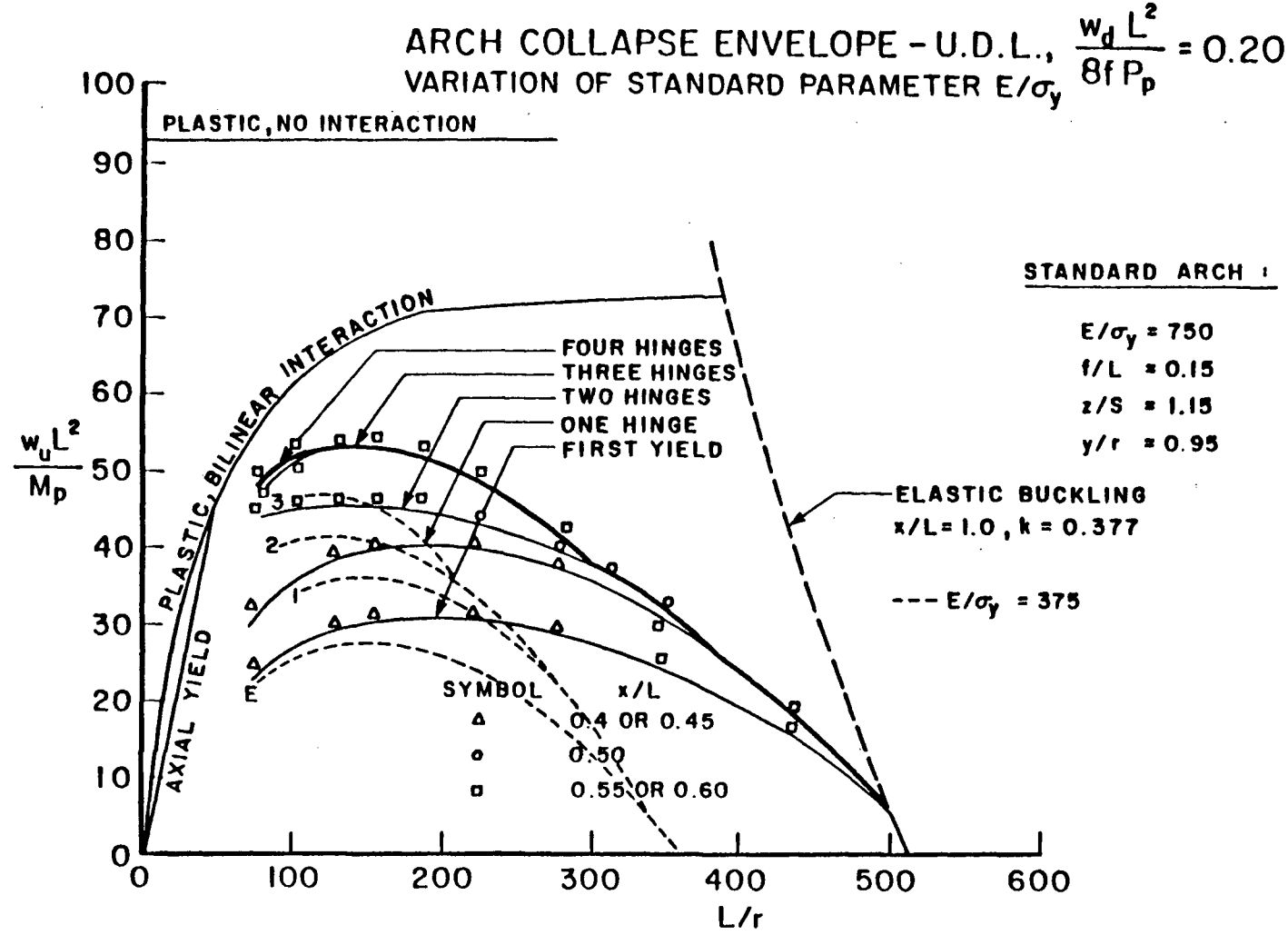

Fig. 40. Sensitivity Analysis of E/σ_y, Uniform Loading, $\alpha = 0.20$

of L/r of 100, the increase in $P_u L/M_p$ due to a change in f/L from 0.15 to 0.25 is only 9%. This behaviour is confirmed by ULA computer analysis for point loading and uniform loading with an f/L value of 0.25. The results are superimposed on standard arch behaviour curves in Figs. 41 through 44.

It is interesting to note that at high L/r, an increase in f/L actually causes a small decrease in the ultimate load parameters. At first, this may appear as an anomaly when compared with Eq. 4.27 describing the analytical bounds for uniform loading at high L/r because $w_u L^2/M_p$ appears to be linearly proportional to f/L. However, the value of K is assumed in the derivation of Eq. 4.27 as a fraction of the span length L when in fact it is more correctly interpreted as a fraction of the arc length l. Eq. 4.27 can be rewritten in the form of Eq. 5.1 using kL as the effective length

$$\frac{w_u L^2}{M_p} = \frac{8(f/L)(L/r)}{(y/r)} \left(\frac{\pi^2}{(kL/r)^2} \frac{E}{\sigma_y} - \alpha\right) \qquad (5.1)$$

Realizing that an increase in f/L causes the effective length kL to increase due to a larger arc length it is evident that increasing f/L at large slenderness can act to reduce the ultimate load parameter. A similar argument holds true for the point loading case.

As a final comment before leaving the discussion of variation of f/L, a practical note is now made. The ratio f/L was changed from 0.15 to 0.25 in the computer analysis by increasing the rise f by that ratio 5/3. For a valid comparison, all other dimensionless ratios must be unchanged. This meant that for the dead load ratio $\alpha = w_d L^2/8fP_p$, the dead load w_d has to be increased by 5/3 to maintain $\alpha = 0.1$ or 0.2. This

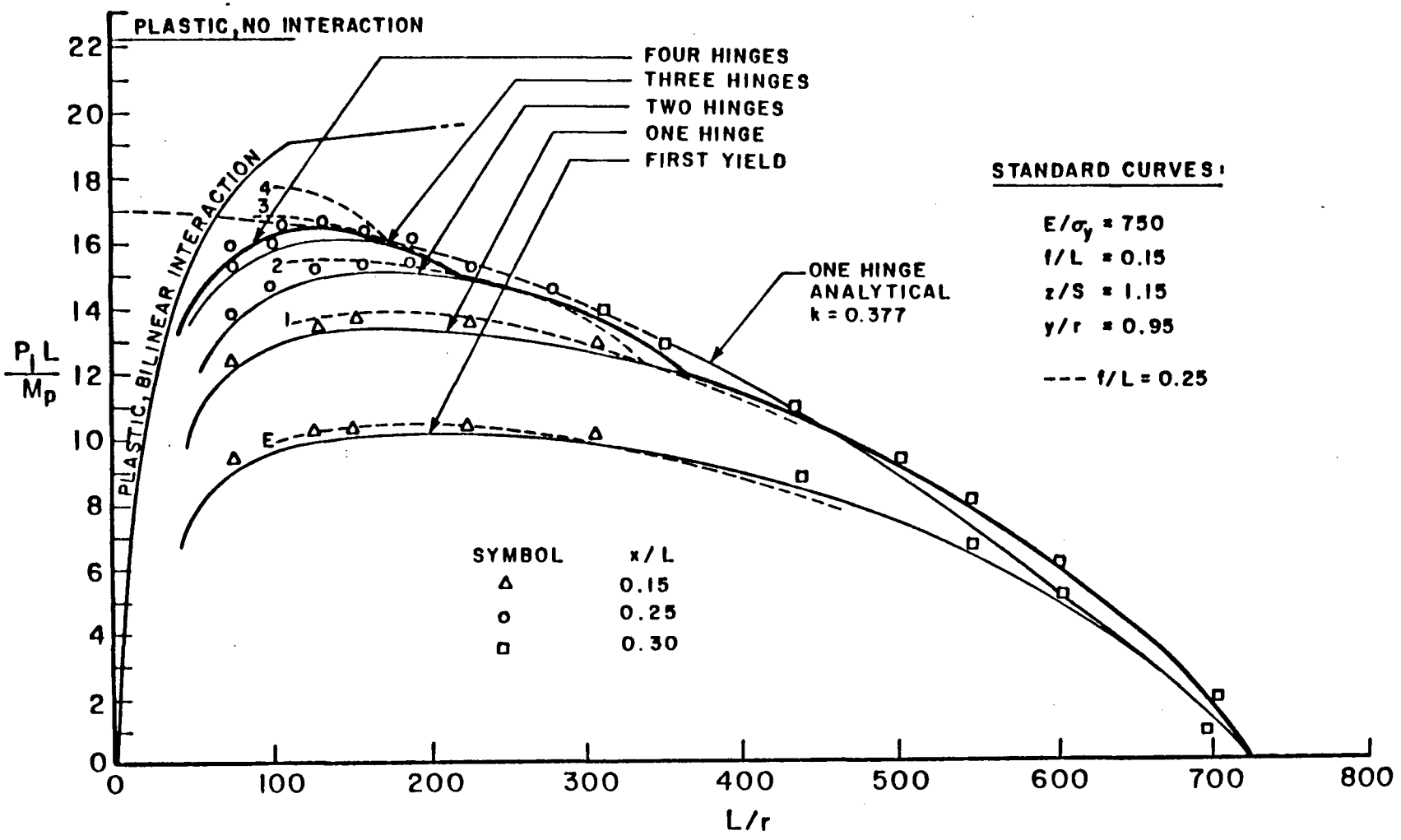

Fig. 41. Sensitivity Analysis of f/L, Point Loading, $\alpha = 0.10$.

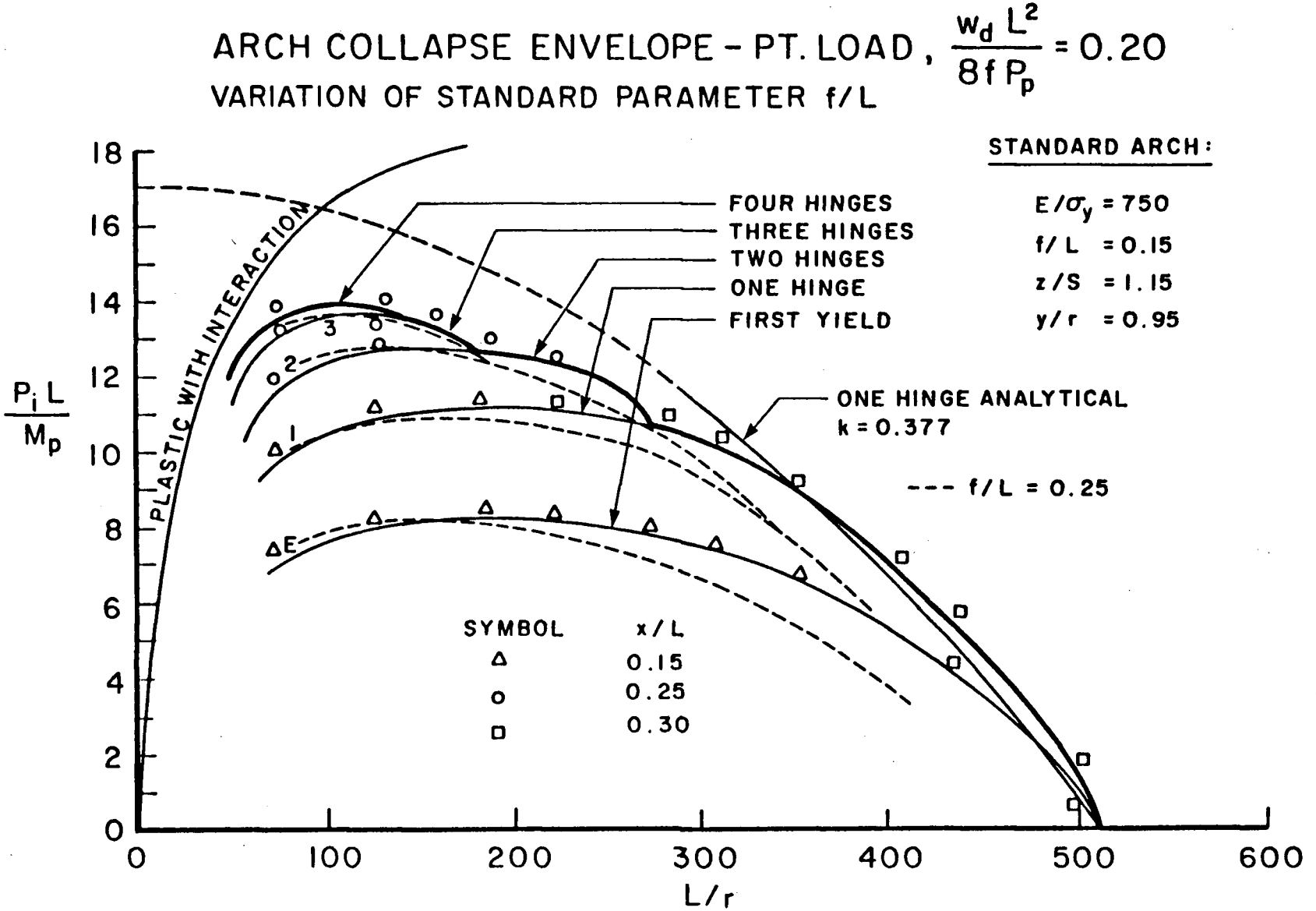

Fig. 42. Sensitivity Analysis of f/L, Point Loading, α = 0.20.

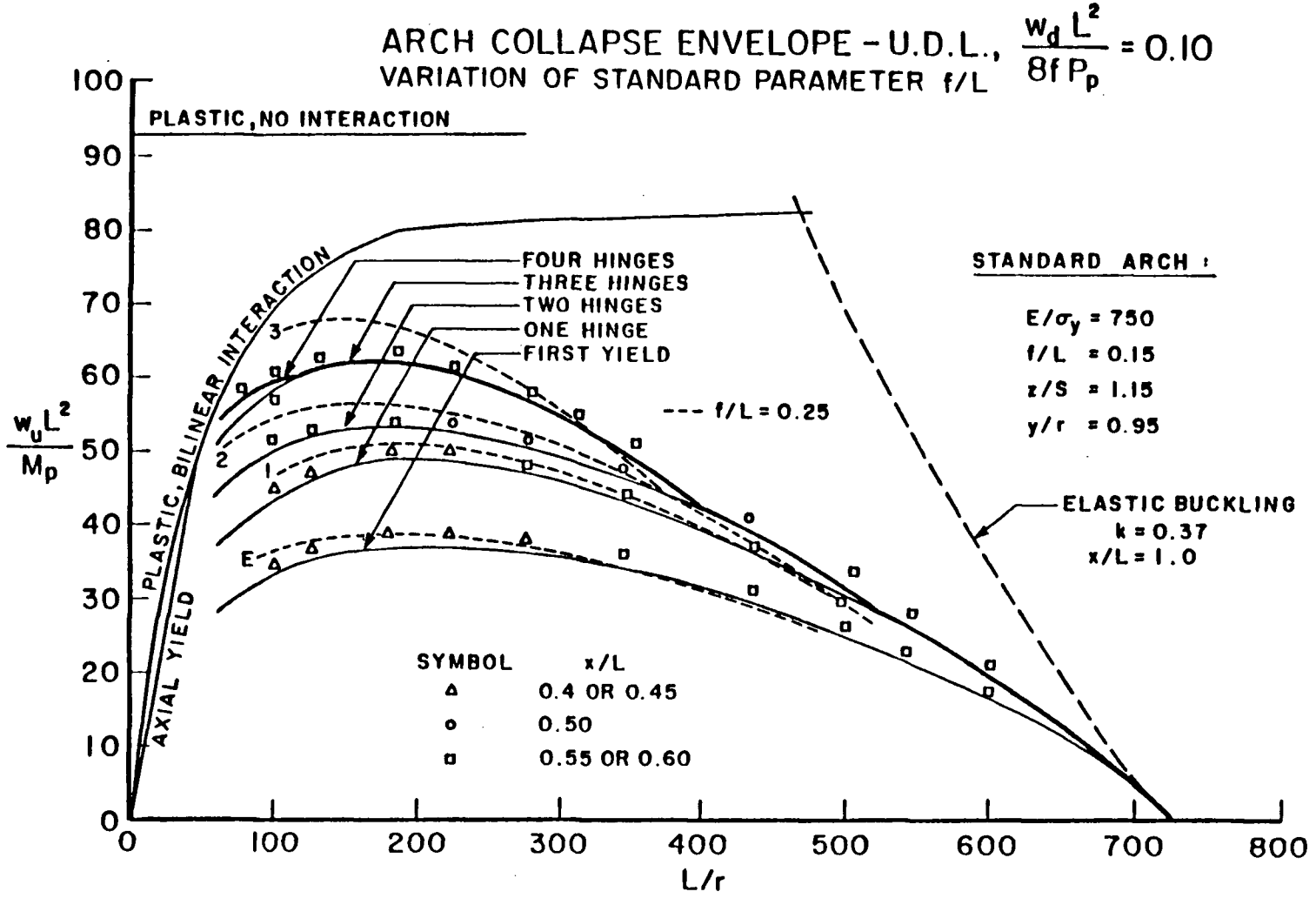

Fig. 43. Sensitivity Analysis of f/L, Uniform Loading, $\alpha = 0.10$.

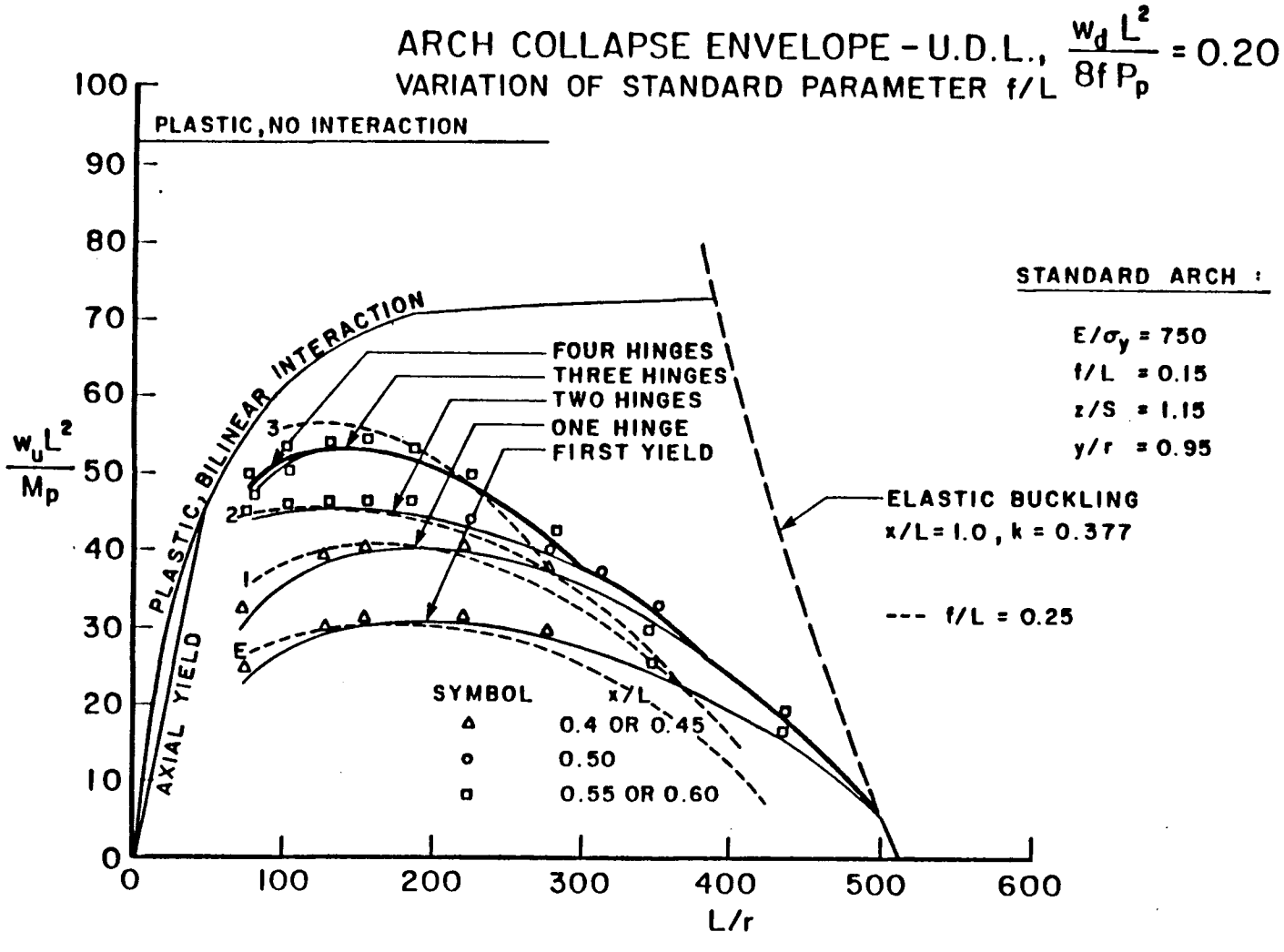

Fig. 44. Sensitivity Analysis of f/L, Uniform Loading, $\alpha = 0.20$.

should be in mind when examining the small effect of varying f/L in Figs. 41 to 44.

5.3 Variation of y/r

The ratio y/r is a cross section property ranging from 0.866 for a solid rectangular section to 1.0 for an idealized section with all of its material concentrated at two flanges.

Again, in Eqs. 4.16 and 4.17 for point loaded plastic collapse and Eqs. 4.22 and 4.23 for U.D.L. plastic collapse the quantity y/r is apparent. An increase in y/r will cause a decrease in the ultimate load parameters. The sensitivity of the load ratios to any change in y/r is the same as for f/L, however, the range of y/r is very limited whereas f/L may vary considerably. As an example, the analytical bound equations at a value of L/r of 100, varying y/r through its entire feasible range from 0.866 to 1.0 only changes $w_u L^2/M_p$ by 4.1 percent, and $P_u L/M_p$ by 0.8 percent. ULA computer analysis confirms the insignificance of the variation of the quantity y/r. It is therefore reasonable to conclude that the standard arch non-linear behaviour curves are practical for all values of y/r. No additional plots are needed.

5.4 Variation of Z/S

The ratio of the plastic section modulus to the elastic section modulus, Z/S is also a ratio of the plastic moment of a cross-section to its yield moment, M_p/M_y and is often referred to as a shape factor. It is a cross-sectional property and varies from 1.0 for an idealized section with all its material at two flanges to 1.50 for a solid rectangular section. The value assumed for the standard arch is 1.15

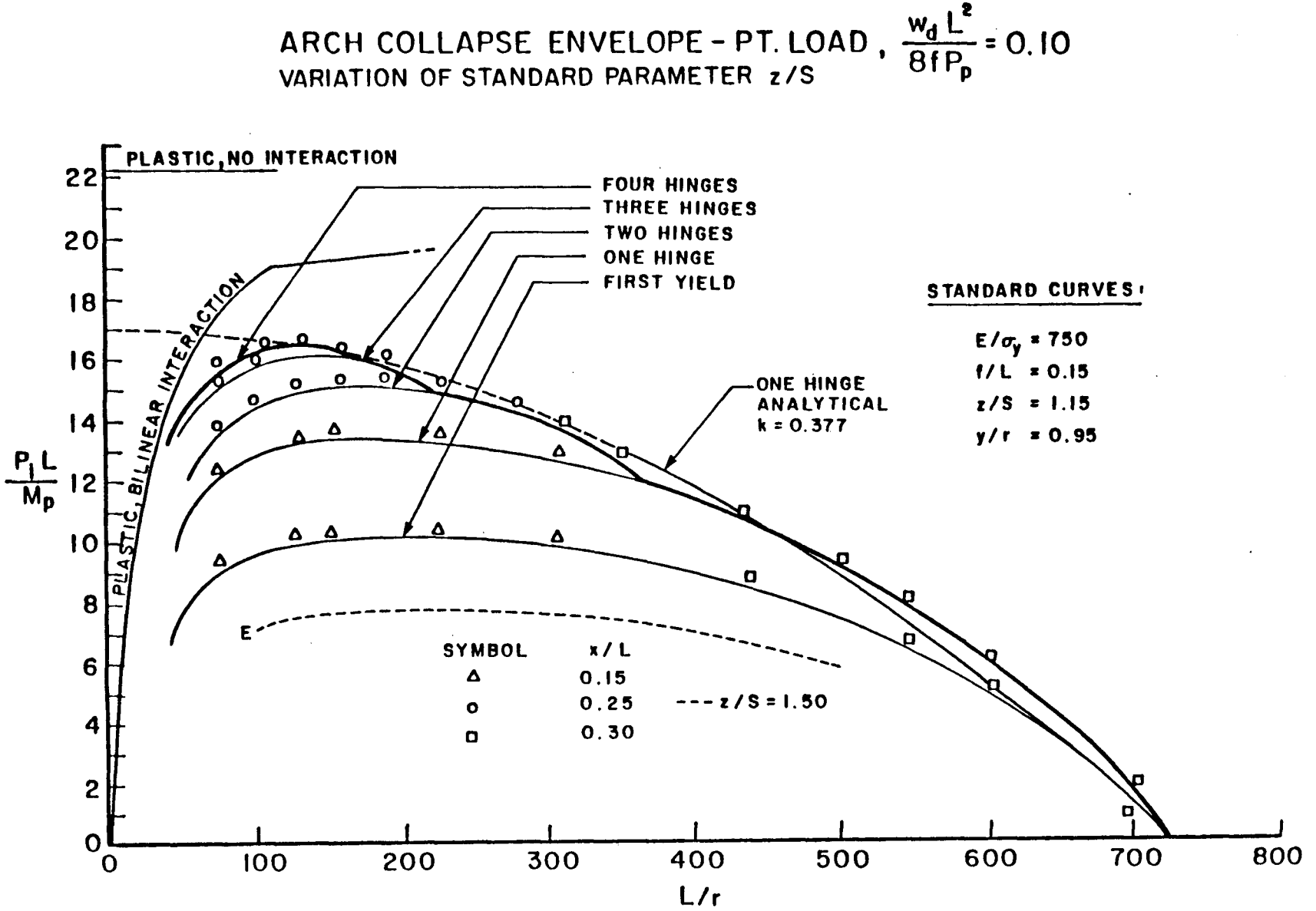

Fig. 45. Sensitivity Analysis of Z/S, Point Loading, α = 0.10.

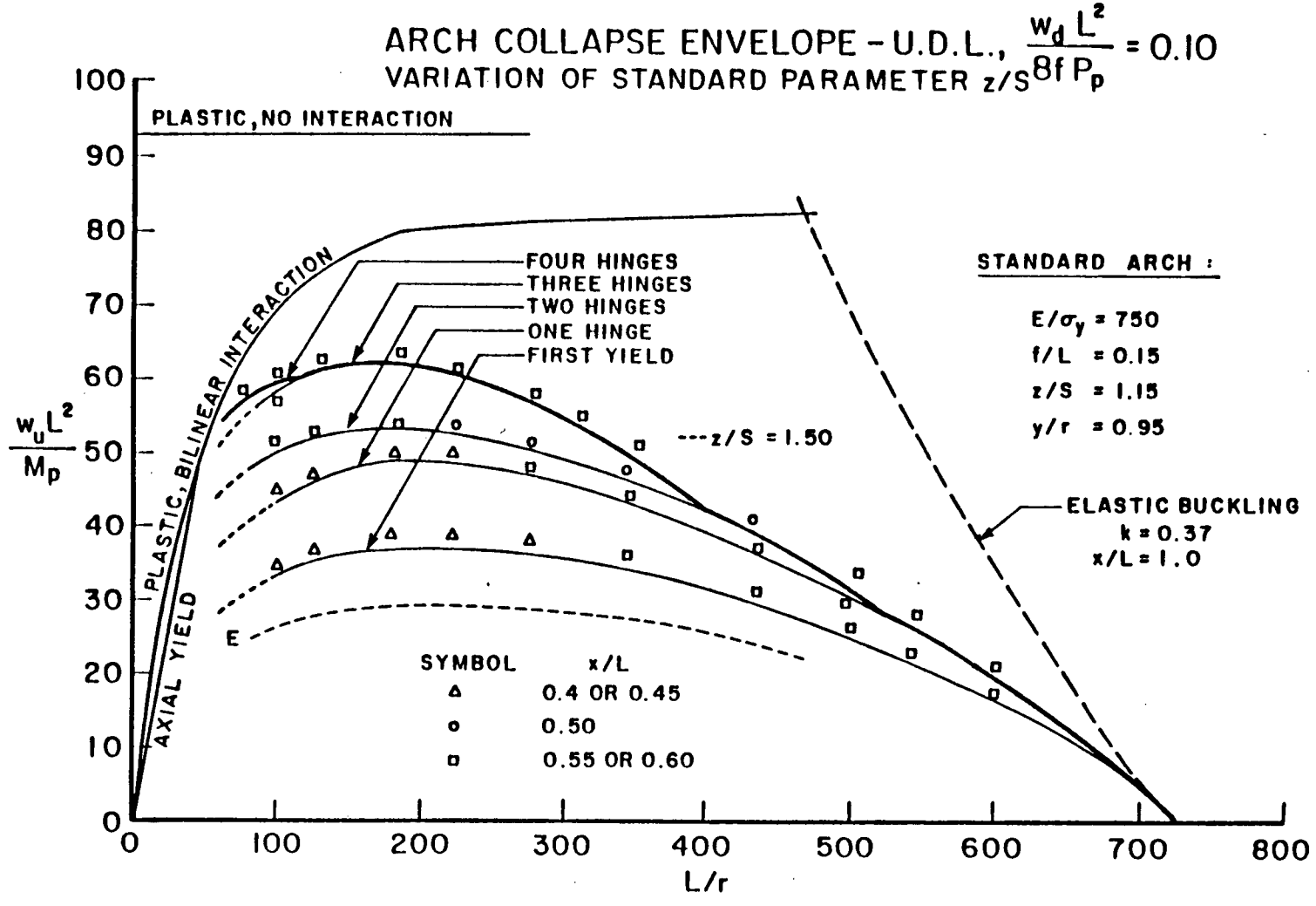

Fig. 46. Sensitivity Analysis of Z/S, Uniform Loading, $\alpha = 0.10$.

corresponding to the approximate shape factor for box and wide flange section.

As pointed out in Chapter 3, the shape factor effects only the first yield condition and not hinge formation or ultimate load. In the limiting case of Z/S = 1.0, the first yield and first hinge curves would coincide. For any other values of the shape factor, the first yield curve must lie below the first hinge curve. It is therefore simple to conclude that increasing Z/S would decrease $P_e L/M_p$ or $w_e L^2/M_p$. This is easily confirmed by second order elastic computer analysis, the results of which are superimposed on standard curves for $\alpha = 0.10$ in Figs. 45 and 46. The shift in the first yield curve in the low and intermediate ranges are very nearly the ratio of the change in Z/S.

By varying the four standard ratios E/σ_y, f/L, Z/S and y/r, an indication of the sensitivity of the load parameters to these ratios was obtained. It is concluded that the standard arch hinge formation curves and collapse envelopes are reasonable for any values of y/r and Z/S and for values of f/L in the range from 0.10 to 0.30. However, as shown clearly in Figs. 37 through 40, the standard arch curves are significantly sensitive to variation in the material parameter E/σ_y. This cannot be overlooked when applying the arch behaviour curves.

CHAPTER 6

CONCLUSION

6.1 Hinge Locations and Formation Sequence

By considering both second order effects and member plasticity the behaviour of standard fixed arches loaded to ultimate has been summarized using hinge formation curves and collapse envelopes. A variation of parameters which defined the standard arch was carried out to examine the sensitivity of the response to these parameters.

Throughout this work, it became clear that the collapse mechanism depends on slenderness and ranges from one hinge instability at high L/r to a four hinge plastic collapse mechanism at low L/r, with a few extremely slender uniformly loaded arches buckling elastically. The location of the plastic hinges and the sequence of formation have yet to be discussed completely. These results are summarized for the different collapse mechanisms in Tables 1 and 2 for point loading and uniform loading respectively. Each row in the tables describes a different collapse mechanism.

The numbers in the body of the table indicate which hinge, if any, formed at a certain location on the arch. For example, three hinge instability under uniform loading occurs with the first hinge forming at the right haunch, the second hinge forming at the left haunch, and the third and final hinge forming near the right quarter point. The loading, defined by x/L is for minimum ultimate strength and is indicated in the collapse envelopes of Figs. 17 to 22.

TABLE I. Hinge Formation Sequence, Point Loading

Point Load	Left Haunch	Near Left 1/4 Point	Near Right 1/4 Point	Right Haunch
4 Hinge Collapse	2	1	4	3
3 Hinge Collapse	2	1		3
2 Hinge Collapse	(2)*	1		(2)*
1 Hinge Collapse		1		

*Second hinge may form at either haunch, depending on L/r and α.

TABLE II. Hinge Formation Sequence, UDL Loading

UDL Load	Left Haunch	Near Left 1/4 Point	Near Right 1/4 Point	Right Haunch
4 Hinge Collapse	1	4	3	2
3 Hinge Collapse	2		3	1
2 Hinge Collapse	2			1
1 Hinge Collapse				1

6.2 Typical Load Deflection Behaviour

It is common to monitor the behaviour or response of a structure due to increasing load level to compare experimental results with analytical work. Unfortunately, no experimental results are available, therefore

different common analytical techniques will be compared on a load-response basis, in the belief that the second order elasto-plastic analysis used in this work closely models actual behaviour.

Figs. 3 and 4 of Chapter 1 contrast first and second order elasto-plastic response of a hypothetical single bay frame. Such a comparison will now be applied to a typical fixed arch. The live load applied is uniformly distributed over six-tenths of the span and the dead load is of course applied to the entire span. The response is the maximum arch deflection. The arch chosen to evaluate load-deflection is a standard arch as previously defined with slenderness $L/r = 222$ and dead load ratio $\alpha = 0.10$. These parameters were chosen as they are indicative of slender arched ribs of highway bridges.

Several load deflection curves are plotted on Fig. 47 for the above mentioned arch. These generated curves contrast the second order elasto-plastic "ULA" response with first order elasto plastic behaviour, with and without moment axial interaction. Because an assumed dead load was included in the analysis, the load deflection curves do not start at the origin. The deflection corresponding to $\omega L^2/M_p = 0.0$ is the dead load deflection.

Several observations can be made from these load-response plots, the most obvious being the significant non-conservatism arising from neglecting second order effects in determining a collapse mechanism. This is best summarized by noticing that at the load level when the first hinge would form according to a first order analysis, the arch has actually either formed, or is very near, a three hinge collapse mechanism.

Any discrepancies between the different load deflection curves would be even more pronounced if the dead load parameter α were greater than

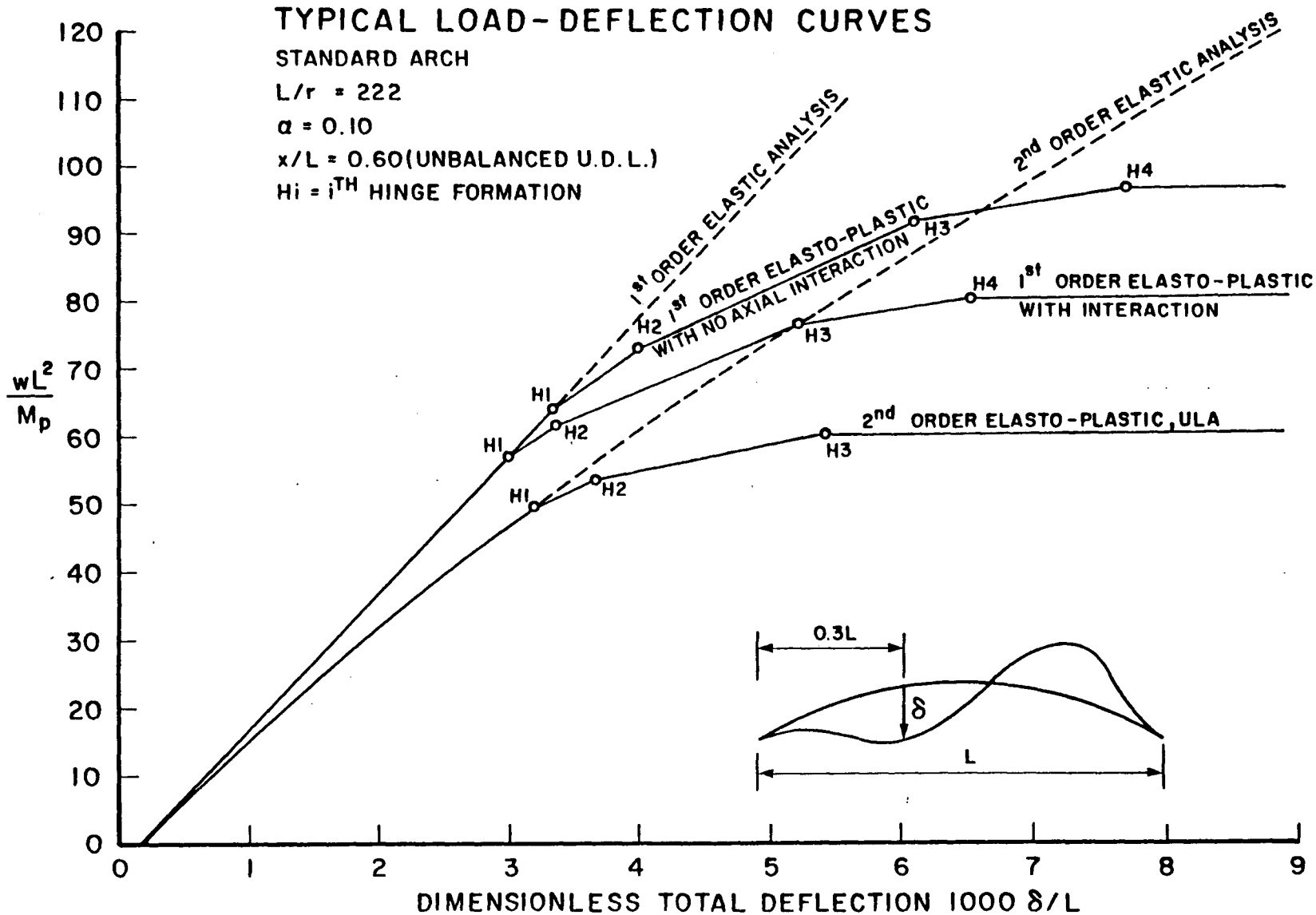

Fig. 47. Load-Response of a Typical Standard Arch.

0.10 because that would increase any second order effects. This is indeed the case for many long span arches with α between 0.10 and 0.20.

6.3 Application of Load and Performance Factors

There has been little discussion thus far on the application of load factors and performance factors as dictated by Limit States Design. The collapse curves and hinge formation curves have all been based on a computer analysis. It must be assumed that all the parameters relating to the curves, be they loads or material properties, are appropriately factored. Thus, before entering the curves, all factors must first be applied when calculating the required dimensionless parameters, then the live load P_i and w_i obtained from the curves are factored loads. This ensures complete flexibility because any factors may be used. For example the dead load w_D must be interpreted as $\alpha_D w_{DS}$ where α_D is the dead load factor and w_{DS} is the specified load. Similarly, the plastic moment M_p indicated as part of several dimensionless ratios must actually be calculated as $\phi Z \sigma_y$. Of course, it will almost certainly be necessary to interpolate between curves with different α ratios to obtain meaningful values of P_i and w_i.

The following section will deal with application of the dimensional analysis to existing arches where load and performance factors must be applied.

6.4 Application to Existing Arches

A very common use of the arch as a structural form is for highway bridge ribs. A span which is too long for a truss, and yet not long enough to warrant a suspension or cable stayed structure, is commonly

bridged by two or more arch ribs. If the foundation conditions are stable enough, a fixed arch can be constructed. Throughout the life of a bridge, it will likely be required to support live loads greater than the original design loads. Most existing arched bridges were designed elastically, and likely by means of an allowable stress approach. Thus properly evaluating an existing bridge, as well as designing a new bridge by Limit States Design both require a knowledge of behaviour beyond the criterion of first yield. If a structure has significant reserve capacity beyond first yield and factored loads cause a response in this region, then the structure may be deemed safe from a strength point of view.

The typical hinge formation curves and collapse envelopes of Figs. 21 to 27 will now be applied to the fixed arches of three existing bridges. These bridges are the La Conner Highway Bridge in Washington State, the Capilano Canyon Highway Bridge in Vancouver, British Columbia, and the Arvida Bridge in Arvida, Quebec. The arched ribs of these bridges are made of structural steel, reinforced concrete and aluminum respectively.

As a result of all three arches having long spans, the designs were governed by lane loading as opposed to truck loading. The arch collapse curves for unbalanced uniform loading will be used. A point load was required in addition to the uniform lane loading for the La Conner and Capilano bridges. The analysis in this work did not include this additional point load, however both loaded lengths are quite long and any error due to the omission of the point load should not be serious.

The original design loads are used along with a Limit States Design dead load factor of 1.3 and performance factor of $\phi = 0.90$ applied to

reduce P_p and M_p. For each bridge rib the value of wL^2/M_p is plotted on the appropriate collapse curves. The value of w is the unfactored uniform design load per rib. This includes an impact factor and sidewalk pedestrian loading. A reduction in gross area due to any rivet or bolt holes was considered in calculating M_p. When calculating r, full cross-sectional area was used. The load case examined here does not include such things as temperature, wind or earthquake and is therefore by no means a complete analysis, however a very good conceptual idea of the load factor required to cause first yield and the load factor required to cause collapse is indicated. In the analysis used for this work, a constant cross-section was assumed. The reality, however, is that a small variation in cross-section is commonly used to increase the moment resistance at the haunch where first yield normally occurs. This results in a variation in M_p and r. Thus, the key dimensionless ratios wL^2/M_p and L/r will not have one single value each, but a range of values. The resulting plots on Figs. 48 and 49 will therefore consist of a service load level region as opposed to a single point for each bridge examined.

6.4.1 The La Conner Bridge

The La Conner Bridge, also known as the Swinomish Chanel Bridge, is located at La Conner, Washington. This fixed steel box arch spans 167.6 metres (550 feet). It was designed by H.R. Powell and Associates of Seattle, Washington in 1955. Data from the design drawings give:

$$f/L = 0.167$$

$$E/\sigma_y = 600$$

$$Z/S = 1.18$$

$$y/r = 0.95$$

$$\alpha = 0.16$$

$$wL^2/M_p = 7.37 \text{ to } 8.89$$

and

$$L/r = 185 \text{ to } 191.$$

The corresponding service load level region is plotted as a square on Fig. 48. The first yield and collapse curves for both $\alpha = 0.10$ and $\alpha = 0.20$ are shown on Fig. 48 so that an interpolation between the two curves can be made by the reader. The actual cruves for the La Conner Arch would plot slightly below the standard arch curves due to the discrepancy between the standard value of $E/\sigma_y = 750$ and the La Conner value of 600.

6.4.2 The Capilano Canyon Bridge

The Capilano Canyon Bridge is part of the Trans-Canada Highway. It includes two reinforced concrete arch ribs which span 103.4 m (339.4 ft.) across the Capilano Canyon supporting a four lane concrete deck. The bridge was designed by Choukalos Woodburn Hooley and McKenzie Ltd. for the B.C. Department of Highways in 1956. Although this research was originally geared towards metal arches, reasonable estimates can be made of the important parmeters describing the arch such as slenderness and a plastic moment. As is common to all concrete arches, the Capilano arch is symmetrically reinforced resulting in as much compression steel as tension steel for bending. This implies significant ductility and capability of hinge formation. A much more noticeable variation in cross-section is apparent in a reinforced concrete arch than a metal arch, thus the service load region plots larger.

Data from the design drawings give:

$$f/L = 0.168$$

$$E/\sigma_y = 900$$

$$\alpha = 0.14$$

$$L/r = 115 \text{ to } 181$$

and

$$wL^2/M_p = 14.6 \text{ to } 20.2 \ .$$

The design load region for the Capilano Canyon bridge is plotted on Fig. 48. The curves shown in Fig. 48 are conservative when applied to the concrete Capilano arch because they correspond to $E/\sigma_y = 750$, when in fact $E/\sigma_y = 900$ for concrete.

6.4.3 The Arvida Bridge

The first aluminum highway bridge on the American continent was built in Arvida, Quebec, in 1950. This, the Arvida Bridge, has a main span which is a fixed arch 88.4 meter (290 ft.) center to center of skewbacks, spanning the Saguenay River. The following dimensionless parameters were calculated from information in an article by C.J. Pimenoff:[5]

$$f/L = 0.16$$

$$Z/S = 1.12$$

$$E/\sigma_y = 210$$

$$L/r = 151 \text{ to } 156$$

$$\alpha = 0.11$$

$$y/r = 0.93$$

and

$$wL^2/M_p = 8.40 \text{ to } 9.84 \ .$$

The available hinge formation curves for $E/\sigma_y = 375$ and 0.10 are applied to the Arvida arches in Fig. 49. Again, the value of E/σ_y is incorrect, however the resulting non-conservatism is not serious at the low L/r corresponding to the Arvida arch.

6.4.4 Further Research

It would be interesting to compare the theoretical solutions presented herein with an experimental study on model arches.

As well, the results herein are centered around a moment axial interaction curve for a material such as steel. Some investigation should be made using the somewhat unique interaction curve for reinforced concrete.

Finally, the current results could possibly be simplified into a design system more realistic than that used today.

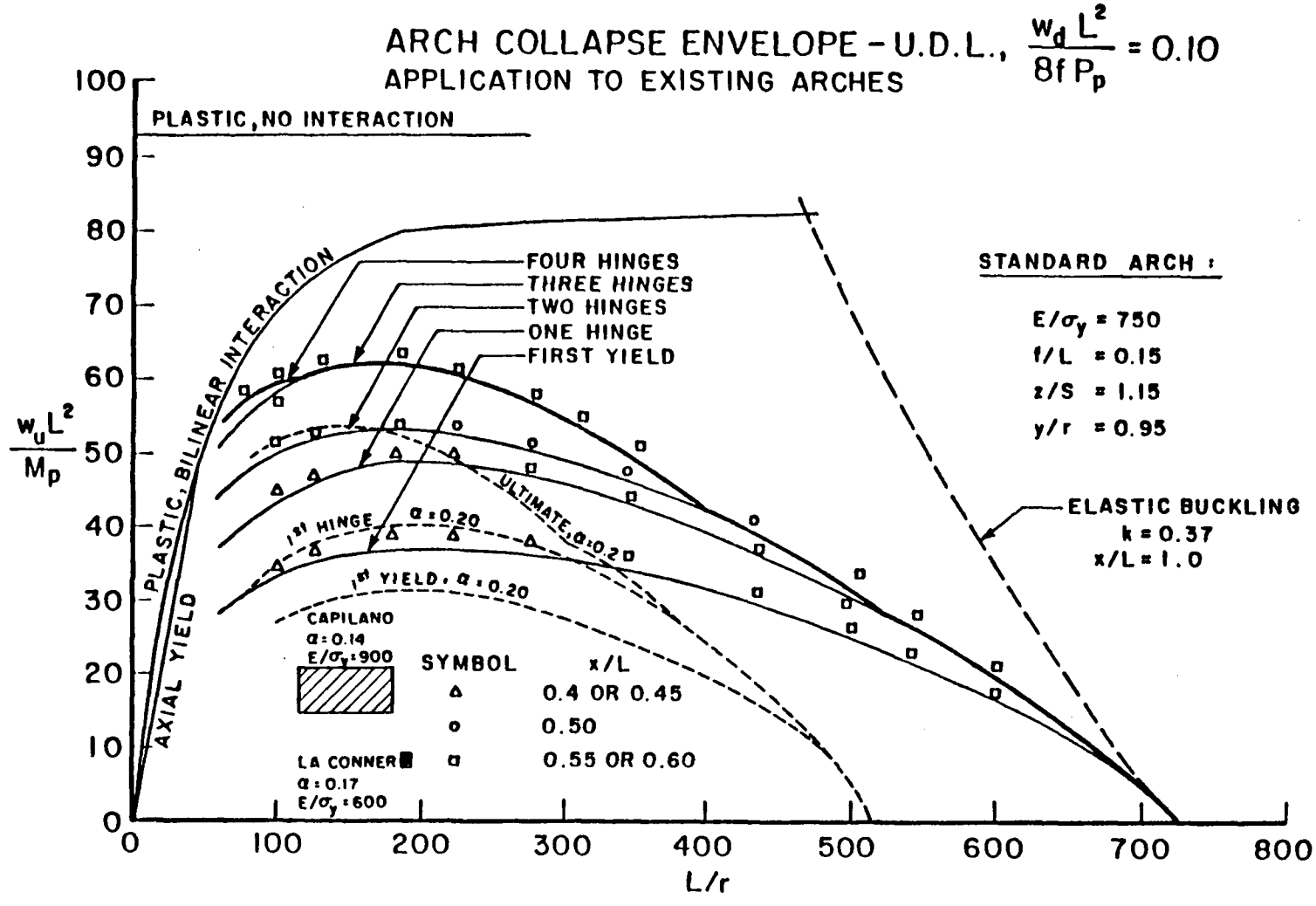

Fig. 48. Application of Collapse Curves to La Conner and Capilano Bridges.

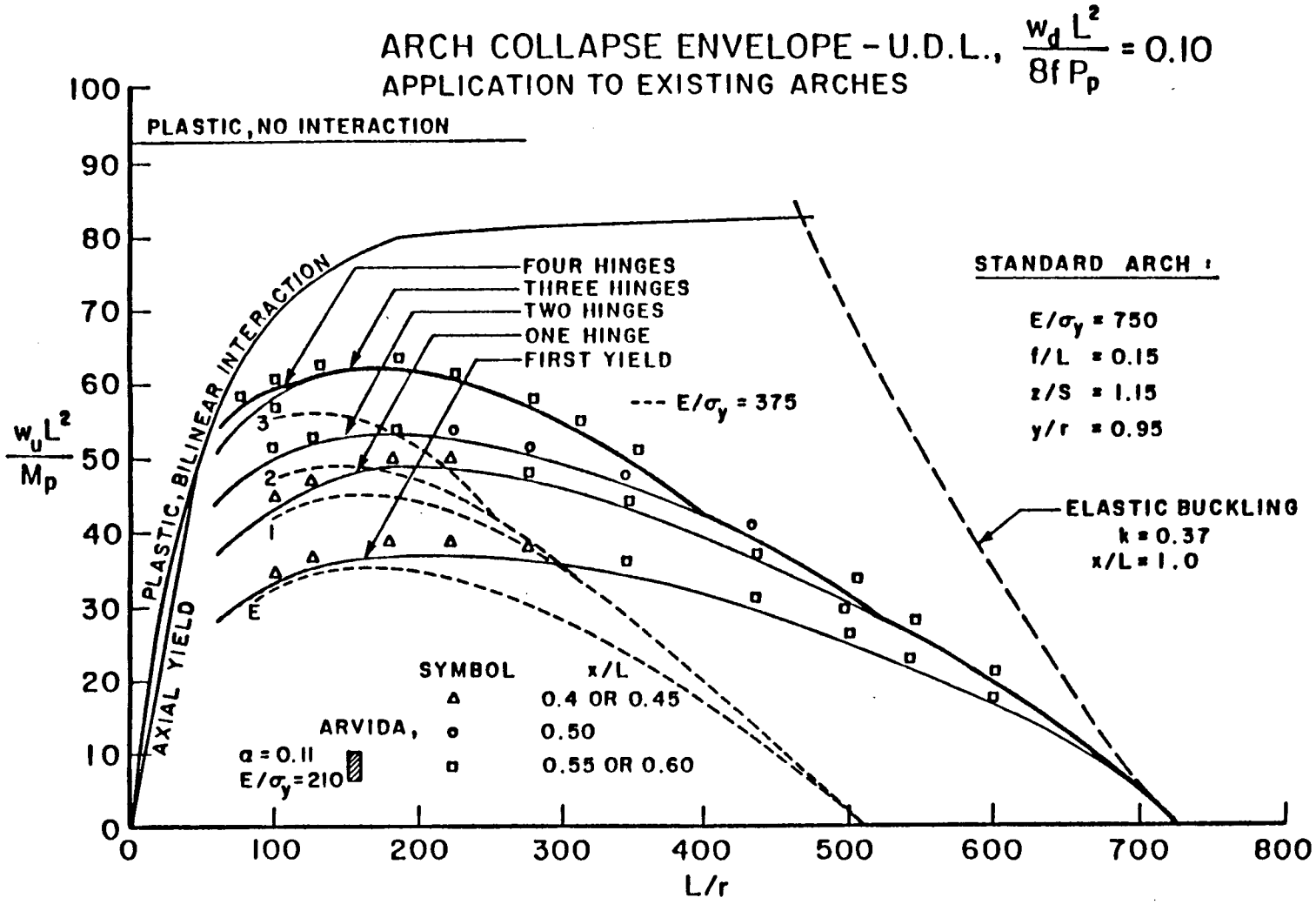

Fig. 49. Application of Collapse Curves to the Arvida Bridge.

REFERENCES

1. Hooley, R.F. and Mulcahy, F.X., 1982. Nonlinear Analysis by Interative Graphics. Canadian Society for Civil Engineering, Annual Conference.

2. Gere, J.M. and Weaver, W., 1965. Analysis of Framed Structures. Van Nostrand Reinhold Co., New York, pp. 428-431.

3. Timoshenko, S., 1936. Theory of Elastic Stability. 1st ed. McGraw-Hill, New York, pp. 36-38.

4. Galambos, T.V. and Ketter, R.L., 1961. Columns Under Combined Bending and Thrust. American Society of Civil Engineers, Transactions, Vol. 126(I).

5. Pimenoff, C.J., 1949. The Arvida Bridge. E.I.C. Journal, Vol. 32, No. 4.